ABSTRACT

Title of Dissertation:	TOWARDS A GENETICALLY-ENGINEERED BACTERIUM FOR GASTROINTESTINAL WOUND HEALING
	Chelsea Ryan Virgile, Doctor of Philosophy, 2017
Dissertation directed by:	Professor William E. Bentley, Fischell Department of Bioengineering

Society and physicians frequently associate the increase of antibiotic-resistant bacteria with the overuse of antibiotics. This proposes a question, “Why use antibiotics to fight bacteria and risk resistance, when one could engineer bacteria to target and kill infectious bacteria?” Bacteria are often thought of as ‘good’ bacteria (e.g., commensals, probiotics) or ‘bad’ bacteria (e.g., pathogens). Synthetic biology enables the augmentation of biosynthetic capabilities and retooling of regulatory structures in the creation of cells with unprecedented ability to make products. One can also, however, think of the cell as the product – a cell that operates in a noisy environment to execute non-native tasks. There have been several recent reports of the rewiring of bacterial cells to function as conveyors of therapeutics. The engineering and rewiring of the bacteria such as *E. coli* into ‘smart' bacteria potentially allows for a broad range of applications, from the treatment of wounds, the elimination of pathogenic strains, to the delivery of vaccines, particularly in the gastrointestinal (GI) tract. I have engineered smart bacteria as a therapeutic delivery vehicle

for wound healing in the GI tract. The approach comprises synthetic biology and microfluidics for the creation of a biological ‘test track' for ensuring the appropriate design and testing of engineered bacteria. Bacterial motility was engineered for response to wound-generating signals such as hydrogen peroxide. Specifically, we have placed a motility enzyme CheZ under the control of the hydrogen-peroxide-responsive oxyR/S gene-promoter pair so that the ‘run’ in the tumble and run scheme of bacterial movement is externally regulated. These engineered cells exploit pseudotaxis for directional swimming towards hydrogen peroxide, a non-native signal. Additionally, the therapeutic enzyme transglutaminase plays an important role in the tissue clotting cascade. Microbial transglutaminase can crosslink fibrinogen, similar in function to human transglutaminases during the clotting cascade, but independently of calcium ions. This allows for a potentially faster, increased wound-healing response. By combining microbial transglutaminase expression with controlling motility and lysis expression using the OxyR/S system, the ‘smart’ bacteria can potentially swim towards and treat at the wound site with subsequent cell lysis. Ultimately, this strategy can lead to new bacterial therapies.

TOWARDS A GENETICALLY-ENGINEERED BACTERIUM FOR GASTROINTESTINAL WOUND HEALING

by

Chelsea Ryan Virgile

Dissertation submitted to the Faculty of the Graduate School of the
University of Maryland, College Park, in partial fulfillment
of the requirements for the degree of
Doctor of Philosophy
2017

Advisory Committee:
Professor William E. Bentley, Chair
Professor Amy J. Karlsson
Professor Donald Milton
Professor Gregory F. Payne
Professor Ian White

Acknowledgements

I would like to acknowledge Dr. William Bentley for advising my project, and Drs. Hsuan-Chen Wu, Chen-Yu Tsao, and Pricila Hauk for providing advice, guidance, and trainings during my PhD. I would like to acknowledge Dr. Hsuan-Chen Wu for engineering the W3110-*ΔcheZ* strain and pFZY1-oxyR-*p*oxyS-cheZ, and for teaching me the transwell experiments. I would like to acknowledge Dr. David Quan for providing and teaching me the transwell Comsol model. Wu Shang performed the static gradient device experiments. Dr. Pricila Hauk aided the Western Blot experiments. Naren Bhokisham taught and provided guidance with the microbial transglutaminase experiments.

Table of Contents

List of Tables

List of Figures

List of Abbreviations and Nomenclature

Abbreviations

Hospital acquired infections (HAIs)

Methicillin-resistant Staphylococcus aureus (MRSA)

Lawrence Livermore National Laboratory (LLNL)

Extended-spectrum β-lactamase (ESBL)

3OC12-HSL (quorum-sensing molecule N-3-oxododecanoyl homoserine lactone)

Hydrogen peroxide (H_2O_2)

Microbial transglutaminase (mTG)

Vascular endothelial growth factor (VEGF)

Gastrointestinal (GI)

Inflammatory bowel disease (IBD)

Ulcerative colitis (UC)

Crohn’s disease (CD)

Reactive oxygen species (ROS)

Quorum sensing (QS)

Acyl homoserine lactones (AHLs)

Methyl-accepting chemotaxis protein (MCP)

Human tissue transglutaminase (htTG)

Glutaredoxin-I (Grx)

Relative quantification (RQ)

Tris-buffered saline + Tween 20 (TBST)

Dulbecco's phosphate-buffered saline (DPBS)

Constant fragment (Fc)

Antigen-binding fragment (Fab)

N-α-carbobenzoxy-L-glutaminyl-glycine (CBZ-Gln-Gly)

Propidium iodide (PI)

Nomenclature

STRAIN: *E. coli* K-12 W3110 (WT) – Native run and tumble (motility, surface display, mTG)

STRAIN: *E. coli* K-12 W3110-*ΔcheZ* (HCW01) – Tumble (motility, lysis)

PLASMID: pFZY1-OxyR-*p*OxyS-CheZ (pHW02) – H_2O_2-controlled running (motility)

PLASMID: pET200-t5-eGFP – constitutive fluorescent protein/reporter (motility, metabolic burden)

STRAIN: *E. coli* K-12 *ΔluxS* (LW12) – Autoinducer-2 sensing (surface display)

PLASMID: pLacUV5-ProteinG-AIDA1 (pG-AIDA1) – IPTG-induced Protein G surface display on bacterial outer surface (surface display)

PLASMID: pST39-OxyR-pOxyS-Trx–proTGase (H_2O_2-Trx-proTGase) – H_2O_2-induced mTG (therapeutic)

PLASMID: pET32aΔ-SNTGA (SNTGA) – IPTG-induced mTG (therapeutic, lysis)

PLASMID: pFZY1-OxyR-*p*OxyS-CheZ-E7 (pHW02-E7) – H_2O_2-controlled running + lysis (motility, lysis)

Chapter 1: Introduction

1.1 Background

1.1.1 Bacteria, Hospital Acquired Infections, and the FDA's Role

In society over the past few years, not a week went by without the news reporting civil unrest or an update on the latest healthcare crisis. Over the past 5 years, the healthcare news updates included Zika, Ebola, enterovirus 68, necrotizing fasciitis (flesh-eating bacteria), and hospital acquired infections (HAIs), specifically methicillin-resistant Staphylococcus aureus (MRSA). Ebola and enterovirus 68 are viruses that cannot be treated with antibiotics; however, necrotizing fasciitis and MRSA are two well-known bacterial infections because of their increasing difficulty to treat. Researchers and physicians report finding an increasing number of necrotizing fasciitis cases with MRSA-origin[1]. This represents one example of the increase in the number of antibiotic-resistant bacteria.

Society and physicians frequently associate the increase of antibiotic-resistant bacteria with the overuse of antibiotics. Therefore, industry and researchers have looked for alternatives to antibiotics, such as utilizing a combination of the gut microbiome, probiotics, and/or disease-specific engineered probiotics. However, bacterial therapy's translational application is in the infancy stages at the FDA. In 2016, the company Seres entered Phase 2 clinical testing of its 'poop pill,' SER-109 for treatment of *Clostridium difficile* bacterial infection; the treatment process involves taking a stool sample from the patient, extracting and purifying 5 to 15 bacterial strains for insertion into the pill, and oral ingestion of the pill to restore gut health and cure the infection; however, they failed the Phase 2 clinical trial due to the inability to reduce the relative risk of *C. diff* recurrence, compared to a placebo, up to eight weeks after treatment. After consultation with the FDA and study investigators, Seres

adjusted the development for SER-109 and entered Phase 3 clinical trials[2]. Other companies were or are also seeking FDA approval for gut health restoration and cure of infection[3]. These companies are taking the first steps toward FDA approval of bacterial therapeutics. This shows there is promise for expanding bacterial therapy as a conventional and/or alternative treatment for bacterial infections and potentially targeted injury-specific or disease-specific therapies.

1.1.2 Relationship Between HAIs, Combat Soldiers Abroad, and Global Health

Combat soldiers face danger every day they are abroad in combat zones in Iraq or Afghanistan; soldiers can see the physical dangers, but they miss the invisible danger – viruses, bacteria, and fungi that live in the soil and possibly in their wounds. Wounded soldiers' lives depend on the evacuation speed, surgeon's ability to properly clean and treat the wound, degree of blood loss, and exposure of the wound to infectious microorganisms. The microorganisms existing in the soil and found in soldiers' wounds vary depending on the region, climate, and microorganism's evolution[4,5]. In order to best protect soldiers from losing limbs to infection and amputation, researchers and physicians must understand and create libraries of these microorganisms and create treatment plans, especially if the bacterial microorganisms have antibiotics resistance.

In response to the public's growing concern with infection and antibiotic-resistant infection control, the military and Department of Defense are also taking the initiative; currently, researchers at the Lawrence Livermore National Laboratory (LLNL) with four other research organizations are creating a library to identify and characterize the phenotypic and genotypic changes of colonizing and infection *E. coli* found in Iraq and Afghanistan combat zones and soldiers' wounds from June 2009 to May 2011[4–6]. They developed a novel detection method, named the Lawrence Livermore Microbial Detection Array, for detecting

bacterial pathogens. Currently, the standard culture method does not detect a bacterial pathogen existing in the infected wound samples they tested. The LLNL's current library contains probes for approximately 3,855 bacteria[6]. In their findings, the researchers frequently classified both the colonizing and infecting isolates as extended-spectrum β-lactamase (ESBL)-producing *E. coli*. This gives rise to concern because the majority of ESBL infected wounds heal unsuccessfully; even though ESBL infections are associated with hospital infections, studies in recent years show an emerging link between ESBL and community-acquired infections[4]. Therefore, by creating a library of infectious and drug-resistant bacteria's phenotypes and genotypes, one can quickly identify the infection and develop a treatment plan.

1.2 Synthetic Biology Approach to Therapeutics

Synthetic biology offers a potential therapeutic alternative to current infection treatment methods, considering the rise of antibiotic-resistant bacteria. Synthetic biologists construct novel genetic/biological systems through genetic rewiring for use in bacteria to treat environmental, energy, and health problems. Recent advances in the field produced bacteria containing switches[7], amplifiers[8,9], oscillators[10,11], and genome recombination methods[12] to create highly specialized bacteria with a variety of biosynthetic abilities, including sense and respond phenotypes[13,14]. By utilizing genetic rewiring, researchers created 'smart' bacteria as the final product for targeting infectious bacteria; most importantly, these groups created the 'smart' bacteria to target to disease or infection sites and deliver therapeutics using the minimal required doses to reduce side effects. One group, Chang *et al.*[14], genetically engineered *E. coli* to sense and kill nearby *P. aeruginosa* via secretion of pyocin S5 (a killing protein specific to the pore-forming activity of P. aeruginosa) in response to its identifying signaling molecule released by *P. aeruginosa*, 3OC12-HSL (quorum-sensing molecule N-3-

oxododecanoyl homoserine lactone); in addition, the bacteria were engineered to later self-destruct. This example is just one of a few that looks to exploit the natural signaling processes that exist in individual bacteria and the methods of rewiring their genetic circuits to produce a desired outcome – target and treatment of an infectious disease.

In combination with the "poop pill" theory addressed in **1.1**, one can engineer smart bacteria to autonomously target, treat, and lyse at a disease or wound site based on the specific density of the bacterial, chemical and/or molecular signals up-regulated at the site; as a starting platform, one can encapsulate the bacteria for oral delivery. By genetically rewiring bacteria, one can create a new, innovative platform for developing and optimizing spatially-sensitive and physiologically-relevant disease-targeting bacteria in combination with the research community, industry, and the FDA.

1.3 Global Objective and Hypothesis

1.3.1 Global Objective

Soldiers wounded in combat abroad face a multitude of obstacles during the critical treatment time, including degree of blood loss, evacuation speed, the military surgeon's ability to completely treat the wound, and the unknown microorganisms that exist in foreign soil; these foreign microorganisms include viruses, bacteria, and fungi, all of which affect wound treatment and healing time. Diminishing and eliminating these foreign microorganisms can be accomplished by using synthetic biology. Specifically, by rewiring the parts of the *E. coli*'s natural genetic circuitry, one can engineer 'smart' bacteria to swim towards the wound site, dock, and either recruit a second therapeutic bacterial population or deliver therapeutics. The type of therapeutic delivery can vary depending on the type of wound and type(s) of foreign microorganisms infecting the wound. This proposal will focus on the swimming towards the injury and aiding wound healing. Considering the possibility of

antibiotic-resistance developing in current types of infections, bacterial therapy would be an alternative treatment to antibiotics; one can use 'smart' bacteria to target, deliver therapeutic aid, and kill infectious bacteria.

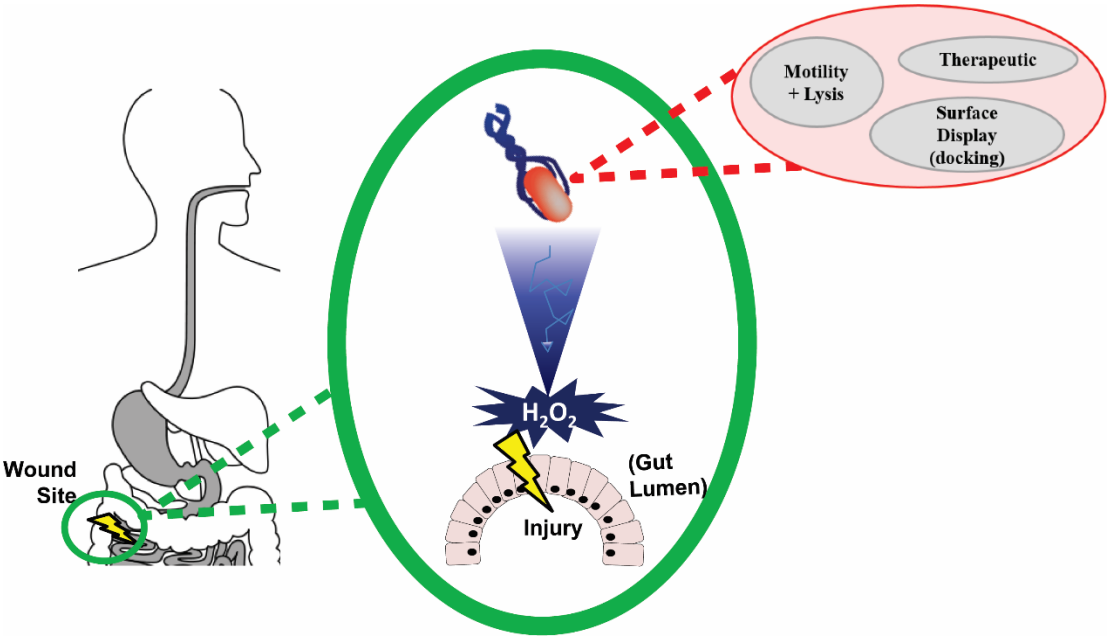

Figure 1 – Schematic of engineered bacteria targeting and treating a gastrointestinal wound.

1.3.2 Hypothesis

To accomplish all of these objectives for this dissertation, the bacteria's natural genetic circuitry must be re-wired and balanced, not overburdened. I will briefly discuss the principles and technologies necessary to genetically engineer and modify the bacteria to accomplish the objectives in the latter part of **Chapter One**. **Chapter Two** will serve to characterize the hydrogen-peroxide (H_2O_2)-controlled bacterial running, specifically CheZ. **Chapter Three** will focus on characterizing the phenotypic response of the engineered motility bacteria to H_2O_2. For therapeutic purposes, I will express microbial transglutaminase (mTG), as opposed to the larger and highly insoluble (in bacteria) recombinant human tissue transglutaminase, in the engineered bacteria as a method to speed wound healing; additionally, genetic machinery for bacterial docking will be described and optimized in

Chapter Four. Finally, a lysis system, also under H_2O_2 control, will be characterized in **Chapter Five**, including whether the therapeutic can be released into the supernatant and maintain activity. By combining mTG expression and the other systems with H_2O_2-controlled CheZ motility and lysis, the 'smart' bacteria can potentially swim towards, dock, and treat the wound site with minimal motility burden from the therapeutic systems expressed.

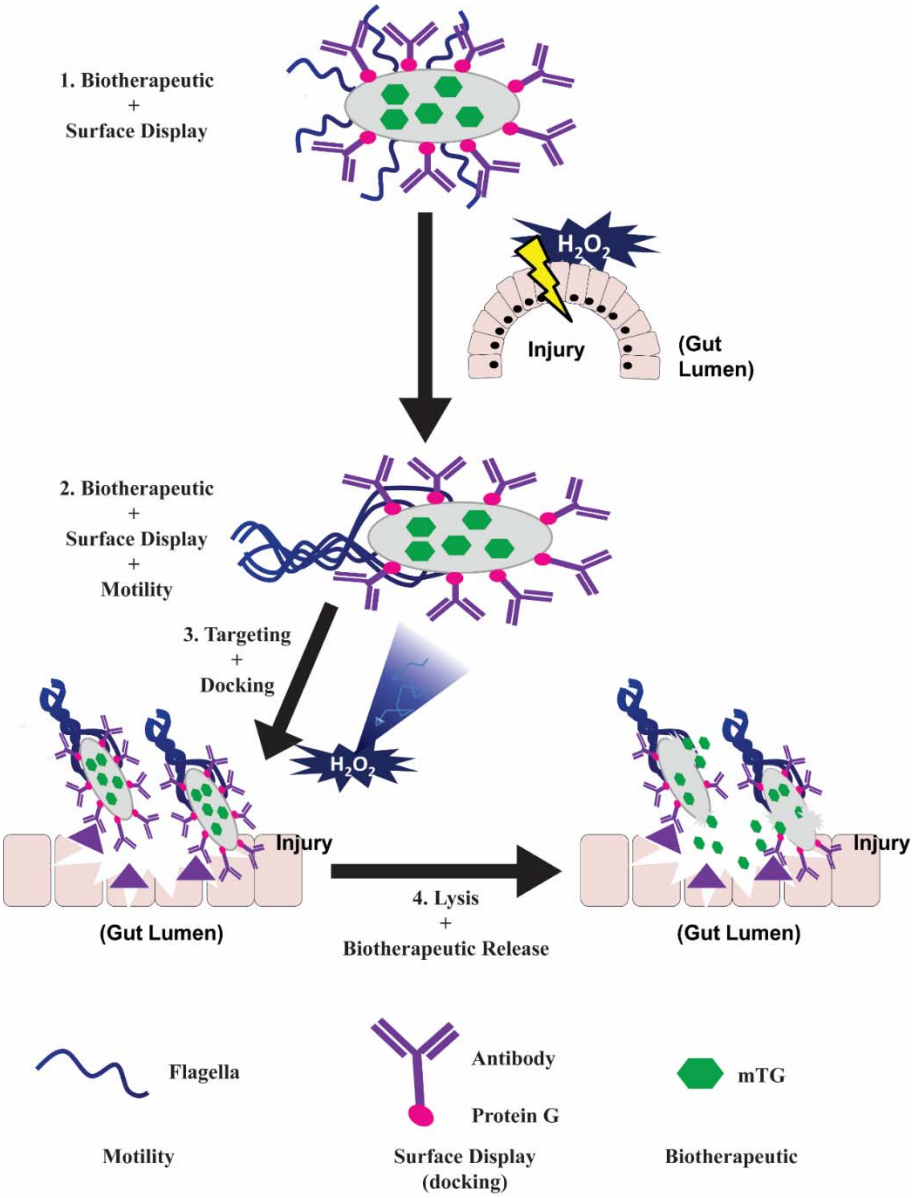

Figure 2 – Schematic of proposed engineered bacteria. *1. The engineered bacteria synthesize the biotherapeutic and surface display Protein G for antibody binding. 2. In response to the H_2O_2 burst release from the wound site,*

the engineered bacteria turn on motility. 3. The engineered bacteria target the H2O2 at the wound site for antibody-specific docking. 4. The engineered bacteria lyse at the wound site, releasing the biotherapeutic.

1.4 Hydrogen Peroxide

1.4.1 Role: Wound Sites

Researchers have extensively documented the phases of epidermal skin wound healing. Immediately after injury occurs, the dynamic wound-healing response starts with a blood clot starting to form; once homeostasis occurs[15,16], the inflammatory phase begins with neutrophils gathering at the wound site for release of bactericidal reactive oxygen species and H_2O_2 to kill bacteria and prevent infection; then, environmental stimuli cue macrophages to arrive, phagocytose (eat) foreign particles, and release vascular endothelial growth factor (VEGF) to modulate angiogenesis via tissue vascularization growth factors[15,17,18].

Specifically for this proposal, gastrointestinal (GI) epithelial wound healing will serve as the model injury/disease state. Naturally, the intestinal epithelial cells form tight and adherens junctions to regulate the passive movement of luminal fluid and solutes, passive diffusion, and intercellular adhesion; importantly, these cells also allow some non-pathological gut microbiota access to the immune system, to promote and evolve immune tolerance. Recent studies have demonstrated the importance of commensal bacteria activating toll-like receptors to inhibit inflammatory responses and maintaining colonic homeostasis[19].

However, injury to the epithelial barriers, especially of the mucosal surfaces of the GI system, is found in a number of states; these include pathological states such as inflammatory diseases, ischemic events, and also mechanical injury from medical intervention or surgical repair[19]. Injury to the (GI) epithelial lumen lining allows an increased absorption of toxic and immunogenic factors, leading to disruption of homeostasis, inflammation, and an uncontrolled immune response. Activation of the wound healing response resembles that of epidermal skin, including the generation of oxygen free radicals (such as H_2O_2); however, these oxygen free radicals initiate a chain reaction for the phospholipid-GI defense system for

inflammatory process and epithelial surface repair[20]. Additionally, researchers discovered that various regulatory peptides, including growth factors and cytokines, along with novel toll-like receptors, particular dietary factors, and gastro-protective agents help regulate intestinal wound repair[19].

Mitchison *et al.*[21] conducted one of the key studies for visualizing and linking rapid wound detection via a tissue-scale H_2O_2 pattern in zebrafish larvae; their findings indicate that the H_2O_2 gradient does not rapidly dissipate once the injury occurs. Therefore, the H_2O_2 gradient can be used as a signaling molecule for recruiting the engineered smart bacteria to the wound site.

Importantly, initial screens suggest that the H_2O_2 concentrations investigated here are within the reported physiological ranges for eventual deployment at wound sites, potentially including those in the GI tract[21]. Researchers demonstrated *in vitro* that H_2O_2 concentrations at 0.1-0.5 mM delayed murine fibroblast cell apoptosis for 24-48 hours, with no apoptosis below 0.1 mM [22]. Notably, *in vivo* studies conducted in zebrafish, a popular vertebrate model system, demonstrated a burst release of H_2O_2 (0.1-0.2 mM at wound site) to recruit immune cells to prevent infection[21]. Additionally, *in vivo* mice studies demonstrated and quantified that dermal wound H_2O_2 levels persisted during the immediate inflammatory days (> 200 μM; 2 days post-wounding) and post-inflammatory days (~150 μM; 5 days post-wounding); when the researchers added a topical low-dose H_2O_2 (1.25 μM/wound) treatment, it increased the wound healing response[23]. Given these initial indications, we performed studies to evaluate H_2O_2 -dependent dynamics of the promoter system, cell growth, and subsequent swimming phenotype. Given these initial indications, we performed studies to evaluate H_2O_2 -dependent dynamics of the promoter system, cell growth, and subsequent swimming phenotype.

1.4.2 Role: Disease States

While this dissertation focuses on using 'smart' bacteria to traffic to and treat at a GI wound site, broader applications apply. When the dynamic wound-healing process continues to evolve and expand without limitations, tumourigenesis begins. Depending on the tumor, different tumourigenesis signaling pathways are activated and upregulated; for solid tumors, the cancer cells hijack and constitutively upregulate the wound repair signaling pathways. In addition, tumor development from wound sites occurs when inflammation does not subside when re-epithelization is complete[16]. By using these upregulated pathways, 'smart' bacteria can be trafficked to the acidic tumor microenvironment and deliver therapeutics.

Additionally, GI diseases including inflammatory bowel disease (IBD), ulcerative colitis (UC), and Crohn's disease (CD) cause oxidative stress to the mucosal cells of the GI tract; mucosal biopsies taken by Bibloni and colleagues expressed increase in *lactobacilli* compared to healthy biopsies. Some species of *Lactobacillus*, *Streptococcus* and *Enterococcus* genera produce substantially high amounts of H_2O_2, compared to the amount released by the immune response[24,25]. Furthering these studies, Strus *et al.* sought to elucidate the relationship between H_2O_2 development and the body's immune response to IBD. They reported increased populations of *Lactobacillus* and *Streptococci* adherent to the IBD lesions; when cultured in vitro, multiple species tested produced a range of 0.3 – 0.6 mM and 0.3 – 1.8 mM H_2O_2 over 4 and 24 hours, respectively. They hypothesized that the increase in the total populations of these aerobic bacteria but not anaerobes in the studied IBD samples indirectly provides evidence of higher oxygen tension present in the inflamed IBD tissues, possibly due to the imbalanced anti-oxidative activity of the IBD mucosa[25]. Specific to our study, potential applications and the natural presence of bacteria in the gut microbiome, we intend to use a wound in the GI tract as the model.

1.4.3 Using H_2O_2 as a Genetic Controller

Bacteria naturally respond to oxidative stressors such as H_2O_2 and other reactive oxygen species (ROS) that are released by eukaryotic cells upon insult such as pathogen infection or wound generation. They possess several mechanisms, including the OxyR/S-mediated response triggered by H_2O_2[26–28], for protection against toxicity. Eukaryotic/prokaryotic organisms also produce ROS as a byproduct of normal aerobic metabolism; thus, they have naturally developed machinery and mechanisms to convert the metabolic ROS side products into non-toxic products thereby maintaining homeostasis[26,29]. At physiological levels of H_2O_2 (~20 nM), OxyR acts as a repressor[28,30,31] of oxyS RNA transcription. OxyS RNA, in turn, is a global oxidative stress regulator mediating the activation or repression of over 40 genes[26,29]. In the presence of elevated H_2O_2 levels, changes in the oxidation state of OxyR's sulfhydryl groups at Cys199 and Cys208 promote the formation of a disulfide bond[26], that, in turn, modulates OxyR's structural conformation leading to subsequent transcriptional activation of many promoters involved in oxidative stress regulon[32–34], including oxyS[26,29] (**Figure 3**). This structural change, involving oxidation and reduction reactions, occurs extremely quickly, at a rate of 9.7 s^{-1} [34].

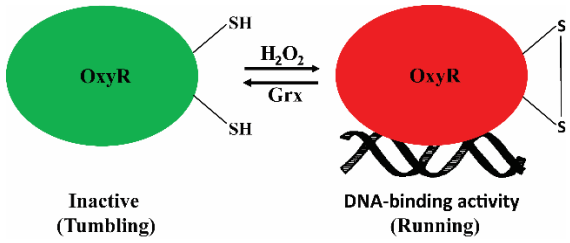

Figure 3 – OxyR activation. *The engineered bacteria tumble when H_2O_2 is not present. When H_2O_2 is present, H_2O_2 oxides the sulfhydral groups to form a disulfide bond, thus activating transcription and translation (for bacteria running) via OxyR binding the DNA.*

1.5 Bacterial Motility

1.5.1 Quorum Sensing-Based Motility

In *E. coli*, quorum sensing (QS) is an organic, complex cell-to-cell communication process that regulates and results in pathogenicity, biofilm formation, virulence, and growth, and cell motility[35–38]. In order to understand bacterial motility and population-based behavior, researchers studied the QS mechanisms in *E. coli* and pathogenic bacteria, such as *P. aeruginosa*, to understand the how the bacteria talk to each other using multi-cellular level interactions. Briefly, bacteria modulate QS by the synthesis, sensing and uptake of small chemical molecules called autoinducers. Using autoinducers, specifically acyl homoserine lactones (AHLs), autoinducer-2, and many other universal signals, the bacteria "talk" by sending, receiving, and processing different forms of these chemical signals. Through "talking," to either their own species or other bacterial species, bacteria enumerate and modulate local bacterial densities to evade the immune host and survive. This leads to the phenotypic expression of cell motility and other factors via population-based recruitment. Low-density bacterial populations express low amounts of QS molecules. However, as the population increases, the amount of QS molecules being expressed and exchanged grows, recruiting more bacteria to the site; this yields exponential QS-based growth towards the favorable, autoinducer-rich environment[35,36].

1.5.2 Bacterial Motility: Chemotaxis versus Pesudotaxis

Similar to QS-based motility, chemotaxis is defined as the biased process by which bacteria move towards a more favorable chemical environment (either a nutrient or food source) or away from a more toxic chemical environment[39–41]. For *E. coli*, Brownian motion (random movement) and viscous drag physically constrain them; however, using gene regulation and propeller-like flagella, bacteria can bias their movement from random

Brownian motion to a more directional swim. To accomplish this, bacteria alternate the rotation of their flagella between clockwise and counterclockwise rotations[41].

Specifically, this dissertation will focus on the CheY/CheZ mechanisms for controlling *E. coli* motility. The cheY gene activation turns the flagella motor in a clockwise motion, resulting in a random tumbling motion (**Figure 4-a**); The cheZ gene activation turns the flagella motor in a counter-clockwise motion, resulting in a more directional, biased run[41] (**Figure 4-b**).

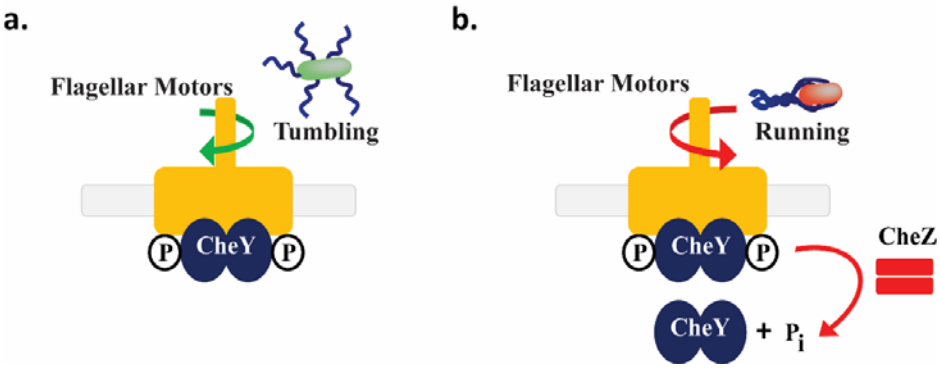

Figure 4 – Bacterial motility. *a. CheY activation. Phosphorylated CheY binds to the flagellar motor complex. The complex rotates clockwise, resulting in tumbling. b. CheZ activation. CheZ dephosphorylates CheY. CheY unbinds from the flagellar motor complex, resulting in counterclockwise rotations and bacterial running.*

Alternatively, to activate directional swimming via CheZ activation, the opposite mechanisms occur. First a chemoattractant binds one of five methyl-accepting chemotaxis protein (MCP) receptors; this signals the MCP-CheW-CheA tertiary complex in the cytoplasm. It allows the MCP to demethylate and CheW (the scaffolding protein) to receive chemical stimuli[39–41]. Dynamically, this also activates CheA, an autokinase, to use ATP to autophosphorylate CheB from a specific CheA histidine residue20. In addition, CheZ dephosphorylates CheY to balance phosphorylation levels. When paired with methylation and phosphorylation of CheB with dephosphorylation of CheY, the tertiary complex becomes an inactive kinase. These dynamic reactions result in the flagella motors turning counter-clockwise, yielding a directional swimming[39,40] (**Figure 5**).

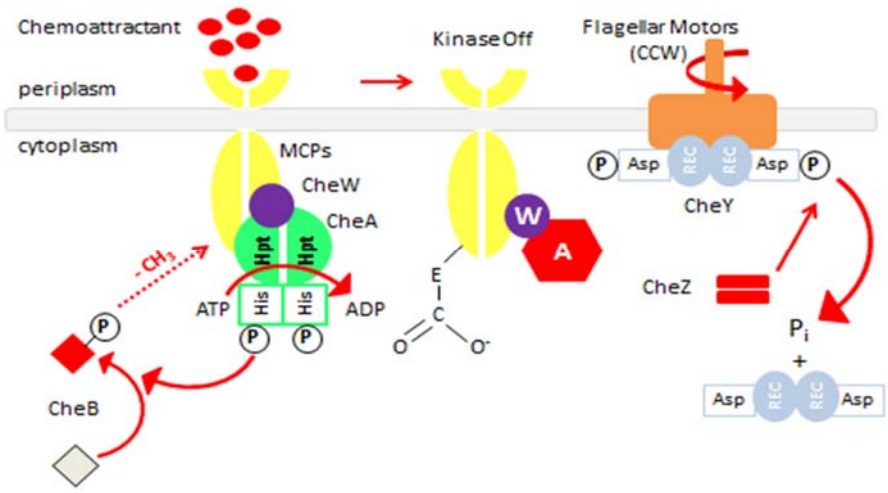

Figure 5 – CheZ mechanistic activation.

Researchers have well-documented the mechanisms of activating CheY and CheZ. The CheY phosphorylation cascade activates bacteria's random tumbling motion. For default CheY activation, first a chemo-repellant binds one of five methyl-accepting chemotaxis protein (MCP) receptors; this signals the MCP-CheW-CheA tertiary complex in the cytoplasm. It allows CheR to methylate the MCP, and CheW (the scaffolding protein) to receive chemical stimuli[39–41]. Dynamically, this also activates CheA, an autokinase, to use ATP to autophosphorylate a specific CheY aspartate residue from its specific histidine residue[39]. To control phosphorylation levels in the bacteria, CheB is dephosphorylated to balance CheY phosphorylation levels. When paired with dephosphorylation of CheA and methylation of a specific glutamic acid in the MCP, the tertiary complex becomes an active kinase. These dynamic reactions result in the flagella motors turning clockwise, yielding a tumbling motion[39–41] (**Figure 6**).

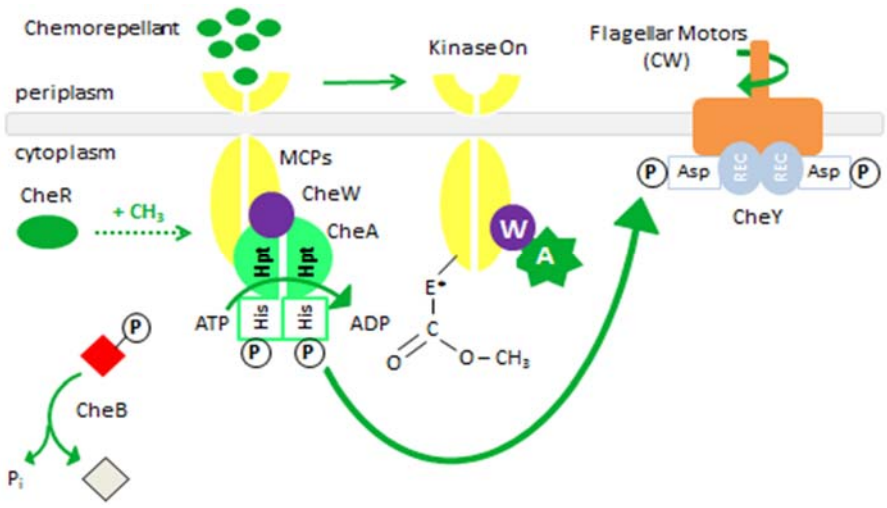

Figure 6 – CheY mechanistic activation.

1.6 Wound Healing: The Clotting Cascade

1.6.1 Transglutaminase's Role

Many approaches to wound treatment exist, from antibiotics and band-aids to suturing to skin grafts. However, many different physiological factors play a dynamic role in wound healing, as discussed previously in **1.4.1**. Human tissue transglutaminase (htTG) plays a large role in epithelial wound healing. htTG is a multifunctional protein with catalytic functions including peptide crosslinking. htTG is a large protein, ~80 kDa[42]. Other transglutaminase genes serve to stabilize the fibrin clot in homeostasis, serve as a structural component of the cytoskeleton, etc[42,43]. However, overexpression of htTG can lead to disease, specifically celiac disease[44]. In order to express human enzymes in bacteria, the human enzyme must be codon-optimized for expression in bacteria. Previous studies conducted by Shi *et al.* found that recombinant htTG2 expressed in bacteria yielded > 90% inactive, insoluble rhtTG protein; attempts to optimize expression temperature and pH yielded no improvements[44]. Therefore, due to its extremely low solubility in *E. coli*, an alternative transglutaminase must be used.

1.6.2 Microbial Transglutaminase: An Alternative and Applicable Approach

Because of htTG's large size and folding sensitivity, mTG serves as a comparable replacement; possibly due to convergent evolution, mTG shares similar crosslinking capabilities expressed by htTG. Additionally, htTG require calcium ions for enzyme activation; mTG does not require calcium to activate and has a more robust stability along a broad range of pH and temperatures[45].

mTG from *Streptomyces mobaraensis* (28 kDa) was first studied by Yokoyama *et al.* to its use in food processing for its effective protein crosslinking activity. Specifically, transglutaminases catalyze the acyl-transfer reaction between ε-amino group of lysine and the γ-carboxyamide group of glutamine in proteins. This crosslinking reaction has been tested in type I collagen[46], type II collagen[47], and gelatin hydrogel[48–50]. More extensive studies examined stability and activity across the different hosts and species. Further studies added a pro-region to mTG to expand mTG's solubility and activity across a broader range of temperature and pH[51].

Therefore, to limit metabolic burden and increase soluble transglutaminase expression, mTG will be used and tested in **Chapter 4**. By using mTG, as opposed to htTG, one can avoid pathogenesis and quicken wound healing by not disrupting htTG homeostasis levels.

1.7 Site-Specific Bacterial Docking

Site-specific bacterial docking requires antibodies to be displayed on the outer surface of *E. coli* that are disease-specific. Previous studies have engineered proteins on the outer surface using well-established phage systems[52]. Specifically, AIDA-I is a more robust system that allows for surface display of enzymes, enzyme inhibitors, and other small peptides or enzymes for several applications[53]. IgA1 protease, the AIDA-like transporter

found in *N. gonorrhoeae* was first described by Pohlner *et al.* in 1987[54]; the autotransporter of the IgA1 protease-like family consists of a signal peptide at the N terminus, one or more domains for transport, and an autotransporter structure at the C terminus. The autotransporter domain forms after translocation through the β-sheet barrel within the outer membrane. The N-terminally attached passenger protein is translocated to the surface through this porin-like barrel[54]. Maurer *et al.* optimized AIDA-I, an *E. coli* adhesin co-expressed with the *orfA* gene for diffuse adherence to HeLa cells, for only efficient surface display and release of soluble recombinant proteins[52–54].

Therefore, in **Chapter 4**, I will discuss using AIDA to surface display Protein G and load antibody for site-specific docking; this serves as a reasonable solution to ensure that the engineered therapeutic bacteria remain at the theoretical GI wound site.

1.8 *E. coli* Lysis Protein E7

Naturally, bacteria do not secrete protein. However, to overcome this issue for protein bio-production in *E. coli*, Saeidi *et al.* designed a synthetic genetic circuit using quorum sensing and the lytic protein colicin E7, native to colicin-producing *E. coli*, to kill the engineered bacteria and release the biotherapeutic[14]. E-group colicins are a group of plasmid-borne bacteriocins that exhibit antibiotic-like inhibition of bacterial growth[55–57]. While less studied than other E-group , E7 lysis causes inner membrane damage and possibly activates outer membrane phospholipase A to permeabilize the outer membrane via lysophospholipid formations[14,58]. Since the E7 lysis protein is extremely small and native to *E. coli*[14,56,58], it can be easily utilized as a dual-purpose protein – ensure biotherapeutic protein release and engineered lysis (**Chapter 5**).

Chapter 2: Bacterial Response to H_2O_2

2.1 Introduction

Synthetic biologists construct innovative genetic/biological systems to treat environmental, energy, and health problems. Many systems employ rewired cells for non-native product synthesis, while a few have employed the rewired cells as 'smart' devices with programmable function. Building on the latter, we developed a genetic construct to control and direct bacterial motility towards H_2O_2, one of the body's immune response signaling molecules. A motivation for this work is the creation of cells that can target and autonomously treat disease, the latter signaled by H_2O_2 release. Bacteria naturally move towards a variety of molecular cues (e.g., nutrients) in the process of chemotaxis. In this work, we engineered bacteria to recognize and move towards H_2O_2, a non-native chemoattractant and potential toxin. The system exploits *oxyRS*, the native oxidative stress regulon of *E. coli*.

Bacteria naturally respond to oxidative stressors such as H_2O_2 and other ROS molecules that are released by eukaryotic cells upon insult such as pathogen infection or wound generation. They possess several mechanisms, including the OxyR/S-mediated response triggered by H_2O_2[26,27,59], for protection against toxicity. Eukaryotic and prokaryotic organisms also produce ROS as a byproduct of normal aerobic metabolism; thus, they have naturally developed machinery and mechanisms to convert the metabolic ROS side products into non-toxic products thereby maintaining homeostasis [26,29]. At physiological levels of H_2O_2 (~20 nM), OxyR acts as a repressor of *oxyS* RNA transcription in *E. coli* [30,31,59]. OxyS RNA, in turn, is a global oxidative stress regulator mediating the activation or repression of over 40 genes[29,60]. In the presence of elevated H_2O_2 levels, changes in the oxidation state of OxyR's

sulfhydryl groups at Cys199 and Cys208 promote the formation of a disulfide bond [26], that, in turn, modulates OxyR's structural conformation leading to subsequent transcriptional activation of many promoters involved in oxidative stress regulon [30,33,34]. These include *oxyS* [29] (**Figure 7**). This structural change, involving oxidation and reduction reactions, occurs extremely quickly, at a rate of 9.7 s^{-1} [34].

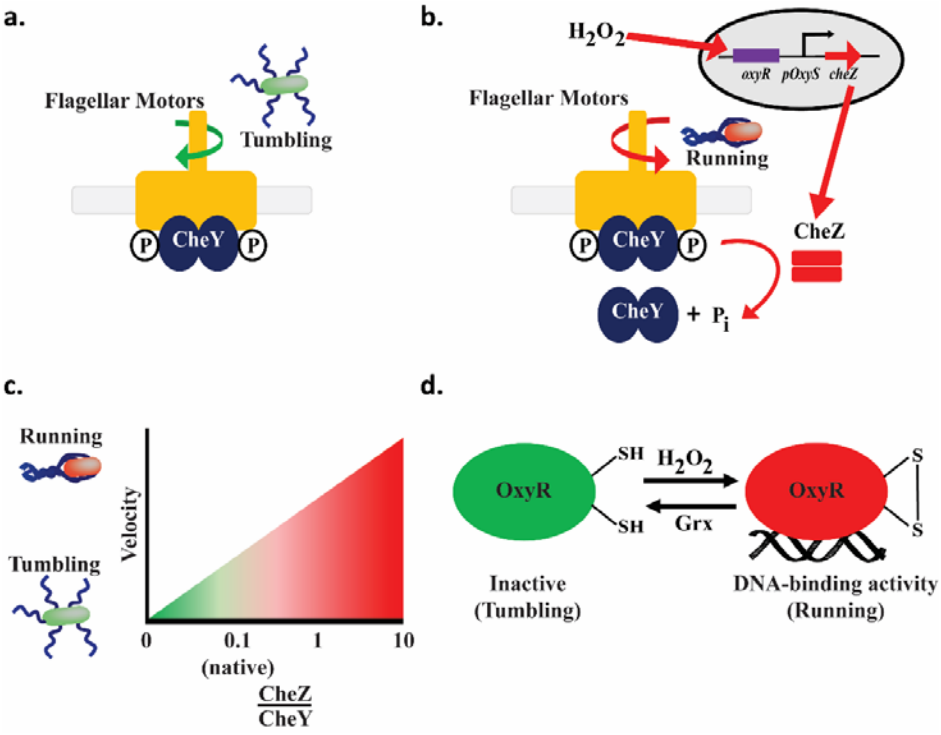

Figure 7 - H_2O_2-controlled bacterial motility. *a. Left. CheY activation. Phosphorylated CheY binds to the flagellar motor complex, counterclockwise rotation resulting in tumbling. Right. CheZ activation and bacterial design. H_2O_2 modulates OxyR, enabling oxyS RNA activation of CheZ. CheZ dephosphorylates CheY, which is released from the flagellar motor resulting in clockwise rotation and a run. c. CheZ-CheY ratio controls run/tumble. As the ratio of CheZ to CheY increases (x axis), the bacteria decreases tumbling time and increases running time. In native E. coli, the ratio of CheY:CheZ expression is approximately 8:1 [61]. d. OxyR-ROS Receptors. The OxyR transcription factor regulates the H_2O_2 oxidative stress response in E. coli. H_2O_2 alters OxyR to activate OxyR DNA binding enabling oxyS RNA transcription. OxyS RNA is a global regulator. OxyR is reduced by intracellularly by glutaredoxin-1 (Grx)* [30].

In the GI tract, mammalian cells produce elevated levels of reactive oxygen species in response to various wounds and diseases, such as IBD, UC, and CD [24,25]. We created a synthetic biology controller employing the *oxyS* promoter and its OxyR regulator within the

native GI bacterium *E. coli,* as a 'smart' device for the eventual autonomous treatment of GI diseases based on wound-specific elicitation of ROS in general, and specifically, H_2O_2.

OxyR's sensitivity to H_2O_2 should allow it to be used as both a monitor of *E. coli's* response to H_2O_2 and as a controller of gene expression [29,32,34,62,63]. Importantly, initial screens suggest that the H_2O_2 concentrations investigated here are within the reported physiological ranges for eventual deployment at wound sites, including those in the GI tract [21]. Notably, *in vivo* studies conducted in zebrafish, a popular vertebrate model system, demonstrated a burst release of H_2O_2 (0.1-0.2 mM) to recruit immune cells that serve to prevent infection[21]. Additionally, *in vivo* mice studies reported H_2O_2 levels of dermal wounds persisted during the immediate inflammatory days (> 200 μM; 2 days post-wounding) as well as post-inflammatory days (~150 μM; 5 days post-wounding)[23]. Given these indications, we performed studies to evaluate dynamics of the *oxyRS* promoter system, bacterial cell growth upon H_2O_2 insult, and our desired H_2O_2-mediated swimming phenotype (**Chapter Three**).

2.2 Materials and Methods

DNA Manipulation and Growth Conditions. The *E. coli* K-12 W3110-*ΔcheZ* strain (HCW01) was constructed using a one-step inactivation method [64]. The genetic constructs developed in this study were assembled using standard molecular biology protocols [65]. Briefly, the *oxyR* and *oxyS* gene-promoter sequence from *E. coli* corresponding to NC_010473:4256210-4257127 (+ strand) and NC_010473:42560054256114 (- strand), respectively and the genomic *che*Z gene were amplified using the primers specified in

Table 1 and subsequently digested using the appropriate site restriction enzymes.

Table 1 – Strain designs and primer designs of pFZY1-oxyR-poxyS-cheZ.

Strain (Short Name)	**Plasmid**	**Phenotype**
W3110 (WT-pFZY1)	**pFZY1 ± pET200-T5-eGFP**	**Run and Tumble**
W3110-*ΔcheZ* (HCW01-pFZY1)	**pFZY1 ± pET200-T5-eGFP**	**Tumble**
W3110-*ΔcheZ* (HCW01-pHW02)	**pFZY1-OxyR-*p*OxyS-CheZ ± pET200-*p*T5-eGFP**	**H_2O_2-controlled Run**
Primer Name	**Primer Sequence**	
BamHI-oxyR (forward primer)	**5'-ATATATATGGATCCTTA AACCGCCTGTTTTAAAACT TTATCGAAATGGCCATCC-3'**	
***p*oxyS-RBS-cheZ-HindIII (reverse primer)**	**3'-GCTCGTCAGCAGGTTTGAT TGATGGTTGCATCATATGTAT ATCTCCTTCTTAAAGTTAAAC TCTCGAAACGGGCAGTGACT TCAAGGGTTAAAAG -5'**	
***p*oxyS-RBS-cheZ (forward primer)**	**5'-CTTTTAACCCTTGAAG TCACTGCCCGTTTCGAGAGTTTA ACTTTAAGAAGGAGATATACATAT GATGCAACCATCAATCAAACCTG CTGACGAGC -3'**	
cheZ (genomic knockout, forward primer)	**5'-ATGCAACCATCAATCAAACCTG CTGACGAGCATTCAGCTGGCG-3'**	
cheZ (genomic knockout, reverse primer)	**3'-CAAAATCCAAGACTATC CAACAAATCGTCCACCTG ATCCTGACTGGC-5'**	

The sequences relative to *oxyR* and *oxyS* promoter or *cheZ* were ligated into the single-copy vector pFZY1 using T4 Ligase (New England Technologies). Ligations were transformed in *E. coli* Top10 cells (Invitrogen) and plated on LB agar plates supplemented with ampicillin

(50 µg/mL) and incubated at 37°C. Plasmid DNA (**Figure 8-a**) from each selected clone was isolated for sequencing using Qiagen miniprep and analyzed via restriction digestion. The same protocol was followed to insert eGFP into pET200 under the T5 promoter (**Figure 8-b**). *E. coli* K-12 wild type (W3110) and *cheZ* knockout strains were transformed with pFZY1 and pFZY1-*oxyR-poxyS-cheZ* (pHW02) or pFZY1, respectively.

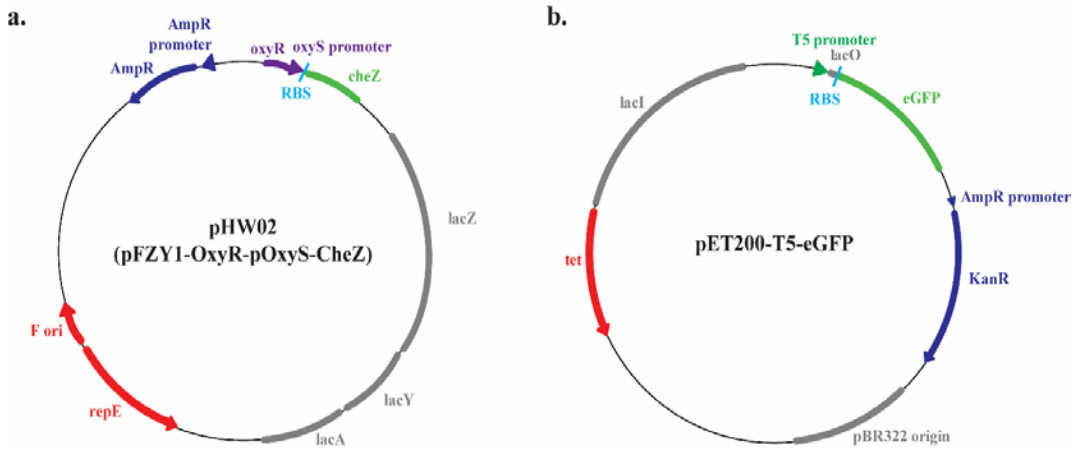

Figure 8 *- a. Plasmid design of pHW02. b. Plasmid design of pET200-t5-eGFP.*

Bacteria were grown in LB media supplemented with ampicillin (50 µg/mL) and incubated at 37°C in a shaker at 250 rpm for all growth experiments. For all overnight inoculations, bacteria were grown from glycerol frozen stock; all morning re-inoculations were adjusted with sterile media to OD_{600} 0.05. Except for motility plates, transwell assays and microfluidic assays, H_2O_2 induced experiments were conducted at 24°C at 250 rpm. The strain-plasmid nomenclature and shortened names are listed in

Table 1.

Motility Plates. *E. coli* W3110-pFZY1 (WT-pFZY1), W3110-*ΔcheZ*-pFZY1 (HCW01-pFZY1), and W3110-*ΔcheZ*-pFZY1-oxyR-*p*oxyS-cheZ (HCW01-pHW02) were grown to OD_{600} ~1.5, diluted to OD_{600} 0.1, and one 2µL droplet of cells ($2x10^5$ cells) was added per motility plate. In turn, H_2O_2 (30% ACS-grade, Fisher Scientific, Pittsburgh, PA) was added to warm motility agar (Bacto Tryptone broth, BD Biosciences, Franklin Lakes, NJ with 0.5% NaCl, Sigma-Aldrich, St. Louis, MO and 0.25% agar, Fisher Scientific, Pittsburgh, PA) and poured into Petri dishes (100 mm diameter, 15 mL per plate) to yield concentrations of H_2O_2 (0-1 mM). Plates were incubated at 30°C for 18 hours. Negative and positive controls were performed in the absence and presence of 100 µM H_2O_2, respectively, added to the plates. For data analysis, technical and biological triplet data were obtained.

Bacterial Growth. *E. coli* WT-pFZY1, HCW01-pFZY1 and HCW01-pHW02 were inoculated into 25 mL of LB in 125 mL flasks. Bacteria were shaken at 37°C and sampled every 30 minutes until OD_{600} ~0.5. After induction, bacteria were shaken at either 24°C or 37°C and sampled every 15 minutes for two hours. For data analysis, technical and biological triplicate data were obtained.

H_2O_2 Consumption. *E. coli* WT-pFZY1, HCW01-pFZY1 and HCW01-pHW02 were inoculated into 10 mL of LB in 50 mL flasks, and shaken at 37°C until OD_{600} ~0.5. Cells were pelleted and resuspended in fresh LB at OD_{600} 0.1 and 0.4. The bacteria were induced with 0-200 µM H_2O_2 in clear 96 well plates (total volume – 200 µL) at 24°C, 250rpm for 5-15 minutes. All samples were assayed for H_2O_2 consumption with standards using the Quantitative Peroxide Assay Kit (Pierce, Thermo Fisher Scientific, Waltham, MA). For data analysis, technical and biological triplet data were obtained.

***cheZ* qPCR.** *E. coli* WT-pFZY1, HCW01-pFZY1 and HCW01-pHW02 were inoculated into 5 mL of LB in culture test tubes, and shaken at 37°C until OD_{600} ~0.5. Cells were induced with 0.125-1 mM H_2O_2 at 24°C, 250rpm for 5-15 minutes and pelleted by centrifugation. RNA extraction was performed using TRIzol (Fisher Scientific) and samples were treated with Dnase I (New England BioLabs) to eliminate possible DNA contamination.

Quantitative PCR conditions were carried out on an Applied Biosystems 7300 Real-Time PCR system using a 2-step cycling protocol. Primers were used at a final concentration of 400 nM, and 10 ng of RNA was used as template in each 20-µl reaction. Each reaction was performed in triplicate, with outlying data removed for select samples. 16s rRNA was used as the endogenous housekeeping gene. To calculate the levels of *cheZ* expression ΔC_T values were calculated by the following equation: $\Delta C_T = C_{T\ Target} - C_{T\ Reference}$. The $\Delta\Delta C_T$ value was calculated as $\Delta\Delta C_T = \Delta C_{T,sample} - \Delta C_{T,Wt}$ where each ΔC_T are represented by the difference between the Target and Reference (16srRNA) values, as above. Also, the relative quantification (RQ) is calculated as $2^{-\Delta\Delta CT}$. Error bars represent the standard deviation of each RQ ($2^{-\Delta\Delta CT+s}$ and $2^{-\Delta\Delta CT-s}$). The relative quantification was based on the relative expression of *cheZ* versus 16S rRNA. Wild type *E. coli* C_T values for *cheZ* were used as reference for all samples.

CheZ Quantification. *E. coli* WT-pFZY1, HCW01-pFZY1 and HCW01-pHW02 either with or without the pET200-T5-eGFP plasmid were grown overnight, reinoculated into 25 mL of LB in 125 mL flasks, and shaken at 37°C until OD_{600} ~0.5. Cells were induced with 0-300 µM H_2O_2 at 24°C, 250rpm for 5, 10, 15, and 60 min and then centrifuged at 4°C, 12,000 rcf for 10 minutes. Bacterial pellets were resuspended with 200 µL BugBuster (BugBuster HT, EMD Millipore) and protease inhibitor (HALT Protease Inhibitor Cocktail (100x), Fisher Scientific). Cell suspensions were shaken at 24°C, 150 rpm for 40 minutes. Insoluble cell

debris were removed by centrifugation at 4°C, 12,000 rcf for 20 minutes and soluble fractions were transferred to new tubes.

Total protein concentration (Pierce BCA Protein Assay, Fisher Scientific) was calculated using the microplate procedure with BugBuster-BSA standards. Pre-stained ladder (Benchmark Prestained Protein Ladder, Fisher Scientific), His_6-CheZ protein, and 25 µL of boiled samples (~110 µg total protein concentration) were loaded into 12% SDS-PAGE gels (Bio-Rad). A Semi-Dry Transfer Apparatus (Bio-Rad) was used to transfer proteins to nitrocellulose membranes (Thermo Scientific Pierce). The membranes were blocked with 10% milk (Blotting Grade Blocker Non Fat Dry Milk, Bio-Rad) overnight at 4°C. Membrane was washed three times using TBS-T buffer and incubated for 1h 30 min with 1:10,000 anti-CheZ polyclonal antibody (produced by New England Peptide). Before incubation with anti-CheZ, it was adsorbed in 25% lysed *E. coli cheZ* knockout strain extract, 5% Bovine serum albumin (BSA), Sigma Aldrich, St. Louis, MO) to decrease nonspecific binding. Membrane was washed three times using TBS-T buffer and incubated with 1:15,000 of anti-rabbit alkaline phosphatase antibody (Sigma Aldrich) solution 5% BSA, Tris-buffered saline + Tween 20 (TBST)). The membranes were developed for 1 hour at 24°C in development buffer (with BCIP/NBT), and the reaction was stopped using deionized H_2O.

Statistical Analysis. For most experiments, one-way ANOVA using a multiple comparisons' Tukey-Kramer post-test were performed using Matlab (version R2015a). ANCOVA linear regression analysis was performed using Prism (Graphpad Prism 7). α values of 0.05, 0.01, and 0.001 were used to indicate statistical significance. Data are reported as mean values and standard deviation of the error, unless otherwise stated.

2.3 Results and Discussion

2.3.1 Understanding H_2O_2's initial effect on bacteria.

Initial screening studies were carried out to test whether engineered cells exhibited enhanced swarming in the presence of H_2O_2. In addition to evaluating whether a potential dose response could be obtained, I was interested to find at what concentration H_2O_2 would prove too toxic so as to permit enhanced motility. In **Figure 9-a**, control experiments using wildtype W3110 cells with empty pFZY1 vector (WT-pFZY1) exposed to 0 or 100 μM H_2O_2 demonstrated a base case cell motility exhibited by ~7 cm rings with no obvious adverse reaction to the H_2O_2. Similarly, isogenic *cheZ* null mutants (HCW01) with empty pFZY1 vector exhibited no spreading in either case, with 0 or 100 □M H_2O_2. Then, using the same null mutants transformed with the *oxyRS* induced CheZ vector, pZY1-*oxyR-poxyS-cheZ*, (HCW01-pHW02) an increasing ring size was observed with increasing H_2O_2 from 0 to 300 μM (2.5-6.5 cm). Interestingly, I found that bacterial spreading decreased dramatically at 500 μM H_2O_2, presumably due to peroxide toxicity. Results from biological triplicates are indicated in **Figure 9-b**.

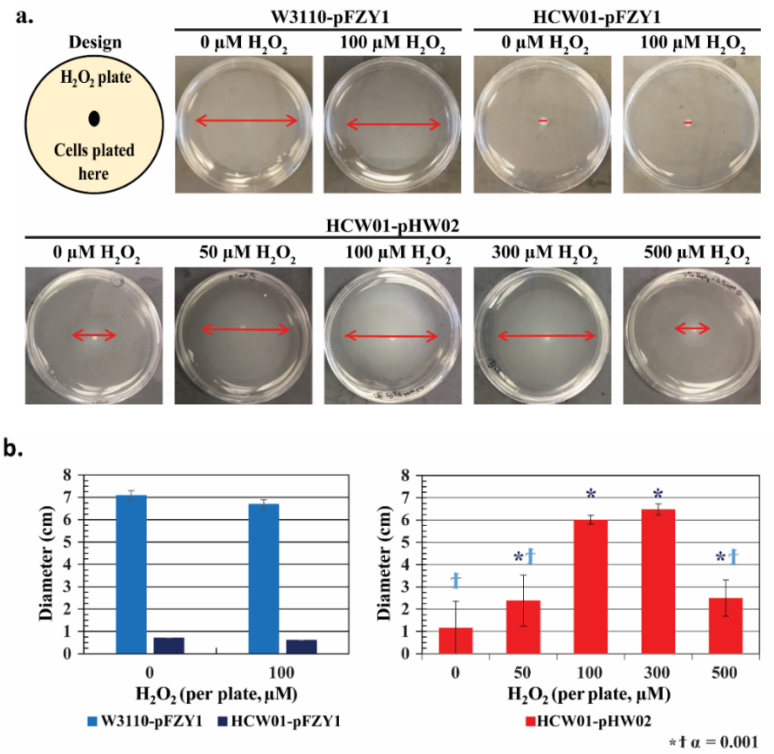

Figure 9 - Bacterial swarming on motility agar exposed to varying concentrations of H_2O_2. *a. Motility plates. Top Row: WT-pFZY1 and HCW01-pFZY1 controls with 0 and 100 µM H_2O_2-infused motility plates. Cultures were grown overnight. Bottom Row: HCW01-pHW02 with 0-500 µM H_2O_2-infused motility plates. b. Motility Spreading. (left) WT-pFZY1 and HCW01-pFZY1 exposed to 0 or 100 mM H_2O_2. (right) Quantification of HCW01-pHW02 with CheZ expression induced by H_2O_2. Tukey-Kramer ANOVA and multiple comparisons analyses were performed with α = 0.05, 0.01 and 0.001. † indicates the samples differed significantly from WT-pFZY1. * indicates the samples differed significantly from HCW01-pFZY1.*

In addition, 1 mM H_2O_2 motility plates resulted in no center colony or spreading (data not shown). I note that the 0 µM plate, which had a minimal but non-zero spread, suggested that some CheZ activity enabled minimal motility, perhaps due to small levels of H_2O_2 through metabolic activity or simple read-through CheZ transcription and translation from our plasmid vector. Interestingly, the 0, 0.5 and 1 mM observations are consistent with previously published data [30]. Bacterial movement or "swarming" on motility plates does not depend on chemotaxis, rather it simply indicates search for nutrients [66–68]. In sum, our initial screening results are consistent with a hypothesis that H_2O_2-induced CheZ enables motility and that the induced motility rescues the wildtype swarming phenotype.

2.3.2 Characterizing H_2O_2 uptake and effect on bacterial growth.

I conducted growth experiments using WT-pFZY1, HCW01-pFZY1, and HCW01-pHW02 (H_2O_2-mediated *oxyS* transcription of CheZ). In addition to CheZ, the motility vector confers (i) resistance to bacteria ampicillin (β-lactamase expression), (ii) utilization of lactose (*lacZ*, *lacY*, *lacA*, expression), and (iii) copy number maintenance by expression of *repE* (mini-F plasmid). In **Figure 10** and **Figure 11**, I grew cells at 37°C until 120 min when I added H_2O_2. At induction, the cultures were split to grow at 24°C and 37ºC to examine how the temperature and H_2O_2 concentrations affect bacterial growth and H_2O_2 consumption. Regression analysis indicated that all preinduction growth rates were similar (data not shown). Then, analogously, after a short transient phase, cultures continuing after OD_{600} ~0.45 all grew at similar rates irrespective H_2O_2 for each temperature level (**Figure 10-b, c** (24ºC)**, Figure 11-a, b** (37ºC)) until H_2O_2 concentrations above 500 µM.

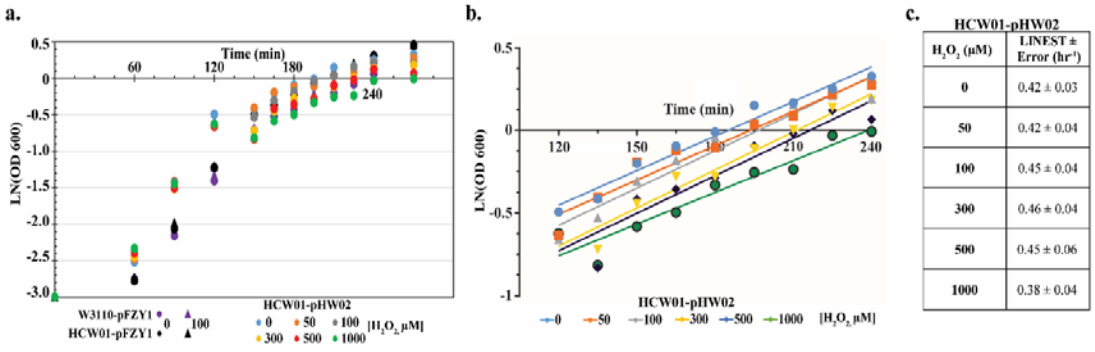

Figure 10. Effects of H_2O_2 on cell growth at 24°C. *a. Cell growth curves. WT-pFZY1 and HCW01-pFZY1 and HCW01-pHW02 vector at different levels of H_2O_2. b. Cell growth curves following H_2O_2 addition. HCW01-pHW02 growth with 0-1000 µM H_2O_2 induction concentrations. Lines indicated are least squares regressed best fits. c. Linear regression analyses. All linear regression analyses for HCW01-pHW02 were compared to 0 µM H_2O_2.*

a.

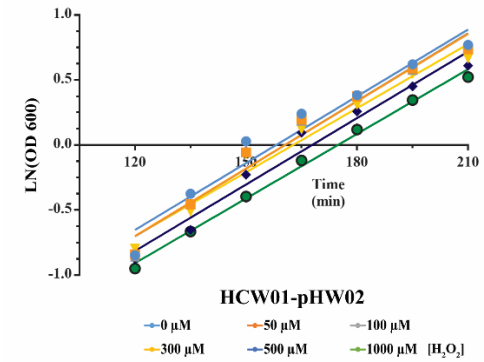

b.

HCW01-pHW02

H_2O_2 (µM)	LINEST ± Error (hr^{-1})
0	1.03 ± 0.11
50	1.04 ± 0.09
100	1.04 ± 0.09
300	0.99 ± 0.08
500	1.02 ± 0.08
1000	0.99 ± 0.03

Figure 11. - Effects of H_2O_2 on cell growth at 37°C. *a. Post-induction growth curves. WT-pFZY1 and HCW01-pFZY1 with and without 100 µM H_2O_2 were controls. b. Tabulated specific growth rates. HCW01-pHW02 growth with 0-1000 µM H_2O_2 induction concentrations. All linear regression analyses for HCW01-pHW02 were compared to 0 µM H_2O_2.*

I noted that swarming experiments indicated reduced motility at concentrations above 300 µM, perhaps suggesting that swarming was more sensitive than cell growth to H_2O_2 at elevated peroxide levels. However, swarming and growth experiments are quite different, particularly in that exposure to H_2O_2 occurs under different time scales. Notably, the growth curves represented a single exposure to H_2O_2 at the start of induction. However, the bacteria in the motility plates were constantly and consistently exposed to the same concentration of H_2O_2 as they swarmed outwards. Therefore, the continuous exposure to H_2O_2 in the motility plates experiments also represented the bacteria's ability to consume H_2O_2 below or above the toxicity threshold and subsequent response (in addition to stimulating swimming).

2.3.3 H_2O_2-mediated *cheZ* transcription.

I conducted studies using qPCR to quantify *cheZ* expression. Data were normalized to 0 µM H_2O_2. For 15 minute H_2O_2 induction (meaning samples taken 15 min after introduction of H_2O_2 at various levels), qPCR data exhibited similar trends to our previous motility plate studies – a rise in gene expression from 0 to 300 µM and a decrease at 500 µM. In this case, to obtain greater resolution, I conducted additional tests at 350 and 400 µM,

finding maximal *cheZ* mRNA levels at 400 µM 15 min post induction. Statistical analyses were performed by lumping tests above 100 µM and demonstrating significance relative to each of the lower levels (multiple comparisons one-way ANOVA, Tukey-Kramer post-test). Importantly, *cheZ* mRNA increased monotonically with H_2O_2 over time for all ranges tested **Figure 12-a**). A more detailed analysis using only 5 &10 min. induction with 12.5-200 µM H_2O_2 showed similar increasing trends (**Figure 12-b**). Interestingly, only 12.5 □M was needed to stimulate *cheZ* expression and this was observed at the first non-zero time point (5 min).

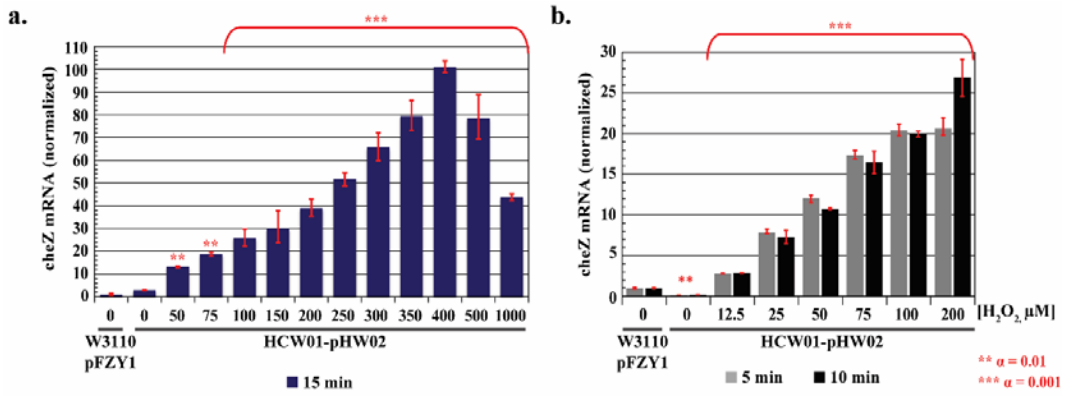

Figure 12. CheZ qPCR. *a. 15 minute qPCR analysis. b. 5-10 minutes qPCR analysis. WT-pFZY1 is used as a control (i.e., genomic cheZ expression). All cheZ levels for HCW01-pHW02 were normalized to 0 µM H_2O_2 wildtype cells. Tukey-Kramer ANOVA and multiple comparisons analyses were performed with α = 0.01 and 0.001.*

2.3.4 H_2O_2-mediated CheZ protein production.

In **Figure 13-a, b**, I used Western blotting to correlate H_2O_2 with CheZ protein levels in the HCW01-pHW02 cells. At 15 min, CheZ levels increased with H_2O_2. I found peak levels at 50-100 µM; this tended to decrease at the higher H_2O_2 levels (although this was not a statistically validated trend) (**Figure 13-a**). Interestingly, the CheZ from uninduced wildtype cells was not revealed, presumably below detection in these blots. Moreover, I found no CheZ bands in the uninduced HCW01-pHW02 cells. Subsequent studies were carried out at shorter induction times and at additional H_2O_2 concentrations (**Figure 13-b**).

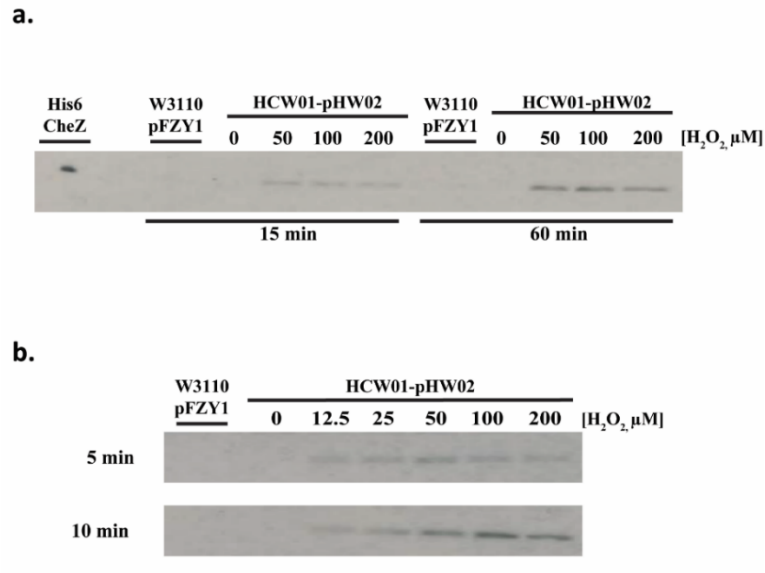

Figure 13. - CheZ Western blot analyses. *CheZ is expressed without a purification tag; Westerns are performed using rabbit anti-CheZ antibody (see Methods). a. H_2O_2 induction for 15 and 60 minutes. b. H_2O_2 induction for 5 and 10 minutes. His6-CheZ and WT-pFZY1 were controls.*

Results were consistent and reveal that at 12.5 µM and 5 min H_2O_2 induction, there was significant CheZ present (significantly more than the wildtype cells). This level increased in time and in peroxide concentration until 100 µM above which perhaps H_2O_2 toxicity prevented further increases. These findings directly corroborated the relatively fast mRNA responses.

2.3.5 Quantifying H_2O_2 consumption and characterizing CheZ expression in the presence of a second constitutive plasmid

Initially, I examined the effects of one plasmid (pHW02) versus two plasmids pHW02, pET200-t5-eGFP) on cheZ genotype. Previous qPCR experiments using pHW02 and varying concentrations of H_2O_2 had shown that within 5-10 minutes, the bacteria turn on cheZ mRNA expression had shown increasing mRNA expression corresponding to increasing H_2O_2 concentrations (12.5-200 µM; data not shown). After 15 minutes of induction for HCW01-pHW02, I clearly can see a statistically significant increase of cheZ mRNA expression in the single plasmid system when induced with 50-100 µM H_2O_2 ($\alpha = 0.005$, 0.001, respectively) compared to WT-pFZY1 (**Figure 14-a**). When examining CheZ protein

levels after 15 versus 60 minutes of H_2O_2 induction, I observed a significant qualitative difference between 1 plasmid versus 2 plasmids. I start to see faint CheZ bands for the 2 plasmid system after 60 minute induction; more discernable bands are visible with the 1 plasmid system after 15 and 60 minute inductions (**Figure 14-b**). This suggests that addition of the second plasmid with the constitutive fluorescence protein attenuates cheZ transcription and translation rates.

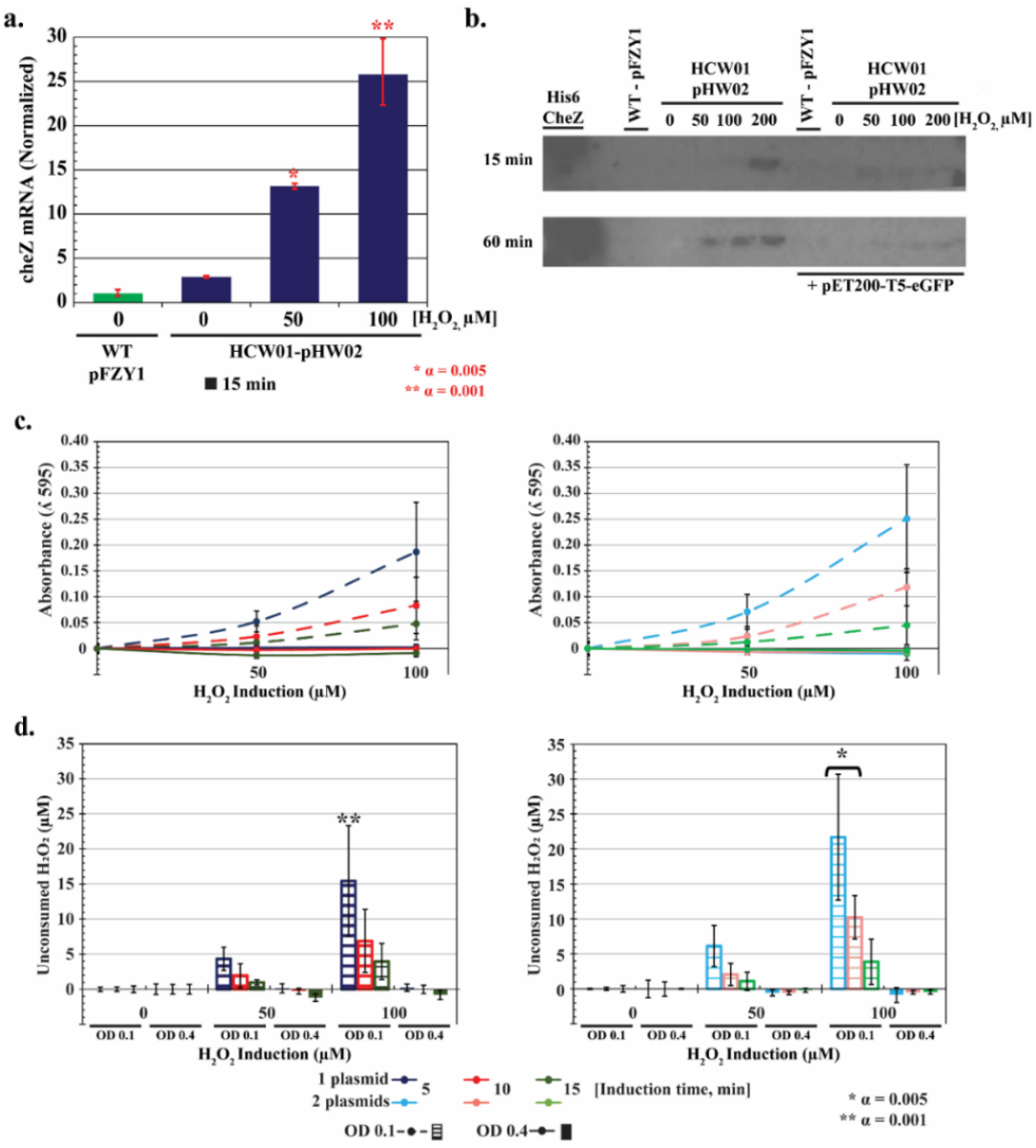

Figure 14 - H_2O_2-induced CheZ production*. a. 1 plasmid – 15 minute qPCR analysis. b. 1 plasmid vs. 2 plasmid CheZ Western Blot. H_2O_2 induction for 15 and 60 minutes. His6-CheZ and WT-pFZY1 were controls. c-d. H_2O_2 consumption absorbance curves. WT-pFZY1 and HCW01-pFZY1 (controls) and HCW01-pHW02 induced with 0-200 µM H_2O_2 for 5-15 minutes at OD 0.1 and 0.4 with absorbance measured at 595 nm. b. Calculated unconsumed H_2O_2. Tukey-Kramer ANOVA and multiple comparisons analyses were performed with * α = 0.005. * indicates the samples differed significantly from all samples.*

Previous studies have examined the effects of plasmid-encoded gene overexpression on quorum sensing and metabolic burden [38], but it is unclear how this overexpression affects H_2O_2 inducer consumption rate and motility. When I induced the 1 and 2 plasmid bacteria at

OD 0.4, all of the H_2O_2 (50, 100 μM) was consumed within 5 minutes (**Figure 14-c, d**). In order to quantify how the second constitutive plasmid affects H_2O_2 consumption rate, bacteria were induced at OD 0.1; after a 5 minute induction with 100 μM H_2O_2, there is a statistically significant amount of H_2O_2 left in the 1 and 2 plasmid systems ($\alpha = 0.001, 0.005$, respectively), and the 2 plasmid system still has significant H_2O_2 unconsumed after 10-15 minutes (**Figure 14-c, d**).

Additionally, I observed different growth and induction rate differences between the one and two plasmid systems (**Figure 15-a**). Linear regression analysis confirmed there is a statistically significant difference at each H_2O_2 concentration when comparing between the one and two plasmid systems (**Figure 15-b, c**). Based on these results, I can definitively state that the second constitutive GFP plasmid burdens metabolic growth; additionally, the induction and expression of CheZ does not affect the metabolic growth. With these results, I can predict and quantify the motility and metabolic burdens when adding and modifying protein expression systems.

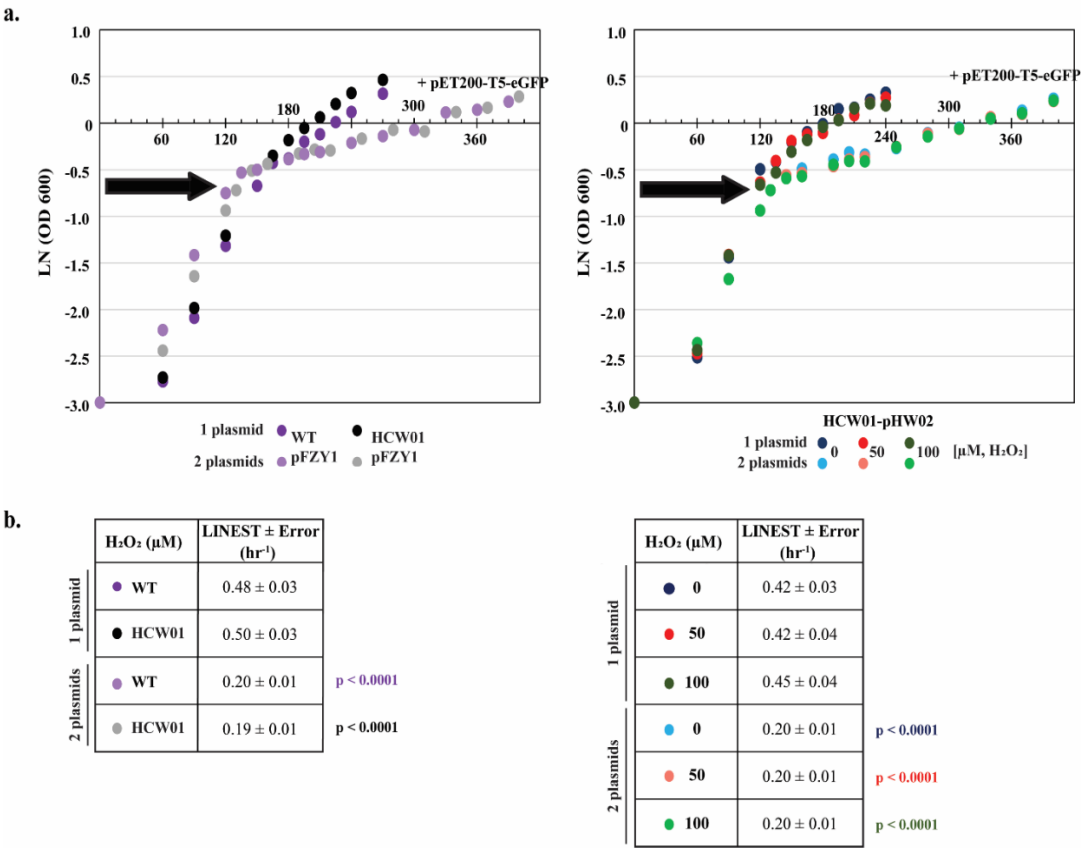

Figure 15 - Standard growth curves. *a. Control and experimental standard growth curves. WT-pFZY1 and HCW01-pFZY1 with and without pET200-t5-eGFP were controls (left). HCW01-pHW02 ± pET200-t5-eGFP with 0-100 μM H_2O_2 induction concentrations (right). The black arrow indicates the induction OD and time. b. Prism linear regression ANCOVA analyses. Linear regression analyses were conducted with samples at induction time. All linear regression analyses compared the two plasmid system to the one plasmid system.*

2.4 Conclusion

We constructed a simple synthetic H_2O_2-responsive promoter system. Complementary studies[31,36,69] demonstrate that additional regulatory constructs based on engineered plasmid controllers and/or engineered host cells enable tight or "tuned" control of gene expression based on signal molecule concentration. We note, however, that significant modification of host genotype can alter cell physiology so as to potentially hinder native phenotypes that are required for optimal cell function [70]. That is, the current system restores swimming motility while only minimally altering native circuitry.

We employed population based analytical methods to characterize the system that enable *E. coli* to sense H_2O_2 in highly-controlled and defined manners. Studies of CheZ expression revealed a practical threshold level of ~12.5 μM was suitable for rapid and sustained induction of CheZ. We noted also that the bacteria were able to quickly consume or otherwise dissipate H_2O_2, diminishing its effects so that over a putative therapeutic range, bacteria exhibited little to no growth inhibition. Thus, we suggest that the synthetic biology framework in this work could be applied for the detailed design of engineered probiotics that would be deployed for directed treatment in the GI tract.

Chapter 3: Engineer Bacteria to Swim In Response to and Towards a H_2O_2-Rich Environment.

3.1 Introduction

In this chapter, I turn to the endogenous, wound-indicating signal molecule, H_2O_2, as a directional cue; I fully recognize the potential conflict in that induced directionality of therapeutic strains could, in turn, lead to their own damage. In order to attract our engineered bacteria toward to a localized injury marked by the presence of H_2O_2, I developed a system that guides *E. coli* swimming towards H_2O_2 by controlling the (i) ratio of run to tumble, and (ii) cell velocity in the presence of an H_2O_2 gradient. Bacterial motility regulator, CheZ, is a phosphatase responsible for controlling the level of phosphorylated CheY, which, in turn, regulates the tumbling mode of bacterial swimming [30,34] (**Figure 7**). For this, *che*Z was expressed under control of the *oxyRS* gene-promoter system induced by the presence of H_2O_2 in *cheZ*⁻ *oxyRS*+ mutants; I retained the native *oxyRS* genes to prevent additional oxidative stress to the bacteria and deleted genomic *cheZ* to examine how exogenous H_2O_2 affects motility.

The CheY and CheZ phosphorylation and dephosphorylation cascade (in conjunction with methylation and demethylation cascades) activates the bacterium's tumbling and running motions [30,34], respectively (**Figure 7**). As noted above, elevated H_2O_2 activates OxyR [30] which then induces OxyS RNA transcription. H_2O_2 concentrations in the $10^2 – 10^3$ μM range causes toxicity to *E. coli* and decreases *E. coli* survival [71]. In physiologically relevant mice studies, researchers showed that a range between 0.1 to 0.3 mM of H_2O_2 was generated at the site of the ROS burst [15,17,72]. Hence, given the potentially 10-fold difference between the physiologically relevant and toxic levels, I hypothesized that engineered bacteria might tolerate, rapidly consume, and swim in response to increased H_2O_2 without suffering

significant oxidative stress. Thus, such engineered H_2O_2-controlled bacteria may allow for a wide range of application for future therapies or applications.

Additionally, in bacterial motility experiments and publications, researchers engineer the bacteria to contain a constitutively-fluorescent protein; this allows researchers to track the bacteria and quantify motility or other parameters with reduced background noise and fewer artifacts compared to phase-contrast tracking. Another focus of this research centers on how constitutively-expressed protein affects engineered motility.

3.2 Materials and Methods

Growth Conditions. Bacteria were grown in LB media supplemented with ampicillin (50 μg/mL) and incubated at 37°C in a shaker at 250 rpm for all growth experiments. For all overnight inoculations, bacteria were grown from glycerol frozen stock; all morning re-inoculations were adjusted with sterile media to OD_{600} 0.05. Except for motility plates, transwell assays and microfluidic assays, H_2O_2 induced experiments were conducted at 24°C at 250 rpm. The strain-plasmid nomenclature and shortened names are listed in

Table 1.

Motility Videos. *E. coli* WT-pFZY1, HCW01-pFZY1 and HCW01-pHW02 (with pET200-T5-eGFP for two plasmid experiments) were inoculated into 5 mL of LB in 25 mL flasks, and shaken at 37°C until OD_{600} ~0.5. Bacteria were split into 1 mL cultures in culture test tubes and induced with 0 μM H_2O_2 (control) and 12.5-100 μM H_2O_2 at 24°C, 250 rpm for 5-15 minutes. The bacteria were centrifuged at 1,000 rpm and 4°C, washed twice, and resuspended in DPBS for brightfield and fluorescence motility videos (CellSense). Videos were recorded for 100 frames for subsequent Tumble Score [73] Matlab (version R2015a) analysis. Phase contrast (brightfield) movies were captured using 50 ms white light exposure without binning (1360x1024 pixel size, 319.48 nm/pixel). For data analysis, technical duplicate and biological triplicate data were obtained.

Transwell Motility Assays. *E. coli* WT-pFZY1, HCW01-pFZY1 and HCW01-pHW02 were grown overnight, reinoculated into 5 mL of LB in 25 mL flasks, and shaken at 37°C until OD_{600} ~0.5. Cells were washed twice and resuspended in DPBS buffer to OD_{600} ~0.15. In a 6 well plate (Corning), 2.5 mL of cell suspension was added. In the top transwell, 1.5 mL of DPBS ± 0-300 μM glucose or 0-300 μM H_2O_2. Transwells were incubated at 37°C for two hours for the DPBS buffer and 25-300 μM glucose transwells; based on the H_2O_2 diffusivity properties dependent on temperature[74] and a Transwell Comsol model[75], the H_2O_2 transwells were incubated at 37°C for 45 minutes to ensure that the H_2O_2 gradient across the transwell membrane persisted throughout the experimental time course. For data analysis, technical duplicate and biological triplicate data were obtained.

Static Gradient Device. *E. coli* WT-pFZY1, HCW01-pFZY1 and HCW01-pHW02 were inoculated into 5 mL of LB in 25 mL flasks, and shaken at 37°C until OD_{600} ~0.5. Cells were centrifuged at 1,000 rpm and 4°C, washed twice, and resuspended in DPBS buffer. The

bottom channel of the motility device (**Figure 22-a**)[76] was pretreated with Pluronic F-127 (Sigma-Aldrich, St. Louis, MO) for 1 hour to minimize nonspecific retention of cells to channel walls. Before cell introduction, DPBS buffer was pumped into both source and sink channels using 1 mL syringe and syringe pump at a rate of 120 μL hr^{-1}. Bacteria were grown until OD_{600} ~0.6-0.8 and then introduced into the bottom channel at the cell inlet. This initially loads bacteria for subsequent filming and study. Both ends of the bottom channel were then wiped and taped to stop flow. They are then exposed to a gradient introduced by providing fluids in the upper source and sink channels, each having different concentrations of the gradient solute. For traditional chemotaxis experiments, a glucose solution (1 mM in DPBS) was then introduced at a rate of 50 μl hr^{-1} to replace DPBS in the source channel and to establish a maximum gradient concentration of 100 μM. The sink channel was maintained with 1 mM DPBS. This methodology rapidly generates a glucose gradient within the bottom channel. Note that there is no flow experienced by the cells in the lower channel (for details, see Shang *et al.*, 2017). The time when glucose was added to the source channel was set to be t = 0. Bright-field images and videos were taken in the middle of the bottom channel at 0, 10, 20 and 30 minutes by a 20X Olympus objective. Then, for pseudotaxis experiments, H_2O_2 solutions (0.5 or 3 mM; diluted in DPBS) were introduced using the same method as the glucose solution, with final maximum H_2O_2 concentration gradients of 50 and 300 μM. Bright-field images were taken at 0, 5, 10, 12, 16, 18, and 20 minutes by a 20X Olympus objective.

Statistical Analysis. For most experiments, one-way ANOVA using a multiple comparisons' Tukey-Kramer post-test were performed using Matlab (version R2015a). α values of 0.05, 0.01, and 0.001 were used to indicate statistical significance. Data are reported as mean values and standard deviation of the error, unless otherwise stated.

3.3 Results and Discussion

3.3.1 Previous phenotypic characterization in response to H_2O_2

Previously in **Chapter 2**, I initially characterized HCW01-pHW02's response to H_2O_2 by using motility plates (**Figure 9**) infused with varying concentrations of H_2O_2; this allowed me to determine an optimal testing range of 0-200 μM H_2O_2 induction, which is also extensively covered and confirmed in literature as the physiological *in vivo* range for various animal models[21,23]. Additionally, standard growth curves showed that, with only pHW02, inducing with varying H_2O_2 concentrations had no statistically significant effect on growth (**Figure 10**); however, adding a second plasmid with constitutively expressed protein added metabolic burden and statistically significantly burdened bacterial growth after H_2O_2 induction (**Figure 15**).

3.3.2 H_2O_2-mediated motility for pHW02

In order to analyze bacterial movements and to differentiate chemotaxis, pseudotaxis, and importantly, swimming from swarming (**Figure 9**), I carried out experiments in 2D using microscopy and cell motility videos. To simplify cell trajectory tracking, I transformed cells with a second plasmid constitutively expressing eGFP. In this way, non-motile cells could be differentiated from dust particles and debris. In **Figure 16-a**, a few eGFP trajectories are depicted from representative traces. That is, a white trace line is produced as a cell moves from the beginning of its trajectory to its end. Similarities between the mutant and engineered cells without H_2O_2 were striking, as were the wildtype cells without H_2O_2 and engineered cells with 100 μM H_2O_2.

In **Figure 16-b**, for cells without the GFP plasmid, Rose plots are depicted wherein many traces are superimposed with the initial points set at the origin of the coordinate axes. First, trajectories were observed in every direction as expected, illustrating random movement. Then, the *E. coli* HCW01-pFZY1 strain without H_2O_2 and *E. coli* WT-pFZY1

behaved as expected; *E. coli* WT-pFZY1 exhibited smooth running trajectories with random, interspersed tumbling while the *E. coli* HCW01-pFZY1 displayed increased tumbling with a few random spurts of running. Notably, the HCW01-pFZY1 cells moved far less from the origin than the WT-pFZY1 cells owing to the *cheZ* deletion and subsequent paucity of runs. Similarly, uninduced (0 µM H_2O_2) HCW01-pHW02 exhibited a phenotypic profile similar to HCW01-pFZY1. When induced with 100 µM H_2O_2, HCW01-pHW02 (**Figure 16-a, b**) showed a phenotype more similar to WT-pFZY1, indicating that motility and CheZ running were recovered to wildtype levels.

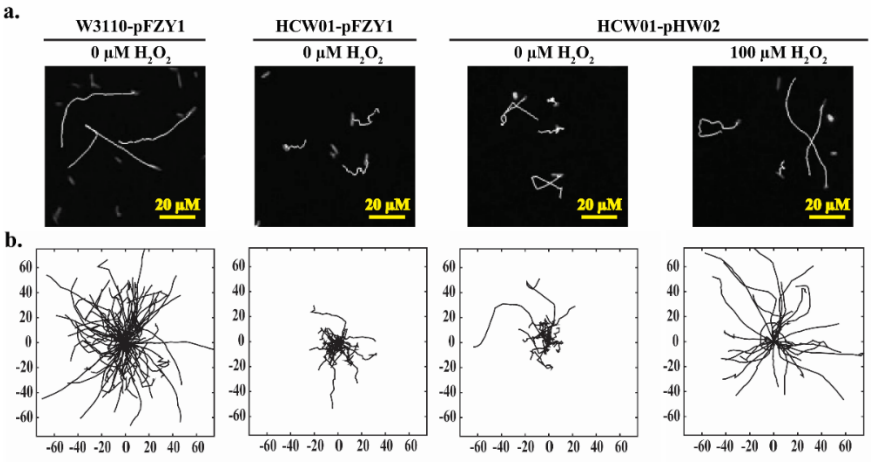

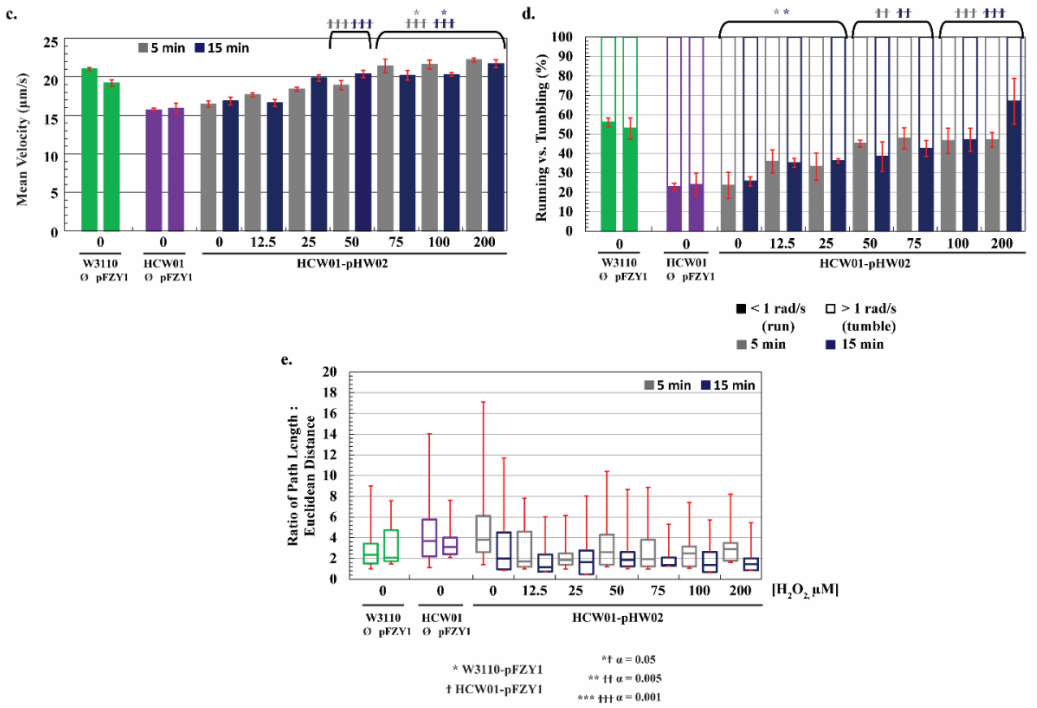

Figure 16 - Characterization of H_2O_2-induced motility. *a. Fluorescent trajectory images. 5 second trajectories of fluorescent WT-pFZY1, HCW01-pFZY1, and HCW01-pHW02 (0 and 100 μM H_2O_2) were mapped. b. Rose graphs of trajectories. 5 second trajectories are displayed from each trajectory's origin to visualize the path lengths and angle changes. c. Average velocities. The average velocities of the control bacteria (WT-pFZY1, HCW01-pFZY1) versus the engineered bacteria (HCW01-pHW02; 0-200 μM H_2O_2). d. Percentage of time within trajectories of running vs. tumbling based on angle change. Trajectories were calculated based on 5 second trajectories for all bacteria. 'Running' trajectories (solid bars) were based on the time it took the bacteria to move < 1 radian/s; 'tumbling' trajectories (lined bars) were based on the time it took the bacteria to move > 1 radian/s. e. Ratio of path length: Euclidean distance. The total distance traveled (path length) versus displacement (Euclidean distance) were calculated based on the initial and final points of 5 second trajectories for all bacteria. Data are presented as box and whisker plots with mean and quartiles indicated in box and extremums as whiskers. All data are quantified for 5 second trajectories. Tukey-Kramer ANOVA and multiple comparisons analyses were performed with α = 0.05. * indicates the samples differed significantly from WT-pFZY1. † indicates the samples differed significantly from HCW01-pFZY1.*

To more directly compare the phenotypic responses, motility movies were again taken also without GFP-yielding plasmids (I had suspected increased burden due to the GFP expression). I used 5-sec trajectories and similar computational analyses, except that all stationary particles were discounted instead of just non-fluorescing particles. Quantified videos thus represent only moving cells. For statistical analysis, mean velocities were analyzed. I found HCW01-pHW02 induced with 50-200 μM H_2O_2 (5, 15 min. induction) had statistically higher (α = 0.001) velocities than the HCW01-pFZY1 control (the two control

bars represent 5 & 15 min samples). Also, CheZ induction with 75-200 μM H_2O_2 for both 5 and 15 minutes showed significant ($\alpha = 0.05$) increases compared to the WT-pFZY1 cells with velocities reaching ~23 μm/s and 19 μm/s, respectively. HCW01-pHW02 with 0 μM H_2O_2 were observed to have similar velocities to the HCW01-pFZY1 cells (~16.5 μm/s, **Figure 16-c**). Velocities were observed to increase monotonically from 12.5 □M to 75 □M H_2O_2.

Another quantity used to characterize swimming is the net angle change as a cell moves from frame to frame. For 5 second trajectories, the percentage of trajectories that exhibited a net angle change of < 1 radian/s and > 1 radian/s [61] were measured; this is calculated by resolving the direction and angle change between subsequent frames and averaging over the 5 second trajectory to classify the bacteria as "running" or "tumbling", respectively. Swimming percentages, which I denote the fraction of time running versus tumbling, were calculated to be ~20-25% for the HCW01-pFZY1 cells and the uninduced HCW01-pHW02. The percent swimming observed for the HCW01-pHW02 induced with 12.5 to 25 μM H_2O_2 were notably higher (~35%). At concentrations above 50 μM H_2O_2, cells were observed to have increased running (~40-48%, solid bars, **Figure 16-d**). Conversely, the increase in percent running per trajectory was inversely proportional to the average angle change per trajectory (**Figure 17-a**). The increased velocity observed with H_2O_2 is consistent with the increased fraction of running within a trajectory. In **Figure 17-b**, I demonstrate that the same conclusions were drawn using both mean and median velocities.

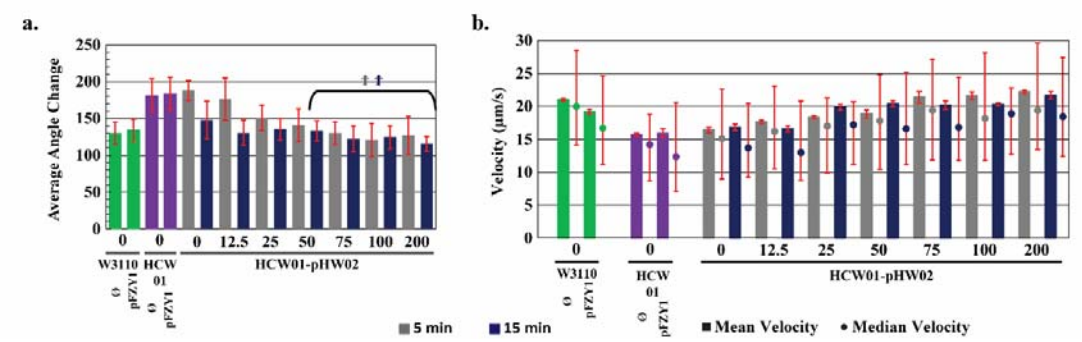

Figure 17 - Phenotypic expression of H_2O_2-induced motility. *a. Average angle change. The average angle change in degrees per 5 second trajectory of the control bacteria (WT-pFZY1, HCW01-pFZY1) versus the engineered bacteria (HCW01-pHW02; 0-200 μM H_2O_2). These values are inversely proportional to the percent running per trajectory. b. Mean vs. median velocity. Quantification and comparison of reported mean vs. median velocities for all bacteria. Slightly lower velocity and higher variability are associated with the median velocity. Median and mean velocities follow similar trends. † (α = 0.05) indicates the samples differed significantly from HCW01-pFZY1.*

Interestingly, I observed that CheZ protein expression increased nearly monotonically with H_2O_2 concentrations until ~100 □M, which mirrored the calculated swimming velocity and percentage of run versus tumble. At H_2O_2 levels above ~100 □M, the CheZ level appeared to drop and the swimming parameters appeared to plateau. Also, the levels reached appeared to match the WT phenotype. This was contra-indicated by the *cheZ* mRNA levels which increased monotonically to ~ 400 □M, suggesting other cellular control mechanisms override continued increases in *cheZ* mRNA.

I did note, however, that the lower concentrations of H_2O_2 yielded higher *variability* in *cheZ* phenotypic expression within the population. For example, I found greater ranges in the standard deviations (25 and 75% quartiles) and extremums in the ratio of path length to Euclidean distance at the lower levels (**Figure 16-e**). This measure is the ratio of the sum of all discrete distances travelled and the net distance from the beginning to end of a trajectory. It had significant variability and thus was an interesting measure to characterize the population distribution and its evolution with H_2O_2. In general, with increasing H_2O_2 concentration and induction time, the heterogeneity among phenotypes within the overall population decreased

towards the observed wildtype values. Similar phenotypic focusing phenomena were observed in response to addition of quorum sensing signaling molecules [36].

3.3.3 Plasmid-encoded protein attenuates bacterial motility

In order to analyze bacterial movements and to differentiate and quantify the burden of the second constitutive protein, I carried out experiments in 2D using phase contrast microscopy and cell motility videos. I used 5s trajectories and computational analyses with all stationary particles discounted. Using this approach, I were able to determine velocity and direction of engineered and wildtype strains. In **Figure 18-a**, a few trajectories are depicted from representative traces; that is, a black trace line is produced as a cell moves from the beginning of its trajectory to its end at the end of a video trace. Similarities between the mutant and engineered cells without H_2O_2 are striking, as are the wildtype cells without H_2O_2 and engineered cells with H_2O_2. I do not discern any differences between the one and two plasmid trajectories. In **Figure 18-b**, Rose plots are depicted wherein many traces are superimposed with the initial points set at origin of the coordinate axes. First, I observed increasing distances with increasing H_2O_2 concentrations with both systems. Second, the trajectories are observed in every direction as expected; however, when comparing the one and two plasmid graphs, the two plasmid system appears to have shorter path lengths compared to the one plasmid system.

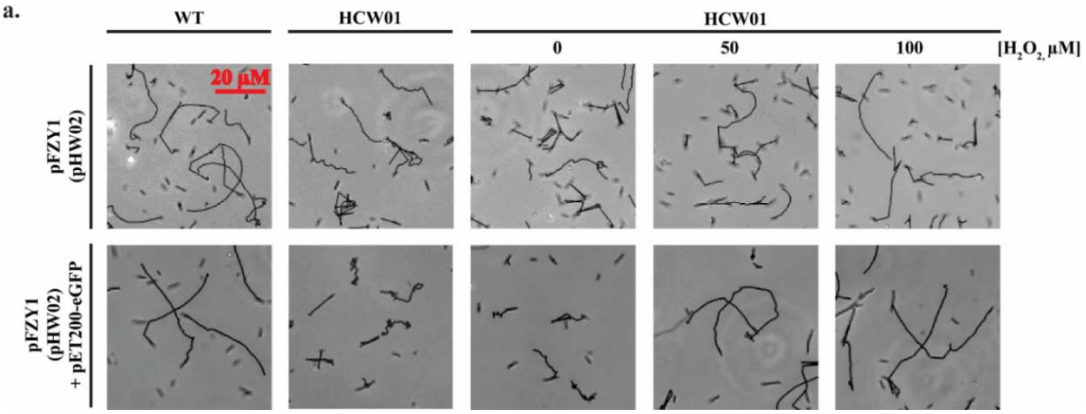

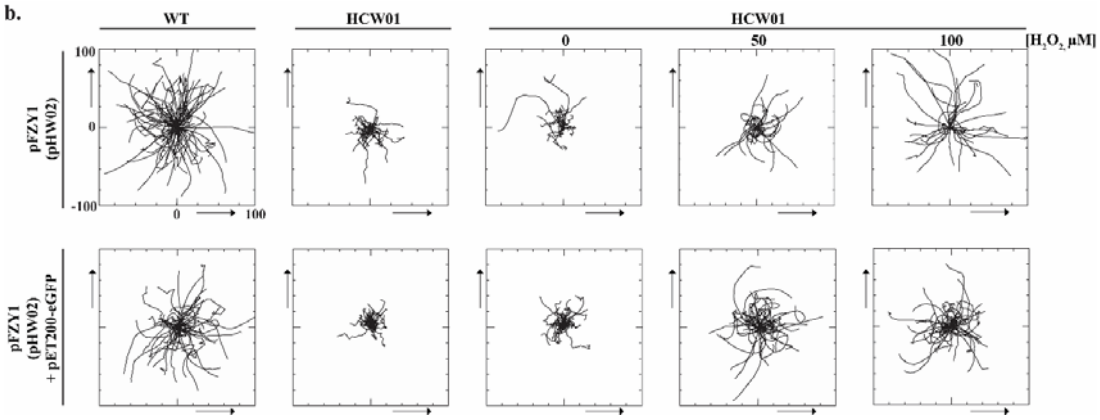

Figure 18 - Phenotypic expression of H_2O_2-induced motility. *a. Phase contrast trajectory images. 5 second trajectories of WT-pFZY1, HCW01-pFZY1, and HCW01-pHW02 (0-100 μM H_2O_2) ± pET200-eGFP were mapped. b. Rose graphs of trajectories. 5 second trajectories are displayed from each trajectory's origin to visualize the path lengths and angle changes with and without the pET200-eGFP plasmid.*

To more directly quantify the phenotypic responses to H_2O_2 with and without constitutive fluorescence, I performed computational analyses [73] of the motility videos. Per trajectory, increases in speed were observed in both the one and two plasmid systems. With H_2O_2 addition, I were able to recover native velocities without a change in growth rate (**Figure 19-a, b**); however, the addition of the constitutive fluorescent protein consistently and significantly slowed down tumbling and running in both the controls and H_2O_2 induced bacteria compared to the one plasmid system. This speed reduction links the effects of metabolic burden previously observed [36] with the direct effect on motility burden.

I note, however, that despite the statistically significant differences in speed, there is no significant difference of percent running (**Figure 19-c, d**) between the H_2O_2 induced one and two plasmid systems. For 5 second trajectories, the percentage of trajectories that exhibited a net angle change of < 1 radian/s and > 1 radian/s were classified as "running" or "tumbling", respectively [61]. WT-pFZY1 and H_2O_2-induced HCW01-pHW02 running times were calculated to be ~40-50%; the H_2O_2-induced bacteria recovered to native run versus tumble percentages. The HCW01-pFZY1 and uninduced HCW01-pHW02 running times

were significantly reduced at ~20-25% (solid bars, **Figure 19-c, d**). Finally, when comparing the ratio of path length to Euclidean distance (**Figure 19-e, f, g**), the bacteria without cheZ in both systems exhibited a more uniform distribution between the median and quartiles 1 and 3 with large whiskers (highest and lowest reported values), indicating a dominance of tumbling. Whereas, with WT-pFZY1 cells, one observes more variation between the median and quartiles 1 and 3 with smaller whiskers in the one plasmid compared to the two plasmid system. With increasing H_2O_2 concentrations and induction time, the quartile and variability (box and whiskers) shrink in size; similar to the controls, the two plasmid system shows less variability between the median and quartiles (**Figure 19-g**) compared to the one plasmid system. Based on the velocity and % running data, I theorize that the constitutive protein slows down and burdens the bacteria to the point where the path length is equivalent to the Euclidean distance.

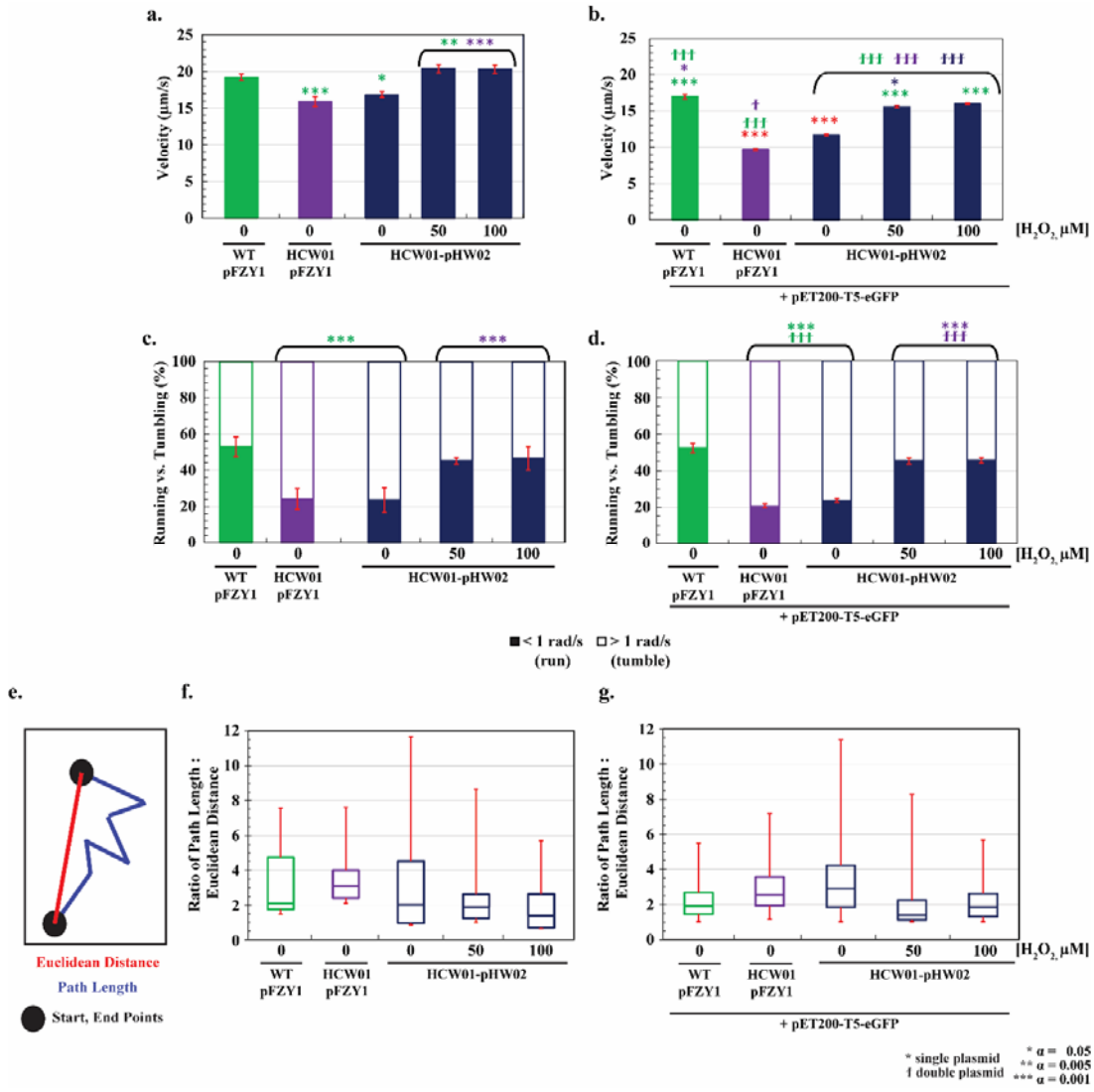

Figure 19 - Phenotypic expression of H_2O_2-induced motility – 1 vs. 2 plasmid*. a-b. Average velocities. The average velocities of the control bacteria (WT-pFZY1, HCW01-pFZY1) versus the engineered bacteria (HCW01-pHW02; 0-200 µM H_2O_2) without (left) and with pET200-eGFP (right). c-d. Percentage of trajectories running vs. tumbling based on angle change percentage. The percentage of trajectories (based on the initial 5 second trajectories of all bacteria) that were 'running" (solid bars) versus "tumbling" (lined bars) based on the time it took to move either < 1 radian/s or > 1 radian/s, respectively. e-g. Ratio of path length: Euclidean distance. The total distance traveled (path length, blue line) versus displacement (Euclidean distance, red line) were calculated based on the initial 5 second trajectories of all bacteria and plotted as box and whisker. All data is quantified for 5 second trajectories. All left columns are the one plasmid system. All right columns are the two plasmid system. Tukey-Kramer ANOVA and multiple comparisons analyses were performed with α = 0.05-0.001. * indicates the samples differed significantly from the one plasmid system. † indicates the samples differed significantly from the two plasmid systems.*

3.3.4 pHW02 – Chemotaxis and Pseudotaxis

Transwell apparatus

Transwell motility assays allow for direct observation of free swimming in 3D, and more specifically, initial analysis of chemotaxic versus pseudotaxic responses. I used Comsol to provide predicted H_2O_2 concentration gradients over time at 37°C for different initial H_2O_2 levels. At time zero, H_2O_2 was assumed to be uniform within the upper chamber, which in turn was assumed quiescent (no flow). In **Figure 20**, I have indicated the predicted concentrations at points A-D over time, without incorporating H_2O_2 consumption by the bacteria. By examining concentrations at various locations relative to each other (e.g., difference between A&B, or C&D), our simulations suggest that the H_2O_2 gradients persisted over the course of the subsequent swimming experiments (**Figure 20-b**).

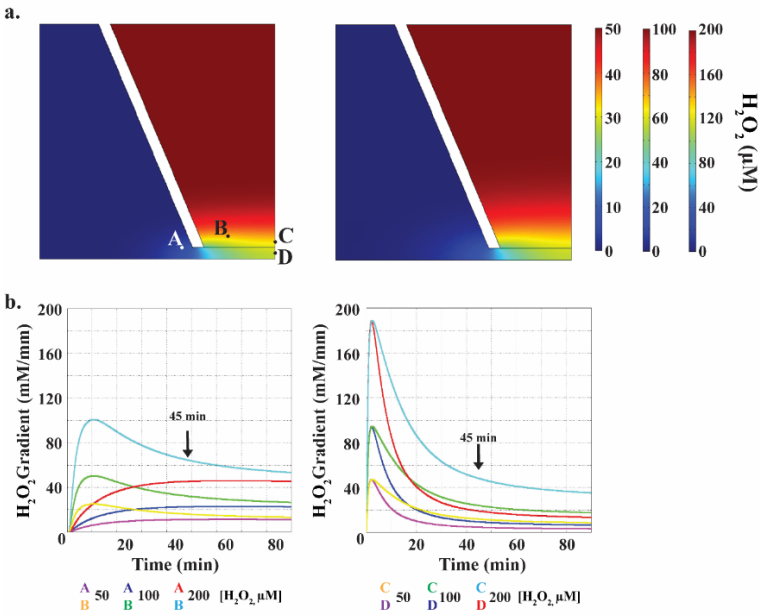

Figure 20 - Simulated H_2O_2 levels (Comsol). *a. Comsol model heat maps. Four points (A-D) were recorded to estimate various H_2O_2 concentration gradients over time. Heat gradient maps were constructed for 45 minute (left) and 90 minute (right) gradients. Heat maps were generated using 50, 100, and 200 μM H_2O_2 starting concentrations. b. H_2O_2 gradient curves over time. For each point (A-B, left; C-D, right), the H_2O_2 gradients were calculated over time to determine dynamics, steady-state conditions, and optimal measurement times (45 minutes).*

I suspended exponentially growing bacteria in the bottom of a transwell apparatus (**Figure 21-a**) containing Dulbecco's phosphate-buffered saline (DPBS) and at time zero, introduced either H_2O_2 or glucose in order to evaluate the swimming of bacteria vertically upward into the upper chamber. Glucose represents a chemotaxis positive control. By analyzing starting conditions with bacteria only present in the lower chamber and ending conditions with swimming bacteria in the upper chamber, I evaluated the extent to which bacteria swim to a chemoattractant such as glucose. These studies are analogous to our previous work [75] wherein bacteria were found to swim towards quorum sensing autoinducer AI-2, another known chemoattractant. In pseudotaxis, if the run of a tumble/run scheme is more frequent and/or of longer duration in the presence of a molecular stimulant, then on average the bacteria will accumulate in the direction of the stimulant [77,78]. In our tests, statistical analysis (multiple comparisons one-way ANOVA, Tukey-Kramer post-test) shows significant differences from WT-pFZY1 with DPBS (control) in the upper chamber compared with WT-pFZY1 with glucose (chemoattractant) in the upper chamber (**Figure 21-b**). Additionally, I found that HCW01-pHW02 induced with H_2O_2 migrated to the upper chamber in an apparent dose-dependent manner (**Figure 21-c**).

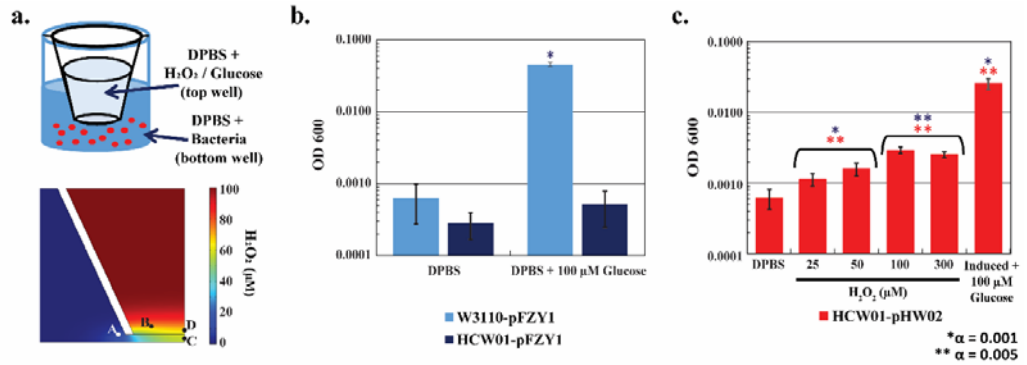

Figure 21 - Chemotaxis versus pseudotaxis bacterial response. *a. Transwell scheme and simulated transwell gradient. Bacteria were suspended in DPBS in the bottom of the transwell apparatus. DPBS, DPBS + 100 μM glucose or DPBS + 100 μM H_2O_2 solutions were loaded into the top of the transwell apparatus for testing. DPBS in both top and bottom served as random motility controls. Chemotaxis (towards glucose), or pseudotaxis (towards H_2O_2), respectively, were also determined. b-c. Quantification of bacterial motility. For chemotaxis, the bacteria cell number was assayed in the upper chamber after 2 hours; for pseudotaxis, the bacteria cell number was assayed in the upper chamber after 45 minutes. Tukey-Kramer ANOVA and multiple comparisons analyses were performed with α = 0.05, 0.01 and 0.001. Blue * indicates the samples differed significantly from HCW01-pFZY1 + DPBS. ** HCW01-pHW02 + DPBS.*

Importantly, while the pseudotaxic response to H_2O_2 was notably lower than the chemotaxic response to glucose, the result that cells swam to the upper chamber was statistically relevant (e.g., different than random swimming). This is particularly noteworthy in that previous findings have shown that bacteria swim away from H_2O_2 [79]; however, our findings suggest that rather than swim away from the potentially toxic ROS molecule, the bacteria instead swam towards H_2O_2. When considering our results from **Figure 10** and **Figure 14**, I suspect that these cells metabolize or dissimilate the potential toxin at the same times they were found to swim towards it. To our knowledge, this is the first such report, and this suggests that pseudotaxis can be controlled by internally regulating the CheZ level via externally applied H_2O_2.

Microfluidic device

While transwells provided a quantitative method for determining globally the directional responses to glucose and H_2O_2, I performed additional studies using a microfluidic motility device [76] to discriminate more precisely the cellular responses due to chemical

gradients. That is, using a well-controlled microfluidic device that employes a well-controlled and more uniform concentration gradient enables one to anaylze the bacteria's phenotypic response both visually and analytically on a per cell basis so that cell and system design parameters for future applications can be estimated more accurately. As noted in Methods, bacteria were introduced into the bottom channel of a dual chamber device at the cell inlet (**Figure 22-a**, **top view**). These cells are localized generally at the inlet but are free to disperse within the bottom channel (**Figure 22-a, cross-section**). As soon as cells are added, the ends are taped to stop flow. Immediately thereafter, DPBS buffer is introduced into the sink channel of the top layer and either glucose or H_2O_2–supplemented DPBS solution was added to the source channel (**Figure 22-a**) which started the experiment (t = 0). The concentration gradient of solute (glucose or H_2O_2) is established in the area indicated by the y-axis arrow (**Figure 22-a, top or cross section views**). The cells in this lower channel are then free to swim according to the emerging gradient. A full description of the device and established gradients is available[76]. At appropriate time intervals, images near the sink, middle, and source were taken to represent the prevailing population and cell density. In **Figure 22-b**, I quantified the WT-pFZY1 chemotaxic response to glucose. Based on data normalized to the cell numbers at time 0 and at the source, I observed a slight increase over time in the source population for WT-pFZY1 with DPBS (no attractant). As I presume there may have been more cells at the source end of the device (closest to the inlet), this represents the natural spreading of the population to unpopulated regions. Then, when the cells were exposed to a glucose gradient, I observed a far greater increase in population at the source. This increase was observed to be sustained for over 20 min. Analogously, in **Figure 22-c**, I examined swimming when bacteria were exposed to H_2O_2. When pHW02 were exposed to

increasing amounts of H_2O_2, I observed an increase in the number of bacteria found at the source (**Figure 22- c**).

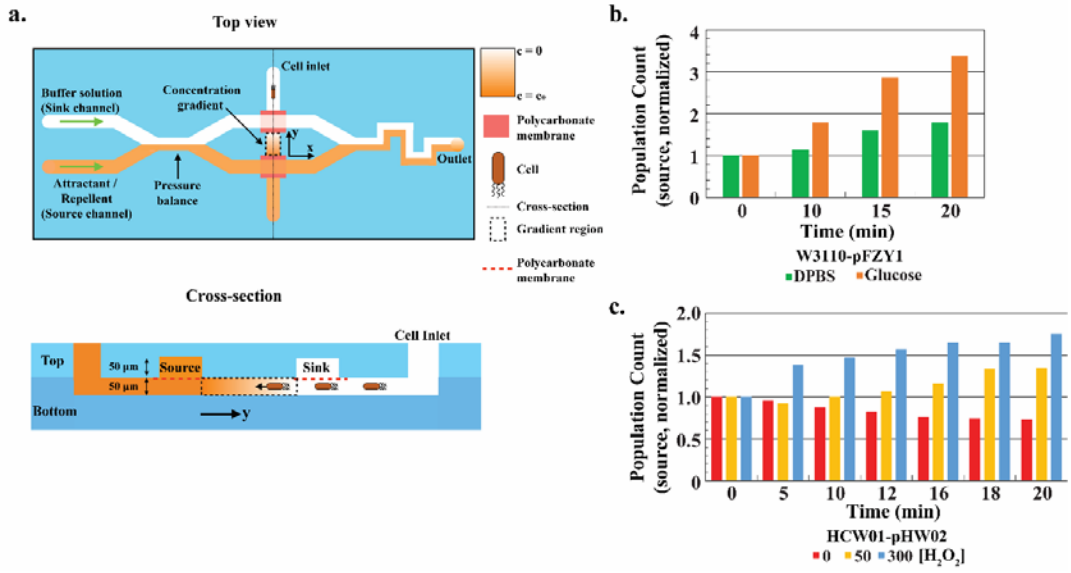

Figure 22 - Pseudotaxis using a gradient-generating microfluidic device. *a. Microfluidic device scheme[76]. Cells are introduced to the cell inlet (Top view) which places cells in the bottom channel (Cross-section). The chemical gradient is established by introducing buffer and attractant in flow at sink and source locations, respectively (see Methods). Cells are imaged near source, sink, and in the middle of the gradient (Top view). b-c. Chemotaxis vs. pesudotaxis population source image analysis. Images were taken at the indicated time intervals with t=0 designated to be the introduction of glucose or H_2O_2 solution into the source channel. All population counts normalized to time 0 population counts at the respective positions. WT-pFZY1 with 100 μM glucose as the source yielded a chemotaxic response (towards glucose source). HCW01-pHW02 with H_2O_2 demonstrated pseudotaxis.*

Moreover, I found that in only 5 minutes exposure to a 300 mM H_2O_2 gradient, a notable increase in bacteria was found. Consistent with our previous results, the cells exposed to lower H_2O_2 concentrations (50 μM) responded more slowly and to a lesser extent. These results again demonstrate that CheZ-engineered bacterial cells can be "programmed" to swim towards H_2O_2. I presume that as cells moved towards the H_2O_2, they also helped to dissipate the level, enabling additional cells behind to swim towards the increasing peroxide level. I did not test, however, such spatially resolved H_2O_2 levels.

3.4 Conclusion

In summary, we engineered a synthetic H_2O_2-responsive promoter system and quantified the additional motile burden caused by constitutive GFP expression. We constructed a simple synthetic H_2O_2-responsive promoter system and used the system to guide bacterial swimming. We employed population based and single cell based analytical methods to characterize the system that enable *E. coli* to sense and pseudotax towards H_2O_2 in highly-controlled and defined manners. Studies of CheZ expression and motility revealed a practical threshold level of 50-200 μM was suitable for rapid and sustained induction of CheZ and cell swimming. Importantly, we identified and quantified how the constitutive GFP expression, a method commonly used by researchers conducting motility experiments [80,81], significantly slows down bacteria without affecting the cheZ network. It is commonly known and characterized that flagella require ATP and ATPases to export protein and rotate flagella [82,83]; this indicated that the two plasmid bacteria experience an energetic metabolic burden, thus reducing the bacterial growth rate and velocity. Despite the burden of GFP, the engineered bacteria quickly consumed the H_2O_2 and turned on bacterial running.

In physiologically relevant settings (e.g., GI tract), reported H_2O_2 concentrations in mice studies were > 200 μM during the inflammatory phase and ~150 μM during the post-inflammatory phase in dermal wounds [84]; additional mice studies have shown that a range of 100-300 μM of H_2O_2 was generated at the site of the ROS burst release [15,17,72]. Correspondingly, our studies have indicated engineered cells functioned satisfactorily when exposed to H_2O_2 levels up to the 100-300 μM range, experiencing diminished CheZ expression, growth and motility at much higher levels (~500 μM). Thus, we suggest that the synthetic biology framework and tracking analysis in this work could be applied for the

detailed design of engineered probiotics that would be deployed for directed treatment in the GI tract.

Chapter 4: Optimize Protein G Surface Display and Express Microbial Transglutaminase in Bacteria in Response to H_2O_2

4.1 Introduction

4.1.1 Protein G Surface Display

In nature, cell surfaces use membrane-bound proteins to bind antibodies at their constant fragment (Fc) region. These protein-bound antibodies are secured to supramolecular structures, such as the cell membrane[85]. The human body and other organisms developed and evolved antibodies with a plethora of different antigen-binding fragment (Fab) variations. These variations allow the antibody to bind the Fab region to a specifically-recognized antigen; numerous antigens are upregulated by the immune system in response to injury, infection, and/or disease. These upregulated antigens serve as excellent targets for innovative bacteriotherapeutics[86]. By utilizing both the Fc and Fab regions of an antibody, a novel antibody display and targeted docking system can be expressed and optimized for *E. coli* and biotherapeutics.

Specifically, in this work, I make use of the AIDA surface display system in combination with Protein G. Protein G is an immunoglobulin binding protein derived from bacterial cell surfaces; it selectively binds the antibody's Fc region, leaving the Fab region free to interact with and bind antigen[87]; importantly, the Protein G-Fc binding stability is aided by hydrogen bonds[88]. Researchers demonstrated *Streptococci* Protein G's ability to bind high amounts of human IgG antibody in various buffers ranging from pH 4-9[89]. Naturally, in the human body, the Fc receptors form a critical link between the humoral and cellular immune response, specifically aiding effector cell functions[90]. Separately, the AIDA surface display autotransporter, found originally in pathogenic bacteria, allows proteins, enzymes,

and peptides to be displayed on the outer surface of bacteria. The use of Protein G as a surface exposed vehicle for the assembly of targeting antibodies will naturally depend on the binding characteristics between the antibody and the protein G and how these might function in the GI tract.

Using AIDA to surface display Protein G, outlined in **Figure 23**, allows the engineered bacteria to be loaded with an antibody to target the disease-specific up-regulated antigen and dock at the site for biotherapeutic release. The approach I am using utilizes and optimizes nature's methods of protein engineering and antibody display. Optimization requires that the engineered *E. coli* uniformly and highly display Protein G on the outer surface in a time-efficient manner and without introducing significant metabolic burden.

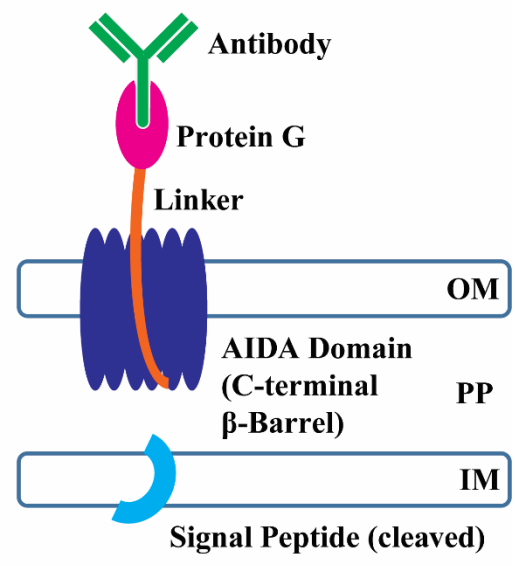

Figure 23 – AIDA1 surface displaying Protein G. *The autotransporter AIDA consists of a signal peptide at the N terminus, one or more domains for transport, and an autotransporter structure at the C terminus. The autotransporter domain forms after translocation through the β-sheet barrel within the outer membrane. The N-terminally attached Protein G is translocated to the surface through this porin-like barrel*[54]*. The Fc region of the antibody binds the surface-displayed Protein G.*

4.1.2 Microbial Transglutaminase

Biologics engineered and expressed in *E. coli* are often purified and introduced into a synthetic drug delivery vehicle; however, more invigorating efforts are being made to use the

engineered bacteria as biotherapeutic delivery vehicles themselves[14,77,86,91]. While Yu *et al.* have used the conventional approach to express high amounts of stable, recombinant mTG, they optimized it for a single-purpose system – protein purification[51]. In this chapter, I look to combine the therapeutic properties of their recombinant mTG with the engineered biotherapeutic *E. coli* delivery system.

The Sn TGase engineered by Yu *et al.* was synthesized as a precursor protein with a preproregion of 82 amino acid residues. This precursor protein allows for higher solubility of folded, inactive protein compared to mature (active) mTG without the preproregion. A high level of soluble Sn TGase with its N-terminal propeptide fused with thioredoxin was expressed in *E. coli*. Bovine trypsin cleaves the propeptide from the TGase to for mature (avtive) TGase. It showed activity over a broad range of pH and temperature; the activity levels are equivalent to the authentic mature TGase[51].

I hypothesize that by utilizing the Sn TGase system in a low copy plasmid under H_2O_2 control, mTG can be made in lower but soluble concentrations for effective therapeutic delivery and activation at the wound site; additionally, the H_2O_2 control allows it to be expressed at the therapeutic site without overburdening the metabolic processes in the engineered bacteria.

4.2 Materials and Methods

4.2.1 Protein G Surface Display

DNA Manipulation and Growth Conditions. The genetic construct developed in this study were assembled using the standard molecular biology protocol[65]. The vector designed for this study was derived from pAIDA-I (low-copy plasmid), which was donated by Larsson[53] and previously used for covalent surface display of fusions up to 110 kDa in size. Briefly, the *protein G IgG Fc binding domain* gene (191 bp) from *Streptococcus sp.* corresponding to

S62801 was amplified using the primers specified in **Table 2**. *Protein G* and pSBP-mCherry[70] (modified from pAIDA-I) were digested with the SalI and XbaI restriction enzymes. The *protein G* and pLacUV5-AIDA1 fragments were ligated using T4 Ligase (New England Technologies). Ligations were transformed in *E. coli* Top10 cells (Invitrogen) and plated on LB agar plates supplemented with chloramphenicol (34 µg/mL) and incubated at 37°C. Plasmid DNA (Figure 24) from each selected clone was isolated for sequencing using Qiagen miniprep and analyzed via restriction digestion. The plasmid was then transformed into *E. coli* K-12 wild type (W3110) and *E. coli* K-12 *ΔluxS* (LW12) (constructed by Wang *et al.*[92]).

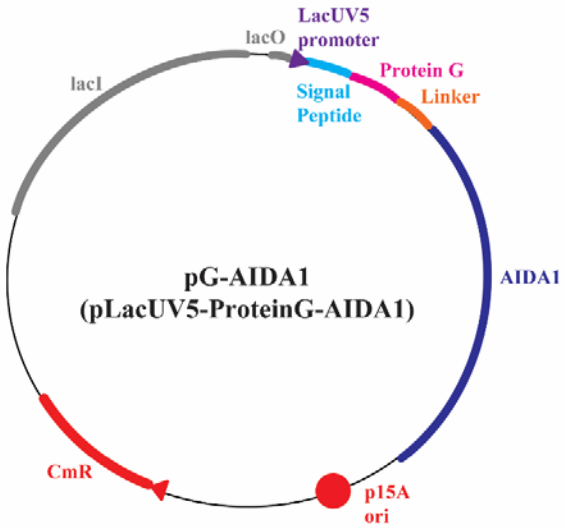

Figure 24 - *Plasmid design of pG-AIDA1.*

Bacteria were grown in LB media supplemented with ampicillin (50 µg/mL) and incubated at 37°C in a shaker at 250 rpm for all growth experiments. For all overnight inoculations, bacteria were grown from glycerol frozen stock; all morning re-inoculations were adjusted with sterile media to OD_{600} 0.05. The strain-plasmid nomenclature and shortened names are listed in **Table 2Table 2**.

Characterizing and Optimizing Protein G Surface Display. *E. coli* WT-pG-AIDA1 and LW12-pG-AIDA1 were inoculated into 100 mL of LB in 500 mL flasks. Bacteria were shaken at 37°C until OD_{600} ~0.25. After induction, bacteria were split into 50mL flasks, induced with 0-1 mM IPTG, and shaken at either 24°C, 30°C, or 37°C. 1mL samples were taken at two, four, and six hours. For quantifying Protein G surface display, 1 mL samples were pelleted and resuspended in PBS with 5 µg/mL of Dylight488 (green) antibody (Goat Anti-Mouse IgG, Jackson Immunoresearch) flow cytometry (FACS). Samples were shaken for 30 minutes, washed multiple times, and resuspended in PBS for flow cytometry (FACS CantoII, BD Bioscience) analysis to quantify Protein G-antibody surface display expression. 2µL samples were taken for simultaneous fluorescent microscopy imaging. BL21(DE3)-pSBP-mCherry[70] served as a negative control and to show that the antibody had no non-specific binding. For data analysis, technical and biological duplicate data were obtained.

Statistical Analysis. For most experiments, one-way ANOVA using a multiple comparisons' Tukey-Kramer post-test were performed using Matlab (version R2015a). α values of 0.05 were used to indicate statistical significance. Data are reported as mean values and standard deviation of the error, unless otherwise stated.

4.2.2 Microbial Transglutaminase

DNA Manipulation and Growth Conditions. The genetic constructs developed in this study were assembled using the standard molecular biology protocol[65] and Gibson Assembly protocol[93]. Briefly, the *oxyR-poxyS* and *Trx–proTGase* genes were amplified using the primers specified in **Table 2**. *oxyR/S* and pST39 (low-copy plasmid) were digested (1 µg each) with the NsiI and XbaI restriction enzymes. The fragments were ligated using T4 Ligase (New England Technologies). Ligations were transformed in *E. coli* Top10 cells (Invitrogen) and plated on LB agar plates supplemented with ampicillin (50 µg/mL) and

incubated at 37°C. Plasmid DNA from each selected clone was isolated for sequencing using Qiagen miniprep and analyzed via restriction digestion. For amplifying pST39-*oxyR/*S, the Gibson primers were designed to have a minimum 15 base pair overlap with the base pairs flanking the insert site. Six histidine residues were added to the beginning of *SNTGA (TGase*, 1562 base pairs*)*. The pST39-*oxyR/S* and *Trx–proTGase* fragments (1:2 ratio) were ligated with Gibson Assembly Master Mix following the Gibson Assembly protocol and subsequently transformed into chemically-competent NEB 5-alpha *E. coli*. Plasmid DNA (**Figure 25**) from each selected clone was isolated for sequencing using Qiagen miniprep. The plasmid was transformed into *E. coli* K-12 (W3110). Additionally, as a positive control, the pET32aΔ-SNTGA plasmid (provided by Dr. Ming-Te Yang)[51] was transformed into *E. coli* K-12 (W3110).

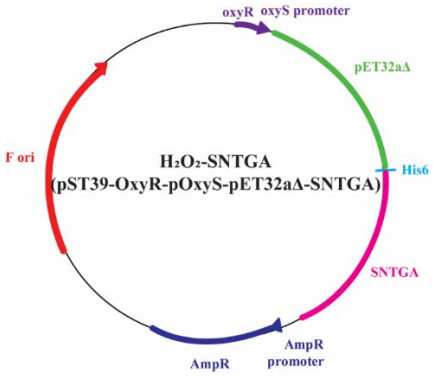

Figure 25 - *Plasmid design of H_2O_2-SNTGA.*

Table 2 - Strain design and primer designs of Protein G and Microbial Transglutaminase.

Strain (Short Name)	**Plasmid**	**Phenotype**
W3110, LW12 (WT-, LW12-pG-AIDA1)	**pLacUV5-ProteinG-AIDA1**	**Surface Display Protein G ("Docking")**
W3110 (WT-SNTGA)	**pET32aΔ-SNTGA**	**mTG (Therapeutic)**

W3110 (WT-H_2O_2-Trx-proTGase)	pST39-OxyR-*p*OxyS-Trx–proTGase	H_2O_2-controlled mTG (Therapeutic)
Primer Name	**Primer Sequence**	
protein G (pLacUV5-AIDA1) (forward primer)	5'-GTCGACATGACA ACTTACAAACTTGTT ATTAATGGTAAAACA TTGAAAGGCGAAAC AACTACTAAAAC-3'	
protein G (pLacUV5-AIDA1) (reverse primer)	3'-AGATCTGCCCAG GTAAAGGCAATGGCA TTTCCAGAATCAG-5'	
oxyR-*p*oxyS (pST39) (forward primer)	5'-CCAATGCATGGAT CCTTAAACCGCCTGT TTTAAAACTTTATC GAAATGGCC-3'	
oxyR-*p*oxyS (pST39) (reverse primer)	3'-CAGTGACGGGC AAAGCTCTCAAATT GAAATTCTTCCTCT ATATAGATCTCG-5'	
Trx–proTGase (pST39) (forward primer)	5'-TTTAAGAAGGAGA TATATCTAGAATAATTTT GTTTAACTTTAAGAAGG AGATATACATATGAGCG ATAAAATTATTC-3'	
Trx–proTGase (pST39) (reverse primer)	3'-ATCGTCGGCCTA GAGAGCTCAGTGCC GGTCGGAACGAA-5'	
pST39-oxyR-*p*oxyS (Gibson forward primer)	5'-CTCGAGAGA TCCGGCTGC-3'	
pST39-oxyR-*p*oxyS (Gibson reverse primer)	3'-AGATCTATATAG AGGAAGAATTTCAA TTTGAGAGCTTTG-5'	

Bacteria were grown in LB media supplemented with ampicillin (50 μg/mL) and incubated at 37°C in a shaker at 250 rpm for all growth experiments. For all overnight inoculations, bacteria were grown from glycerol frozen stock; all morning re-inoculations were adjusted with sterile media to OD_{600} 0.05. The strain-plasmid nomenclature and shortened names are listed in **Table 2**.

Microbial Transglutaminase Expression and Purification. *E. coli* WT-SNTGA and WT-H_2O_2-Trx-proTGase were grown overnight, reinoculated into 50 mL of LB in 250 mL flasks, and shaken at 37°C until OD_{600} ~0.5. Cells were induced with either 0.5mM IPTG or 300 μM H_2O_2 at 24°C or 24°C, 250rpm for 6, 12, and 18 hours and then centrifuged at 4°C, 12,000 rcf for 10 minutes. Bacterial pellets were resuspended with 200 μL BugBuster (BugBuster HT, EMD Millipore) and protease inhibitor (HALT Protease Inhibitor Cocktail (100x), Fisher Scientific). Cell suspensions were shaken at 24°C, 150 rpm for 1 hour. Insoluble cell debris were removed by centrifugation at 4°C, 12,000 rcf for 20 minutes and soluble fractions were transferred to new tubes.

His_6-tagged mTG (Trx-proTGase) was purified using TALON Metal Affinity Resin (Clontech Laboratories). Briefly, resin was washed with 10mM imidazole for protein binding. The resin was pelleted in a swinging-bucket rotor at 4°C, and the supernatant was discarded. The supernatant was added to the resin, vortexed, and shaken for 20 min. at room temperature. The resin was pelleted, and the supernatant was discarded. The resin was washed three times with PBS in an ice bath, shaking for 20 minutes per wash. Trx-proTGase-His6 bound to the resin was eluted with 300 μL of 250mM imidazole. The elution was briefly vortexed and centrifuged. The supernatant from each sample was collected, and protein concentrations were measured using the Nanodrop (Nanodrop 1000, Thermo Scientific).

Pre-stained ladder (PageRuler Plus Prestained Protein Ladder, ThermoFisher Scientific) and 25 µL of boiled samples were loaded into 12% SDS-PAGE gels (Bio-Rad). The SDS-PAGE gel was stained overnight with Coomassie Blue and destained (45% methanol, 10% glacial acetic acid). The gel image was obtained using AlphaImager HP.

Microbial Transglutaminase Activity Assay. To activate the transglutaminase, each sample was incubated with a 1:100 dilution of trypsin (0.25% Trypsin-EDTA, Life Technologies) at 4°C, 24°C, 30°C, and 37°C overnight. The colorimetric hydroxamate procedure by Sigma-Aldrich, modified from Folk and Cole[94], using N-α-carbobenzoxy-L-glutaminyl-glycine (CBZ-Gln-Gly) as a substrate was used for determination of TGase activity. 100 µL of the reaction mixture (2 mL of 0.1 M Tris–acetate buffer (pH 6.0), 5 mL of 200 mM hydroxylamine and 20mM glutathione-reduced form, and 120 mg of CBZ-Gln-Gly; per 10mL total volume), and 15 µL of enzyme solution, was incubated at 37°C for 10 min. The reaction was stopped by adding 250 µL of 12% (v/v) trichloroacetic acid (TCA) and 250 µL of 5% (w/v) $FeCl_3$. After centrifugation at 4,000×g for 15 min, the supernatant was collected and the absorbance at 525 nm was measured with BugBuster serving as the test blank. L-Glutamic acid γ-monohydroxamate was used as a standard. One unit of enzyme TGase activity was defined as the amount of enzyme which catalyzed the formation of 1 µM hydroxamic acid per minute under the assay conditions. For data analysis, technical and biological duplicate data were obtained.

4.3 Results and Discussion

4.3.1 Characterizing Protein G's surface display

Initial growth and induction studies were carried out to test the surface display efficiency of the engineered LW12-pG-AIDA1 cells and whether they exhibited temperature and/or time-dependent expression. Previous studies performed by Wang *et al.* had shown

strain, growth media, and temperature-dependent surface display of protein Z (a model protein) in AIDA. They conducted studies in OmpT mutants to minimize the proteolysis of protein Z and maximize surface expression at various temperatures[53]. For the initial LW12-pG-AIDA1 studies, I conducted temperature, dose, and time-dependent experiments. In **Figure 26**, I grew cells at 37°C until OD ~0.25; the cultures were split, induced with IPTG, and grown at 30°C and 37ºC to examine how the temperature and IPTG concentrations affect bacterial growth and Protein G-AIDA1 expression over time. In **Figure 26-a**, I observed similar growth rates, regardless of temperature and IPTG concentration.

I also conducted AF488 antibody-binding experiments to quantitatively and qualitatively characterize Protein G surface display efficiency. A more nuanced analysis of the FACS data was conducted by quantifying the different levels of fluorescence (**Figure 26-b, c** and **Figure 27-a**) to correlate Protein G surface display with percentage and levels of AF488 fluorescence. Gates were set to show either low (Gate 1), high (Gate 2), or very high (Gate 3) Protein G-AF488 expression (**Figure 27-a**). For pG-AIDA1 induced and expressed at 30°C (**Figure 26-b**), there was a statistically significant difference ($\alpha = 0.05$) between 2 (60%-65%) and 4-6 hours (~80% and 85%, respectively) induction time. When induced, FACS gating analysis (**Figure 27-a**) showed that the majority of fluorescence was high (10^3-10^4 mean fluorescence units). This indicated that there was efficient and relatively uniform amounts of Protein G surface displayed (with AF488 bound) across all cells. However, when pG-AIDA1 was induced at 37°C (**Figure 26-c**), there was overall a statistically significant decrease in expression compared to 30°C (**Figure 26-b, c**). There was a statistically significant increase ($\alpha = 0.05$) in AF488 expression (bound to Protein G) between 2 hours (20%-25%) and 4-6 hours (~60% and 70%, respectively) induction time and decrease compared to 30°C induction ($ł = 0.05$). Importantly, compared to 30°C, FACS gating

analysis of 37°C showed that the fluorescence was split between low and high amounts of bound AF488. This indicated that there was more variable amounts of Protein G surface displayed (with AF488 bound) across all cells over time. Additionally, independent of temperature, there was little leaky expression (not induced) over time compared to the induced samples. There was no dose-dependent response to IPTG induction, regardless of temperature; this indicated that only a small concentration of inducer is required to activate pG-AIDA1. Overall, similar to the studies conducted by Gustavsson *et al.*[53], I found the efficiency to be temperature-dependent but independent of culture media.

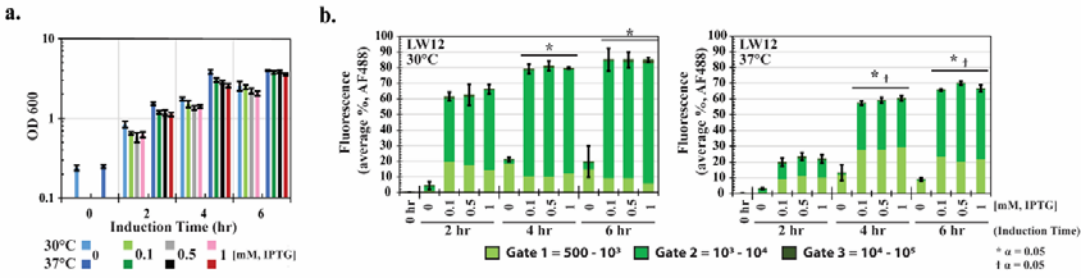

Figure 26 – Characterizing effects of temperature on Protein G surface display efficiency. *a. Cell growth bar chart. b. FACS average percentage of cells with AF488 antibody bound to Protein G. LW12-pG-AIDA1 were induced with 0-1 mM IPTG, and sampled 2 hours. Tukey-Kramer ANOVA and multiple comparisons analyses were performed with α = 0.05. * indicates the samples differed significantly from 24°C. † indicates the samples differed significantly from 37°C.*

Simultaneous to the FACS experiments, the samples were also imaged using fluorescent microscopy for qualitative analysis. Previously, I had grown and induced pSBP-mCherry cells as a negative control to show if the AF488 antibody was non-specifically binding (**Figure 27-c**). Fluorescent microscopy paired with the FACS analysis showed that with time, the cells more uniformly and highly surface display Protein G at 30°C compared to 37°C (**Figure 26-b, c** and **Figure 27-d**). When not induced samples were imaged, there were very few dim (low GFP fluorescence) compared to the number of cells imaged using phase contrast (**Figure 27-d, 0 mM IPTG**). However, when induced samples were imaged using phase contrast and GFP fluorescence, there were an increasing number of green cells over

time. Confirming and correlating FACS results and previous studies by Gustavsson *et al*, Protein G induction at 30°C showed higher numbers of green cells and brighter cells compared to 37°C (**Figure 27-d, 0.1-1 mM IPTG**).

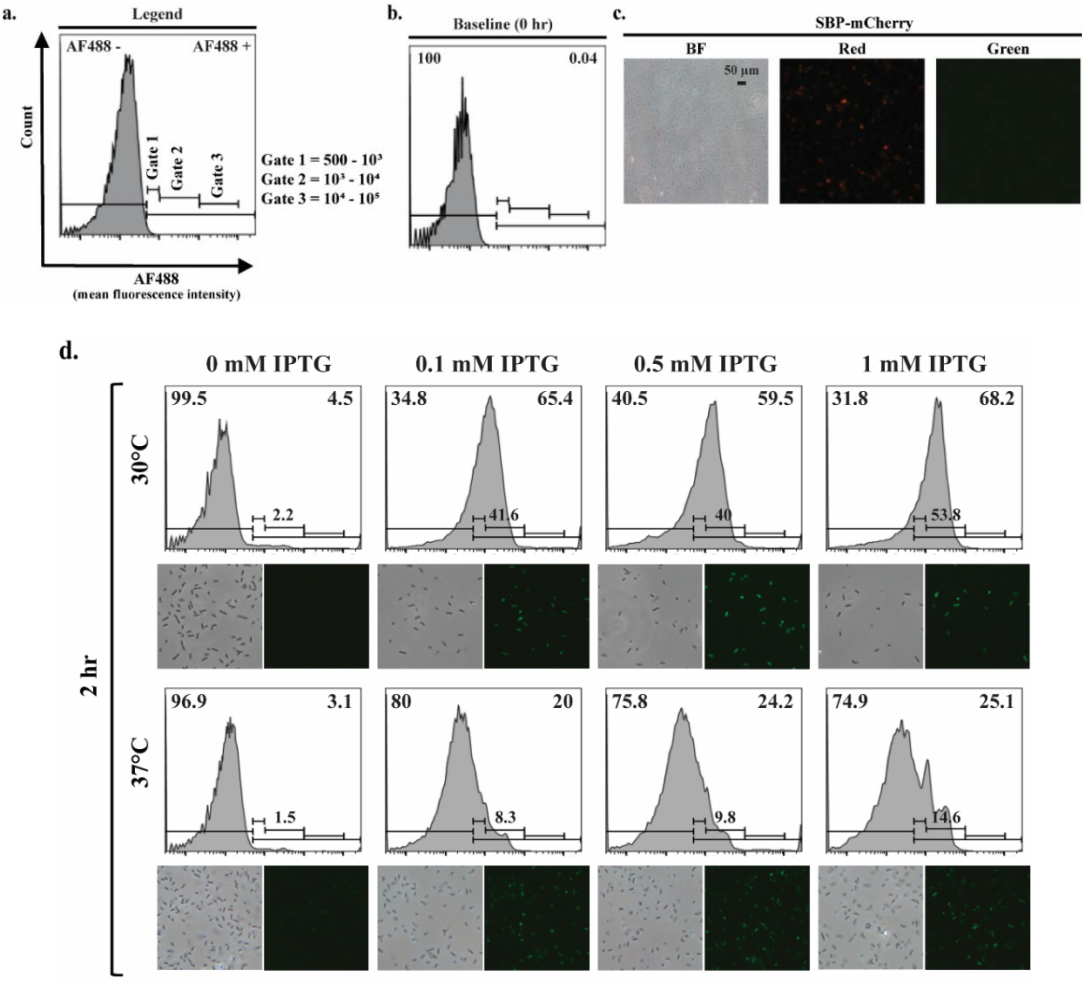

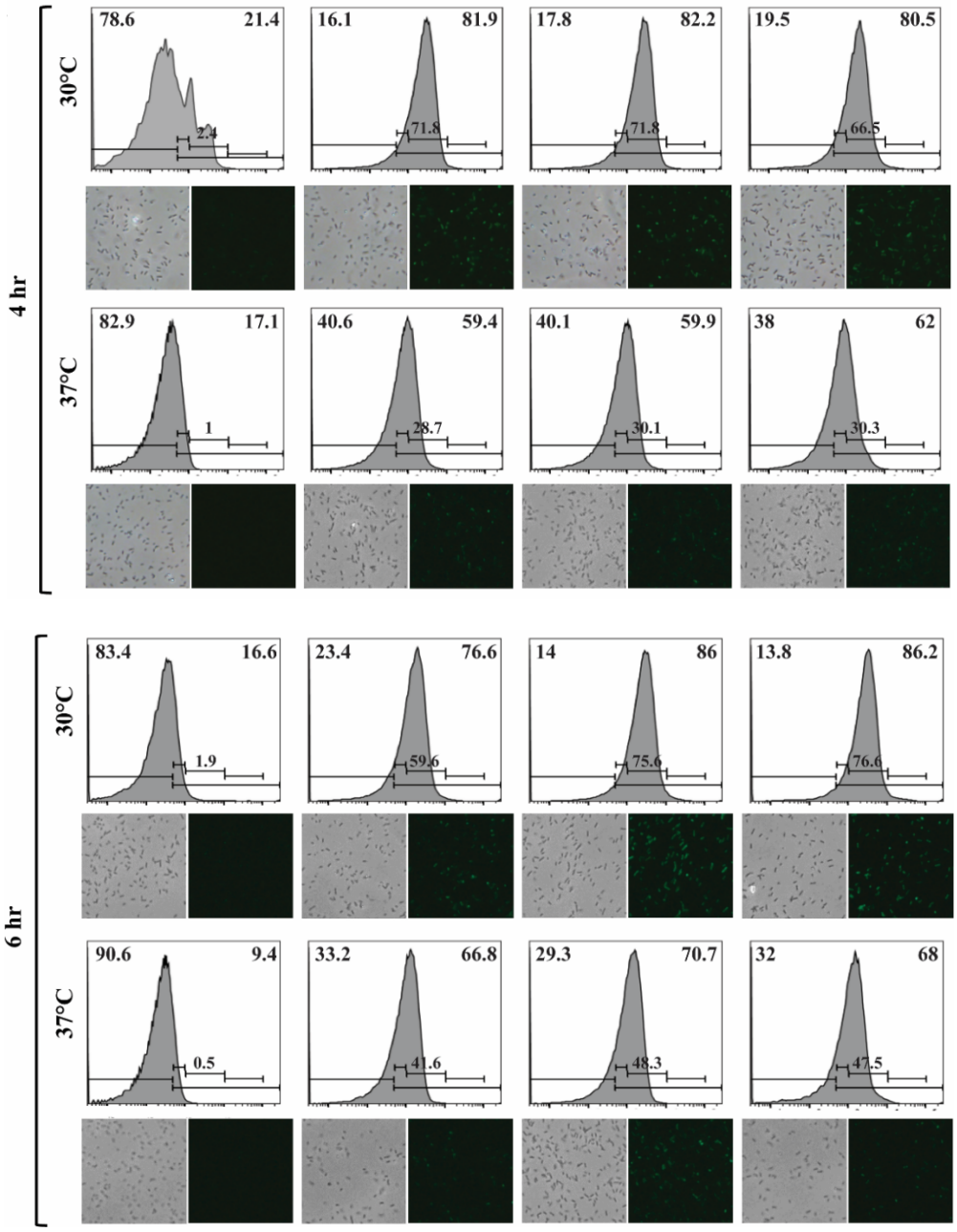

Figure 27 – FACS Histograms of initial Protein G-AIDA1 surface display. *a. FACS histogram legend for AF488 loaded cells. The percentages of non-bound (no surface display) and bound AF488 (to Protein G) on cells are in the upper left and right corners, respectively. b. Baseline histogram and control images. The Baseline histogram is the 0 hr timepoint for IPTG induction of LW12-pG-AIDA1. Control microscopy images are BL21(DE3)-pLysS-pSBP-mCherry with AF488 antibody incubation to check for non-specific binding. d. FACS histograms and microscopy images of LW12-pG-AIDA1 with AF488 antibody binding.*

4.3.2 Optimizing Protein G's surface display

In order to further optimize Protein G surface display, I conducted experiments with the *E. coli* K12 wildtype strain, W3110, and tested induction at 24°C for both LW12- pG-AIDA1 and WT-pG-AIDA1. Additionally, because OmpT cleaves cysteine-rich proteins[53], and Protein G is not cysteine-rich, it is not necessary to perform the experiments in *ompT*- W3110. In **Figure 28**, I grew cells at 37°C until OD ~0.25; the cultures were split, induced with IPTG, and grown at 24°C (LW12, WT) and 37°C (WT) to examine how the temperature and IPTG concentrations affect bacterial growth between strains and optimize Protein G-AIDA1 expression over time. In **Figure 28-a**, I observed similar growth rates, regardless of strain and IPTG concentration.

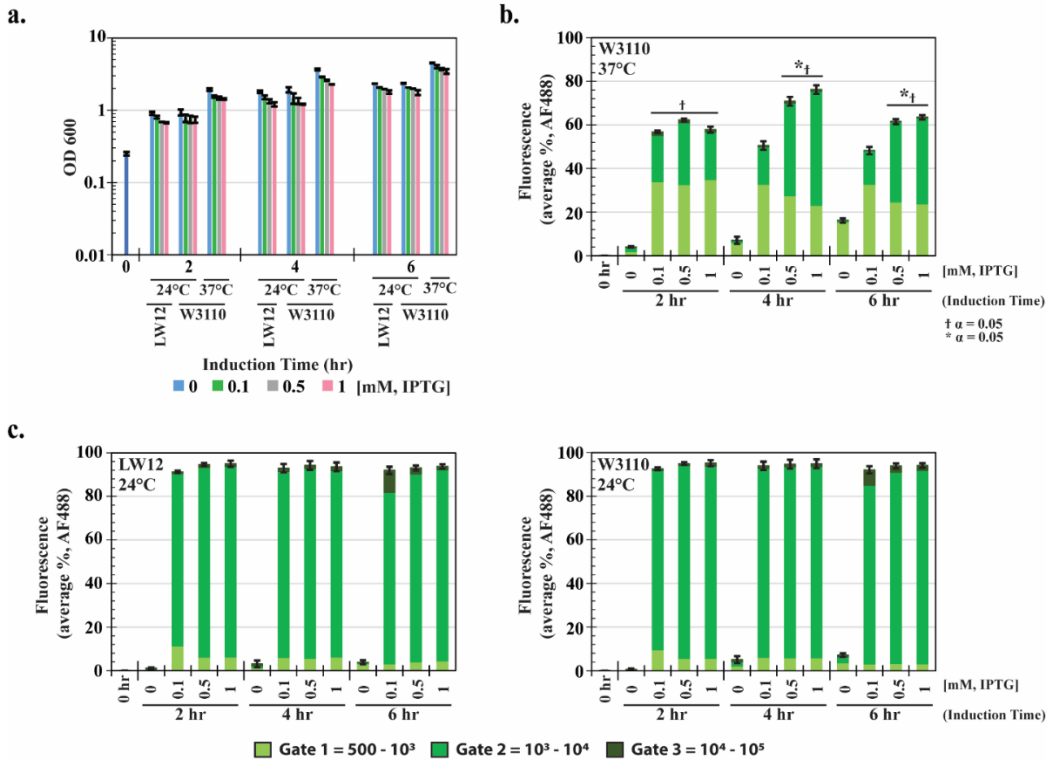

Figure 28 – Comparing Protein G surface display efficiency based on temperature and strain. *a. Cell growth bar chart. b. FACS average percentage of cells with AF488 antibody bound to Protein G. WT-pG-AIDA1 were induced with 0-1 mM IPTG at 37°C and sampled every 2 hours. c. FACS average percentage of cells with AF488 antibody bound to Protein G. LW12-pG-AIDA1 and WT-pG-AIDA1 were induced with 0-1 mM IPTG at 24°C and sampled every 2 hours. Tukey-Kramer ANOVA and multiple comparisons analyses were performed with α = 0.05. * indicates the samples differed significantly from 24°C. † indicates the samples differed significantly from 37°C.*

Additional AF488 antibody-binding experiments quantitatively characterized Protein G surface display efficiency (**Figure 28-b-d**). For WT-pG-AIDA1 induced and expressed at 37°C (**Figure 28-b**), there was a statistically significant increase ($\alpha = 0.05$) in expression between 2 hours (50%-60%) and 4-6 hours (~70%, respectively) induction time for 0.5 and 1mM IPTG. Among the samples, there was low, non-uniform expression to high, saturating expression of Protein G surface displayed over time; based on the FACS data, significant amounts of low antibody binding (Gate 1) per bacteria indicated that low levels of Protein G were being surface displayed.

In addition to induction concentrations and folding time, many proteins are temperature-sensitive for proper folding, including mTG. Importantly, when both LW12-pG-AIDA1 and WT-pG-AIDA1 were tested at 24°C, all induced samples had uniform high antibody binding (**Figure 28-c, d**); this directly correlates to the amount of Protein G surface displayed, indicating that uniformly saturating amounts (> 90% cells with bound, high concentration of AF488 per cell) of Protein G was surface displayed from 2-6 hours. Additionally, there was very little leaky expression (not induced, < 10% with low levels of bound AF488 and Protein G expression) over time at 24°C. There was no dose-dependent response to IPTG induction, regardless of temperature; this indicated that only 2 hours and a small concentration of inducer (≤ 0.1 mM IPTG) is required to activate pG-AIDA1 and fully display Protein G on the outer surface. Similar to the studies conducted by Wang *et al.*[53], I found the protein folding and surface display efficiency to be temperature-dependent (24°C optimal) but independent of culture media and strain for surface displaying Protein G.

4.3.2 Engineering microbial transglutaminase under H_2O_2 control

I conducted studies to test Trx-proTGase's expression and activity under the H_2O_2 promoter in a low copy plasmid over time. Previous studies by Yu *et al.* characterized and

optimized the process to express and activate Trx-proTGase.[51] Compared to these studies, I conducted experiments to minimize expression time while maintaining activity. WT-H_2O_2-Trx-proTGase was induced with 300 µM H_2O_2 for 6, 12, and18 hours at 24°C and 37°C to determine mTG solubility and activity over time. The purified His_6-tagged Trx-proTGase was run on an SDS-PAGE gel to confirm purification results (**Figure 29**). As seen in the plasmid rendering (**Figure 25**), the His_6 tag was engineered at the N-terminus of mTG (after the Trx-pro region). An mTG mixture (provided by Dr. Gregory F. Payne) served as a positive control (**Figure 29-Lane 3**). Similar to Yu *et al.*[51], we observed three bands with our purified proteins – Trx-proTGase (~57 kDa), mature TGase (~39 kDa), and Trx-pro region (~18 kDa). There was noticeably lower concentrations (≥ 10-fold) of purified protein when incubated at 37°C, compared to 24°C (0.05-0.2 mg/mL).

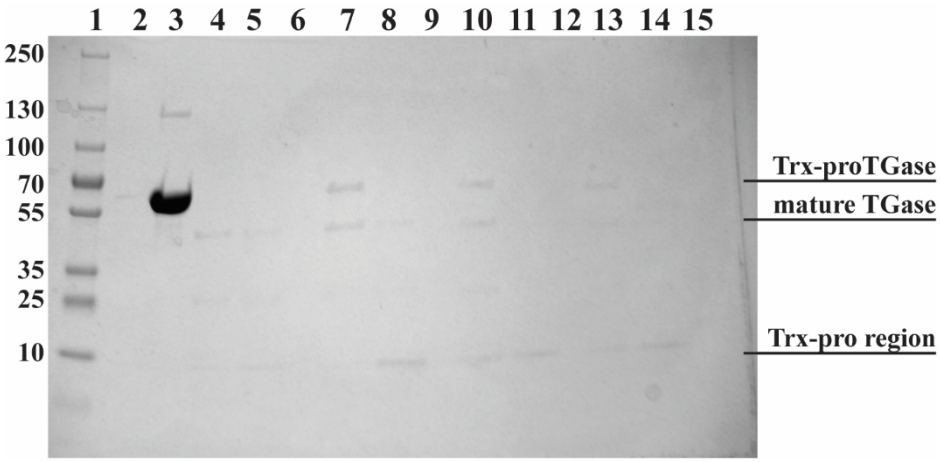

Figure 29 – Trx-proTGase SDS-PAGE. *Lane 1 is the PageRuler Plus Prestained Ladder. Lane 3 is the mTG positive control. Lanes 4-5 are purified SNTGA from 24°C and 37°C inductions, respectively. Lanes 7-8 are purified H_2O_2-Trx-proTGase induced for 6 hours at 24°C and 37°C, respectively. Lanes 10-11 are purified H_2O_2-Trx-proTGase induced for 12 hours at 24°C and 37°C, respectively. Lanes 13-14 are purified H_2O_2-Trx-proTGase induced for 18 hours at 24°C and 37°C, respectively. Lanes 2, 6, 9, 12, and 15 are empty.*

The colormetric activity assay was used to test mTG activity after 16 hour incubation with 100:1 ratio of purified H_2O_2-Trx-proTGase to trypsin to fully cleave the Trx-pro region. H_2O_2-SNTGase induced for 6, 12, and 18 hours at 24°C yielded the highest activity for

cleavage at 4°C. H_2O_2-SNTGase induced at 37°C yielded low activity for cleavage at 4°C. As cleavage temperature was increased (24°C, 30°C, and 37°C), activity decreased from 3.0 U/mg to ~0.5 U/mg.

Table 3 – H_2O_2-SNTGase activity.

Induction Temperature (°C)	Induction Time (hr)	AVG (U/mg)	STDEV
24°C	6	5.2	0.6
	12	3.0	0.7
	18	1.9	0.7
37°C	6-18	1.6	0.7

As a control, WT-SNTGA was induced for 18 hours at 24°C; purified SNTGA was cleaved at 4°C, yielding a specific activity of 17.2 ± 2.4 U/mg enzyme which is comparable to the specific activity determined by Yu *et al.* after extensive optimization.[51] Additionally, purified SNTGA cleaved at 30°C and 37°C yielded a specific activity of 15.7 ± 0.1 U/mg.

4.4 Conclusion

For efficient and uniform Protein G surface display with AF488 binding, pG-AIDA1 yielded > 90% uniform, saturating amounts of Protein G surface display within 2 hours at 24°C, independent of strain design. However, as induction temperature increased, variation of surface display increased and percentage of Protein G surface-displayed decreased; lower surface-display expression (20-25% LW12, 55-60% WT) was found, and increased time was required to achieve > 60% of surface display at 37°C for both WT and LW12. The fast and highly efficient Protein G surface display within 2 hours at 24°C allows the pG-AIDA1 system to be used for both quorum-sensing and non-quorum sensing platforms and biotherapeutics. Specifically for wound-healing based biotherapeutics, a human IgG Annexin 2 antibody can be bound to the surface displayed Protein G for site-specific bacterial docking

at the wound site. As noted in the previous chapter, the binding between Protein G and a targeting antibody (e.g., Annexin 2) would be subject to further study. Importantly, the Annexin 2 is only upregulated at the wound site, as they enhance wound healing via signaling pathways and aid the intestinal epithelial cells' cytoskeleton remodeling[19,95].

Separately, using the H_2O_2-SNTGase yielded soluble protein in significantly shorter time. Yu *et al.* developed and characterized the SNTGase system was for overexpression and optimal activity; however, expressing the H_2O_2-SNTGase for only 6 hours at 24°C yielded up to 0.2 mg/mL of soluble protein, with a reported activity of ~5.5 U/mL. This activity is 3-4-fold lower compared to the optimized, overexpressed conditions; however, the active mTG can aid crosslinking in a time-efficient manner compared to no mTG. Importantly, the lower mTG concentrations produced in our work potentially benefits the therapeutic application, since an increased expression of transglutaminase is linked to Celiac disease[44,96]; additionally, the food industry's increased use of mTG for various processing and manufacturing applications[96] leads to more questions of health and the complications caused from daily mTG consumption.

Thus, a balance needs to be achieved in the biotherapeutics – low but active mTG and delivered only at the targeted site. In conclusion, by lowering the temperature to 24°C and reducing the induction concentration and time needed for Protein G surface display, the conditions were optimized for mTG and other temperature-sensitive biotherapeutic expression for a future single bacterial-based biotherapeutic.

Chapter 5: Single Bacterial System: Motility, Therapeutic Expression, and Self Lysis

5.1 Introduction

In order to construct a single *E. coli* biotherapeutic delivery system, the *E. coli* need to release the biotherapeutic at the wound site and subsequently die. Previous studies have accomplished this using T4 bacteriophage lytic proteins to lyse *E. coli*, but this method requires toxic inducers for regulation[55]. Naturally, *E. coli* trigger the colicin lysis protein E7 via the SOS response system due to stressful environmental conditions[97]. More recent studies looked to construct synthetic circuits that express E7 in response to arabinose[55], 3OC12HSL (from *P. aeruginosa*)[14], and the antibiotic mitomycin C[58]. Therefore, I hypothesize that E7 lysis can be achieved in the pHW02 system, using H_2O_2 as a lysis controller.

Specifically, in this work, I engineer E7 after CheZ in the pHW02 system for H_2O_2 induced lysis. Because the *cheZ* gene is directly after the promoter and CheZ expression is extremely fast, it is possible for the bacteria to pseudotax before E7 lysis expression begins. Since E7 lysis occurs by damaging the inner membrane and permeabilizing the outer membrane[14,58], it allows for protein to be released into the supernatant, including a biotherapeutic. I hypothesize if [1]whether there is lysis in an H_2O_2 dose-dependent response, [2]the effects of metabolic burden on lysis, and [3]whether mTG can be expressed as a therapeutic, released into the supernatant via E7 lysis, and retain activity. To model mTG biotherapeutic release and subsequent activity, I used pET32aΔ-SNTGA.

5.2 Materials and Methods

DNA Manipulation and Growth Conditions. The *E. coli* K-12 W3110-*ΔcheZ* strain (HCW01) was constructed using a one-step inactivation method [64]. The genetic constructs

developed in this study were assembled using the Gibson Assembly protocol[93]. Briefly, *RBS-E7* gene (170 base pairs, provided by Dr. Matthew Wook Chang) was amplified using the Gibson primers specified in

Table 4. The primers were designed to have a minimum 15 base pair overlap with the base pairs flanking the insert site; the reverse primer was designed to remove the end codon after *cheZ*. Separately, 1 µg of pHW02 was digested with the HindIII restriction enzyme. The *RBS-E7* and pHW02 fragments (5:1 ratio) were ligated with Gibson Assembly Master Mix following the Gibson Assembly protocol, with saturating amounts of *RBS-E7* added and subsequently transformed into chemically-competent NEB 5-alpha *E. coli*. Plasmid DNA (**Figure 30**) from each selected clone was isolated for sequencing using Qiagen miniprep.

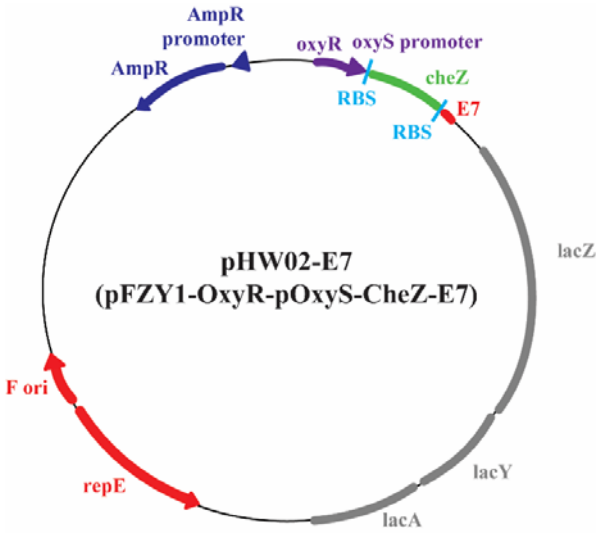

Figure 30 – Plasmid design of pHW02-E7.

The correct sequence plasmid (no mutations) was transformed into *E. coli* K-12 *cheZ* knockout strain (HCW01); additionally, plasmid DNA (**Figure 30**) from each selected *E. coli* clone was isolated for sequencing using Qiagen miniprep, and the clones with no mutations were kept in glycerol stocks for the experiments. The same Gibson protocol was followed to replace the ampicillin resistance with kanamycin resistance in pET32aΔ-SNTGA. The

transformation and sequencing protocols were followed to co-transform pHW02-E7 with either pET200-T5-eGFP or pET32aΔ-SNTGA.

Table 4 – Strain designs and primer designs of pFZY1-oxyR-poxyS-cheZ-E7.

Strain (Short Name)	**Plasmid**	**Phenotype**
W3110-*ΔcheZ* (HCW01-pHW02-E7)	**pFZY1-OxyR-*p*OxyS-CheZ-E7**	**H_2O_2-Controlled Run + Lysis**
	pET200-t5-eGFP	**Constitutive Green Fluorescence**
	pET32aΔ-SNTGA	**mTG (Therapeutic)**
Primer Name	**Primer Sequence**	
RBS-E7 (pFZY1-oxyR/S-cheZ) (Gibson forward primer)	**5'-CATATGATGGGACATCATCATCATCATGACGCCG -3'**	
RBS-E7 (pFZY1-oxyR/S-cheZ) (Gibson reverse primer)	**3'-TGCCCCCGGGGGGATGGGGAGTAAGCTTCTCGAGTCACGG-5'**	
Kanamycin (pET32aΔ-SNTGA) (Gibson forward primer)	**5'-GAGTAAACTTGGTCTGACAGTTCAAATATGTATCCGCTC-3'**	
Kanamycin (pET32aΔ-SNTGA) (Gibson reverse primer)	**3'-AACAAATAAAAAGATTTATGTAGTCTTCTTGAGCAGTTC-5'**	
pET32aΔ-SNTGA (Gibson forward primer)	**5'-TGTATTTAGAAAAATAAACAAATAGGGGTTCCGC-3'**	
pET32aΔ-SNTGA (Gibson reverse primer)	**3'-GACAGTCTGGTTCAAATGAGTATATATGAAATCTAAC-5'**	

Bacteria were grown in LB media supplemented with either ampicillin (50 μg/mL) or ampicillin and kanamycin (50 μg/mL) and incubated at 37°C in a shaker at 250 rpm for all growth experiments. For all overnight inoculations, bacteria were grown from glycerol frozen stock; all morning re-inoculations were adjusted with sterile media to OD_{600} 0.05. The strain-plasmid nomenclature and shortened names are listed in

Table 4.

E7 Growth Characterization. *E. coli* HCW01-pHW02-E7 (with pET200-t5-eGFP for two plasmid experiments) were inoculated into 200 mL of LB in 1000 mL flasks, and shaken at 37°C until OD_{600} ~0.4. Cells were gently pelleted and resuspended in MOPS media (0.5% glucose, Teknova) at OD_{600} 0.4 and shaken at 37°C for 10 minutes to allow for metabolic adjustment. The bacteria were split into 25 mL samples in 125 mL flasks for lysis induction with 0-200 μM H_2O_2 and shaken at 24°C and 37°C. 1.5 mL samples were taken at 2, 4, and 6 hours; after sample volumes were removed, the volume was replaced with another dose of H_2O_2. For the 2 and 6 hour timepoints, 20 μL of bacteria was plated on LB agar plates supplemented with ampicillin (50 μg/mL) and incubated at 37°C overnight.

Quantifying E7 Lysis. The cell pellets were resuspended in PBS and stained with 5 μg/mL of propidium iodide (PI, Sigma Aldrich) for 10 minutes. PI cannot penetrate the bacterial membrane, so only porous bacteria could be stained with PI. Multiple wash steps with PBS were performed, and samples were fixed with 4% paraformaldehyde at room temperature, shaking for 30 min. Multiple wash steps with PBS were performed. Samples were resuspended in PBS and stored in 4°C overnight. For FACS analysis and confocal microscopy, technical and biological duplicates were obtained. For phase-contrast microscopy, images were obtained before the bacteria were fixed.

For FACS experiments, WT-pFZY1 (unstained), HCW01-pHW02-E7 (dead), and HCW01-pHW02 + pET200-T5-eGFP (live, green, 2 plasmid experiments) were controls for setting the scattering and laser(s). The FACS PE (red) laser was used to quantify dead cells. For the two plasmid bacteria, the FITC (green) laser was used to identify only eGFP. For the FACS experiments with eGFP, compensation was performed on the PE (red, dead) laser. Compensation accounts for the spectral emission overlap between the two lasers; compensation was performed on the single-stained PI control to calculate and subtract the green (eGFP) bleed-over into the red (PI) detector (**Figure 36-c**). This was performed using the compensation tool in the BD FACS Diva software. Briefly, the single-stained PI control was plotted on a log-log scatter plot; the x-axis was PE fluorescence, and the y-axis was FITC fluorescence. 15% FITC fluorochrome spectral overlap into the PE fluorochrome was calculated to negate the small percentage of FITC scattering in the log-log plot.

E7 Supernatant Protein Characterization. Bacteria timepoint samples were gently centrifuged to prevent the cells from shearing and releasing protein into the supernatant. Uniform amounts of supernatant were filter-concentrated (Amicon Ultra – 0.5 mL, 10 kDA cut-off, EMD Millipore). Concentrated samples were boiled with 2x SDS dye. Pre-stained ladder (PageRuler Plus Prestained Protein Ladder, ThermoFisher Scientific) and 25 µL of boiled samples were loaded into 12% SDS-PAGE gels (Bio-Rad). The SDS-PAGE gel was stained overnight with Coomassie Blue and destained (45% methanol, 10% glacial acetic acid). The gel image was obtained using the ChemiDoc Touch Imaging System (Bio-Rad). Line profile analysis was conducted using FIJI software[98] to determine the mean greyscale pixel intensity across the protein band. Multiple line measurements across different heights of the band were taken to make a total mean intensity. Induced samples \50-200 µM H_2O_2) were averaged together for comparison to the not induced samples.

Microbial Transglutaminase Expression via Lysis. *E. coli* HCW01-pHW02-E7 with pET32aΔ-SNTGA were inoculated into 200 mL of LB in 1000 mL flasks, and shaken at 37°C until OD_{600} ~0.25. Cells were gently pelleted and resuspended in MOPS media (0.5% glucose, Teknova) at OD_{600} 0.25 and shaken at 37°C for 10 minutes to allow for metabolic adjustment. The bacteria was then induced with 0.5mM IPTG to initiate mTG expression. For aerobic conditions, the bacteria was shaken at 24° for 6 hours; for anaerobic conditions, the bacteria was placed (without shaking) in an anaerobic chamber (nitrogen, 2% hydrogen) for 6 hours. After mTG induction for 6 hours, the bacterial culture were split into 50 mL samples in 250 mL flasks for lysis induction with 0 or 200 μM H_2O_2 and shaken at 24°C and 37°C for 2 hours. The bacteria samples were gently centrifuged. The supernatant was filter-concentrated (Amicon Ultra – 15 mL, 3 kDA cut-off, EMD Millipore). mTG was purified from the supernatant and tested for activity using the protocols outlined in **4.2.2**.

Statistical Analysis. For most experiments, one-way ANOVA using a multiple comparisons' Tukey-Kramer post-test were performed using Matlab (version R2015a). ANCOVA linear regression analysis was performed using Prism (Graphpad Prism 7). α values of 0.05 were used to indicate statistical significance. Data are reported as mean values and standard deviation of the error, unless otherwise stated.

5.3 Results and Discussion

5.3.1 Characterizing H_2O_2-controlled bacterial lysis via E7 using pHW02

Initial growth studies were carried out to test whether the engineered pHW02-E7 cells exhibited enhanced lysis in the presence of H_2O_2. In addition to evaluating whether a potential dose response could be obtained, I was interested to find whether lysis increased with time and if the bacteria would adapt to survive lysis. In **Chapter 2**, I had quantified pHW02's survival threshold in response to increasing H_2O_2 concentrations and induction

temperatures. With the addition of the E7 lysis protein, I conducted growth experiments using HCW01-pHW02-E7 (H_2O_2-mediated *oxyS* transcription of CheZ and E7). In **Figure 31**, I grew cells at 37°C until OD ~0.4, gently spun down the cells and resuspended them in MOPS media; after the cells were shaken for 10-15 minutes for metabolic adjustment, the cultures were split, induced with H_2O_2, and grown at 24°C and 37ºC to examine how the temperature and H_2O_2 concentrations affect bacterial growth. Regression analysis indicated that all preinduction growth rates were similar (data not shown). Then, analogously, after a short transient phase, cultures induced at 24°C all grew at similar rates irrespective of H_2O_2; however, linear regression analysis confirmed that the cultures induced at 37°C significantly varied from both the uninduced 37°C culture and all 24°C growth concentrations (**Figure 31-b, c**). These results indicate that growth could be occurring at both 24°C and 37°C regardless of H_2O_2 dose and with higher efficiency at 24°C, but more analyses were required.

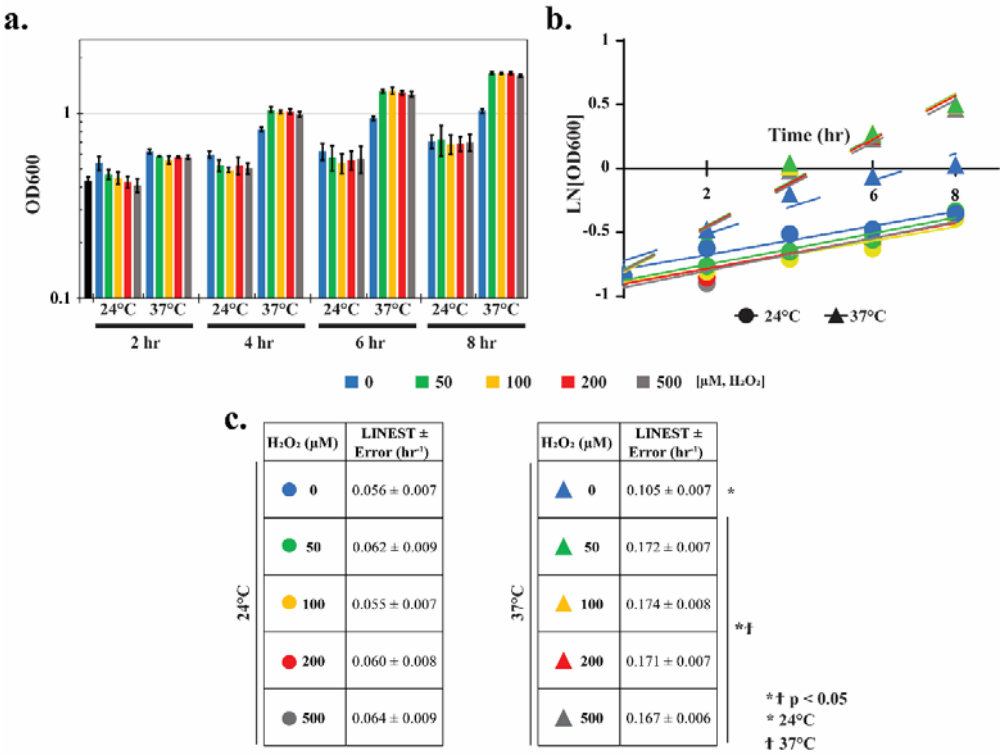

Figure 31 – Effects of H_2O_2-E7 lysis on cell growth. *a. Cell growth bar chart. HCW01-pHW02-E7 growth at different levels of H_2O_2 and induction temperatures over time. b. Post-induction growth curves. HCW01-pHW02-E7 growth with 0-500 μM H_2O_2 induction concentrations at 24°C and 37°C. Lines indicated are least squares regressed best fits. c. Tabulated specific growth rates. HCW01-pHW02-E7 growth with 0-500 μM H_2O_2 induction concentrations Linear regression analyses are reported as * † with $p < 0.05$. * indicates the samples differed significantly from 24°C. . † indicates the samples differed significantly from 37°C.*

To quantitatively characterize E7 lysis, I conducted FACS experiments (**Figure 32**) using the same samples from the growth studies. Briefly, HCW01-pHW02-E7 samples were stained red with PI and fixed to identify and quantify the cells in which E7 lysis ruptured occurred. PI can only penetrate cells through ruptured membranes, not cells with intact membranes. WT-pFZY1 and dead HCW01-pHW02-E7 samples were used to set the voltage, scattering, and gating (**Figure 32-b, c**) for live (unstained) versus dead (PI, stained), respectively. To ensure lysis, overnight HCW01-pHW02-E7 culture was induced with > 100 mM H_2O_2. At H_2O_2-lysis induction, a baseline dead value was reported at ~30% (**Figure 32-c**); as a control, HCW01-pHW02 death (no E7 lysis) also at OD 0.4 was recorded as ~35%. As time increased, there was a statistically signifcant decrease in cell death, regardless of

H_2O_2 dose. At 2 hours, I observed a population shift to the right, indicating that an increased number of bacteria were dying (**Figure 32-d**, 37°C shown). However, as time increased, a bimodal population emerged, indicating that a population of bacteria were dying, but there was also a population living and/or surviving (**Figure 32-d**).

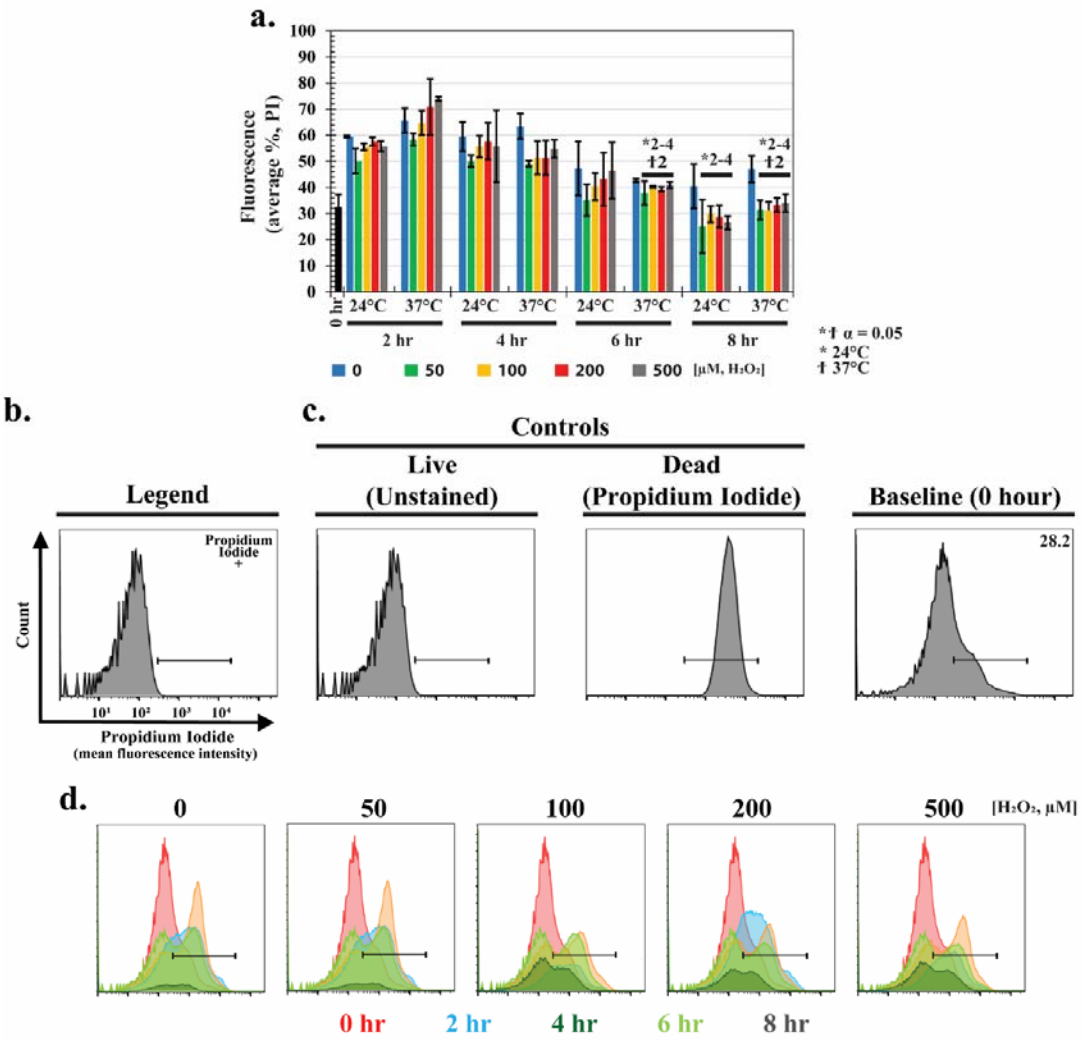

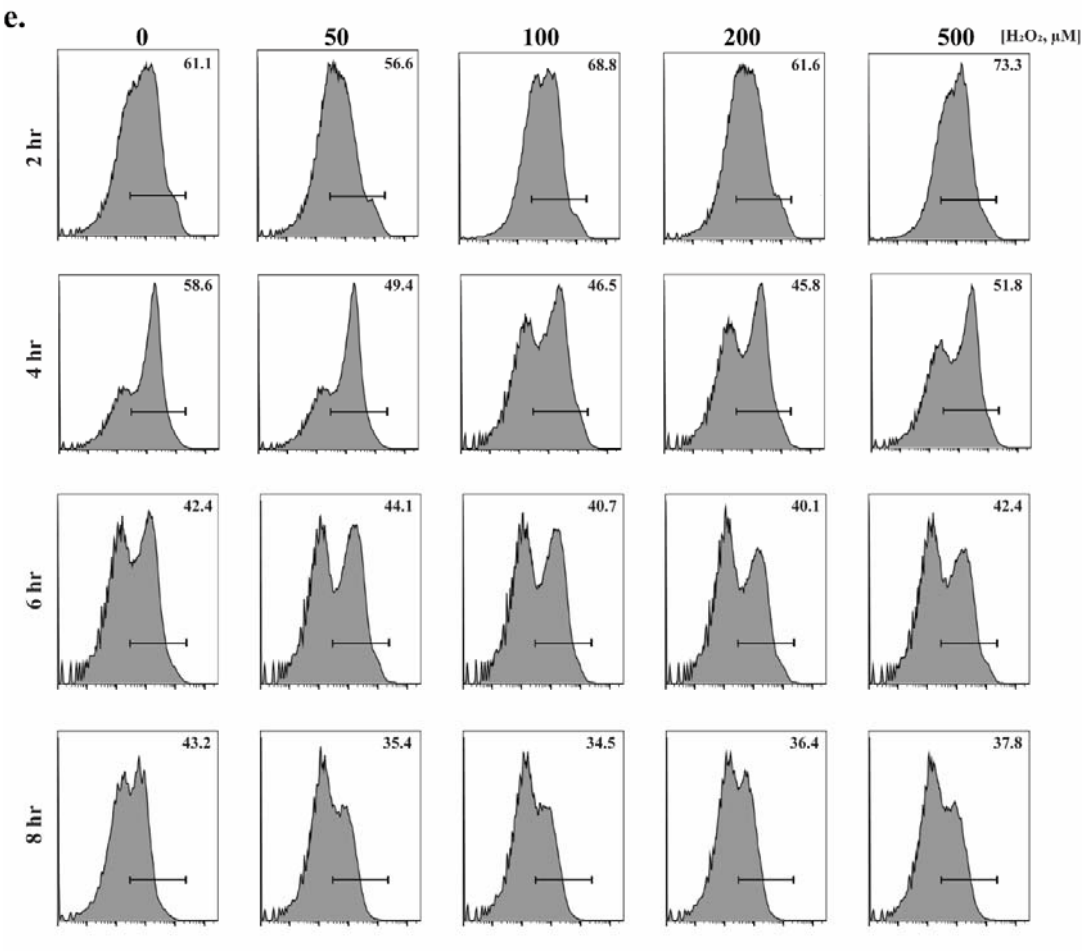

Figure 32 – FACS Analysis of H_2O_2-dosing-E7 lysis. *a. Average percentage of propidium-iodide (dead) stained cells. HCW01-pHW02-E7 were induced with 0-200 µM H_2O_2, and sampled and dosed every 2 hours. Tukey-Kramer ANOVA and multiple comparisons analyses were performed with α = 0.05. * indicates the samples differed significantly from 24°C. † indicates the samples differed significantly from 37°C. b. FACS histogram legend for PI-stained cells. The percentage of PI-stained (dead) cells is in the upper right corner. c. Control and Baseline histograms. Control histograms are unstained WT-pHW02 and dead HCW01-pHW02-E7 cells. The Baseline histogram is the 0 hr timepoint for HCW01-pHW02-E7 lysis. d. HCW01-pHW02-E7 37°C histogram overlay. e. HCW01-pHW02-E7 37°C histograms.*

In order to observe the effects of lysis on intracellular protein release, the supernatants from the growth/FACS experimental samples (0, 2-6 hrs) were concentrated and loaded in an SDS-PAGE gel (**Figure 33**). While there were significantly marked bands visible in the WT-pFZY1 (non-lysed) sample, they were distinct, discrete bands (**Figure 33-a, b; Lane 1**) similar to the 0 hr sample (**Figure 33-a, b; Lane 3**), compared to HCW01-pHW02-E7. For samples induced at 24°C (**Figure 33-a**), I observed low levels of protein

across all sizes. Importantly, when samples were induced at 37°C (**Figure 33-b**), increased levels of protein were visible across all time points; markedly more protein was observed after 4 hours (Lanes 8-11, 0-200 µM) and 6 hours (Lanes 12-15, 0-200 µM) compared to 2 hours (Lanes 4-7, 0-200 µM). These results indicated that despite the bimodal population over time and decrease in percentage of dead cells, the intracellular protein was still released into the supernatant.

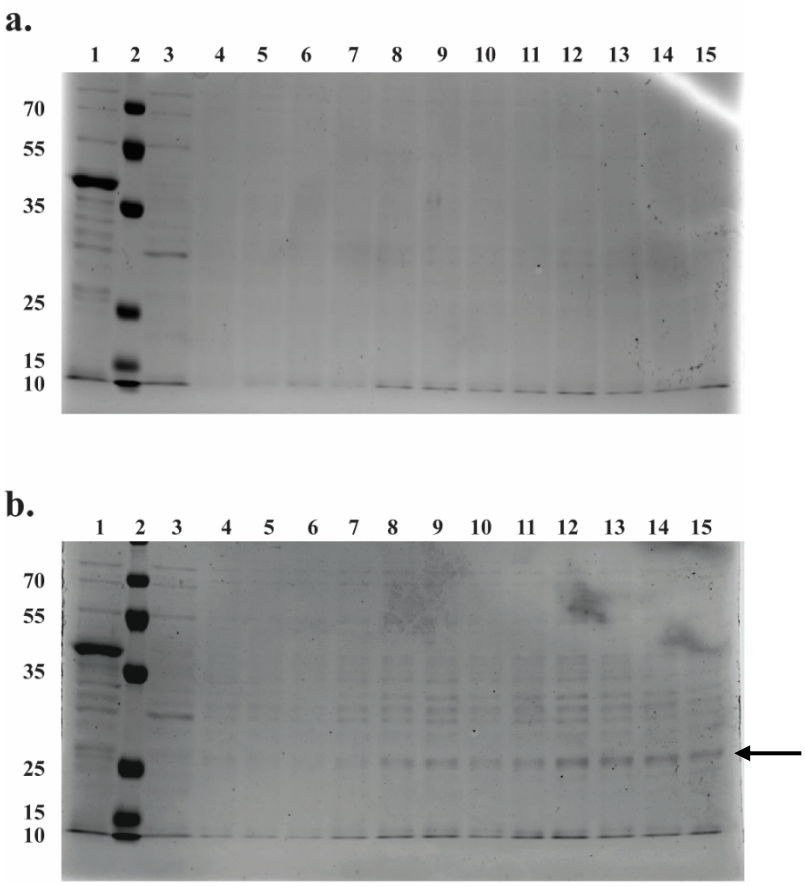

Figure 33 – HCW01-pHW02-E7 cell supernatant SDS PAGE. *a. HCW01-pHW02-E7 induced at 24°C. b. HCW01-pHW02-E7 induced at 37°C. For a and b, Lane 1 is WT-pFZY1. Lane 2 is the PageRuler Plus Prestained Ladder. Lane 3 is the 0 hour timepoint. Lanes 4-7 are the cell surpernatant after 2 hours of induction (0-200 µM H_2O_2). Lanes 8-11 are the cell surpernatant after 2 hours of induction (0-200 µM H_2O_2). Lanes 12-15 are the cell surpernatant after 2 hours of induction (0-200 µM H_2O_2). b. HCW01-pHW02-E7 + pET200-t5-eGFP samples induced at 37°C. Lane 1 is the PageRuler Plus Prestained Ladder. Lane 2 Lanes 3-6 are the cell surpernatant after 2 hours of induction (0-200 µM H_2O_2). Lanes 7-10 are the cell surpernatant after 2 hours of induction (0-200 µM H_2O_2). Lanes 11-14 are the cell surpernatant after 2 hours of induction (0-200 µM H_2O_2).*

Additionally, in order to observe and characterize whether the bimodal population indicated if cells were still alive, I plated 20 µL of cells from designated induction concentrations and times (**Figure 34**). Despite induction with 200 µM H_2O_2 for 6 hours at 24°C and 37°C, all plates grew bacterial lawns.

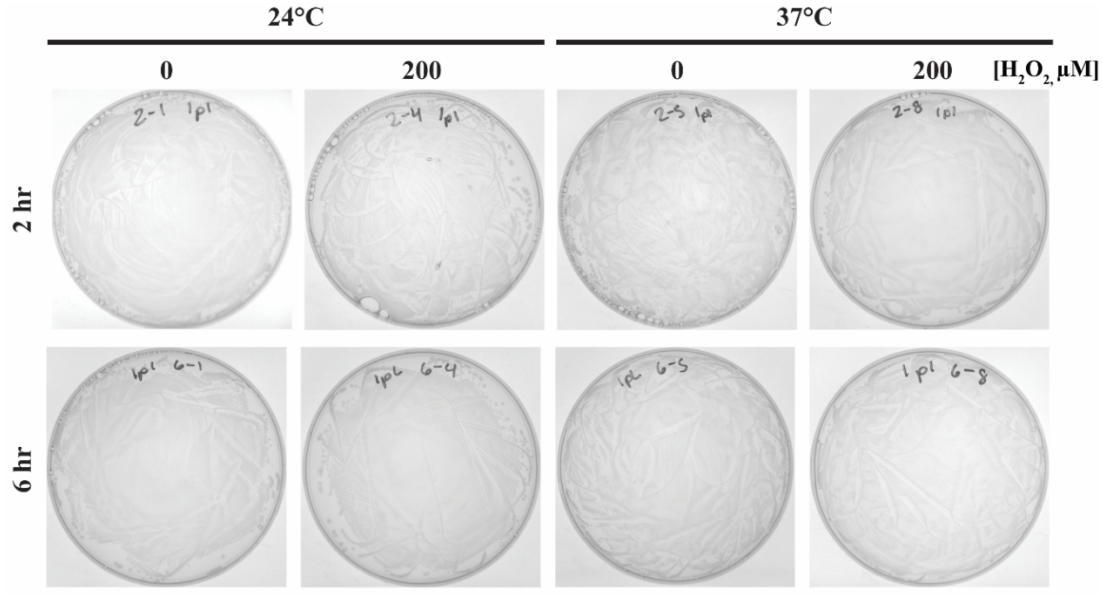

Figure 34 – HCW01-pHW02-E7 survival. *20 µL of cells from the designated H_2O_2 induction, temperature, and time were plated on LB agar plates (ampicillin, 50 µg/mL) to compare H_2O_2-induced E7 lysis efficiency. Plates were incubated overnight at 37°C.*

5.3.2 Characterizing pHW02-E7 lysis with increased metabolic burden

In **2.3.5**, I examined the motility burden placed on HCW01-pHW02 with a second plasmid encoding constitutive protein expression, pET200-t5-eGFP; this addition of a second plasmid also conferred reduced H_2O_2 uptake rates. Using these results, I examined how adding pET200-t5-eGFP affected bacterial growth, lysis, and amount of protein release into the supernatant when co-expressed with pHW02-E7. The lysis experiments conducted in this section (**Figure 35**) mirror those conducted in **5.3.1**. The biological replicates (B.R.1, B.R.2, B.R.3) were analyzed separately due to their differences in growth and lysis behaviors over the course of the experiments. Regression analysis indicated that all preinduction growth rates

were similar (data not shown). Then, analogously, after a short transient phase, B.R.1 and B.R.3 cultures induced at 24°C all grew at similar rates irrespective of H_2O_2; however, linear regression analysis confirmed that the B.R.2 cultures induced at 37°C significantly varied compared to all 24°C growth concentrations (**Figure 35-b; left column**). These results indicated that lysis could be occurring at both 24°C and 37°C regardless of H_2O_2 dose and with higher efficiency at 24°C, but more analyses were required. Separately, B.R.2 cultures induced with 100 and 200 μM H_2O_2 at 24°C ad 37°C were statistically significantly lower ($p < 0.05$) than uninduced (0 μM H_2O_2) and 50 μM H_2O_2 cultures; however, linear regression analysis confirmed that the B.R.2 cultures induced at 37°C were significantly higher ($p < 0.05$) compared to all 24°C growth concentrations (**Figure 35-b; right column**). These results indicate that with the metabolic burden, dose-dependent and high percentages of lysis could be occurring at both 24°C and 37°C when dosed with higher amounts of H_2O_2 over time.

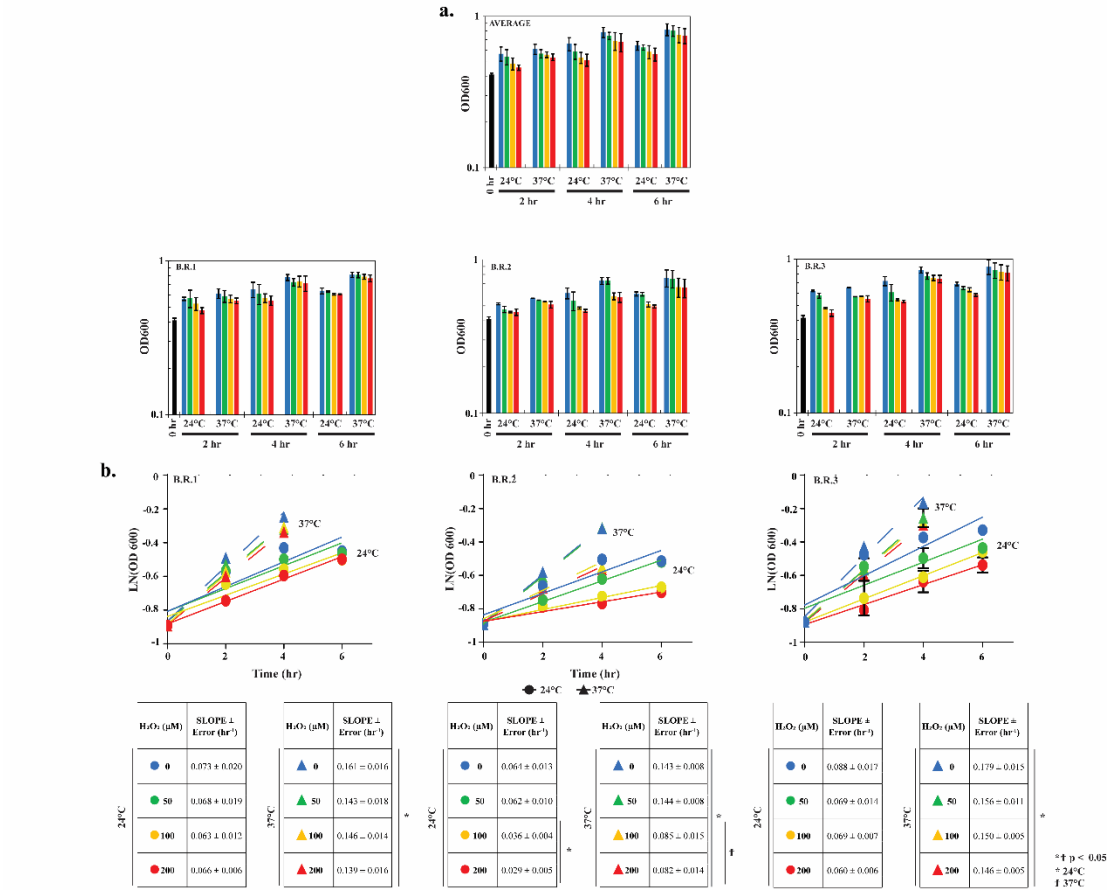

Figure 35 – Effects of H_2O_2-E7 lysis on cell growth with increased metabolic burden. *a. Cell growth bar chart. HCW01-pHW02-E7 + pET200-t5-eGFP growth at different levels of H_2O_2 and induction temperatures over time. b. Cell growth curves following H_2O_2 addition. Linear regression of biological replicates with 0-200 μM H_2O_2 induction concentrations at 24°C and 37°C. Lines indicated are least squares regressed best fits. c. Linear regression analyses. Linear regression analyses are reported as * † with $p < 0.05$. * indicates the samples differed significantly from 24°C. † indicates the samples differed significantly from 37°C. Biological replicates were analyzed separately.*

To quantitatively characterize E7 lysis with increased metabolic burden, I conducted FACS experiments (**Figure 36**) using the same samples from the growth studies. Briefly, HCW01-pHW02-E7 + pET200-t5-eGFP samples were stained red with PI and fixed to identify and quantify the cells in which E7 lysis ruptured occurred. WT-pFZY1, HCW01-pET200-t5-eGFP, and dead HCW01-pHW02-E7 samples were used to set the voltage, scattering, and gating (**Figure 36-b, c**) for unstained (no eGFP or PI present), live (FITC,

unstained), and dead (PE, stained), respectively. As a positive control and to ensure lysis, overnight HCW01-pHW02-E7 culture was induced with > 100 mM H_2O_2. All samples were compensated for the green spectal bleedover into the red spectrum; only the dead. At H_2O_2-lysis induction, a baseline dead value (0 hr) was reported at ~80% (**Figure 36-c**). As a control, HCW01-pHW02 + pET200-t5-eGFP death (no E7 lysis) also at OD 0.4 was recorded as ~55%. These values were markedly higher than just pHW02-E7, possibly due to increased metabolic burden and leaky expression of the H_2O_2 promoter. As time increased, there was a statistically signifcant decrease in cell death, regardless of H_2O_2 dose. At 2 hours, I observed a large percentage of the population were dead (70%-80%), regardless of dose, temperature, and biological sample (**Figure 36-d, e**). However, as time increased for B.R.1 and B.R.3, the percentage of dead bacteria decreased over time when induced at 37°C, while those induced at 24°C remained unchanged (**Figure 36-a, d**). However, when analyzing B.R.2 results, there was a statistically significant decrease in growth and increase in percentage of PI-stained cells when induced with 200 μM H_2O_2 at 24°C ad 37°C. Conversely, while lysis remained high at 4-6 hours for 24°C induction, lysis decreased at 4-6 hours (0-100 μM H_2O_2) for 37°C induction. These results generally confirmed the standard growth curve trends discussed previously.

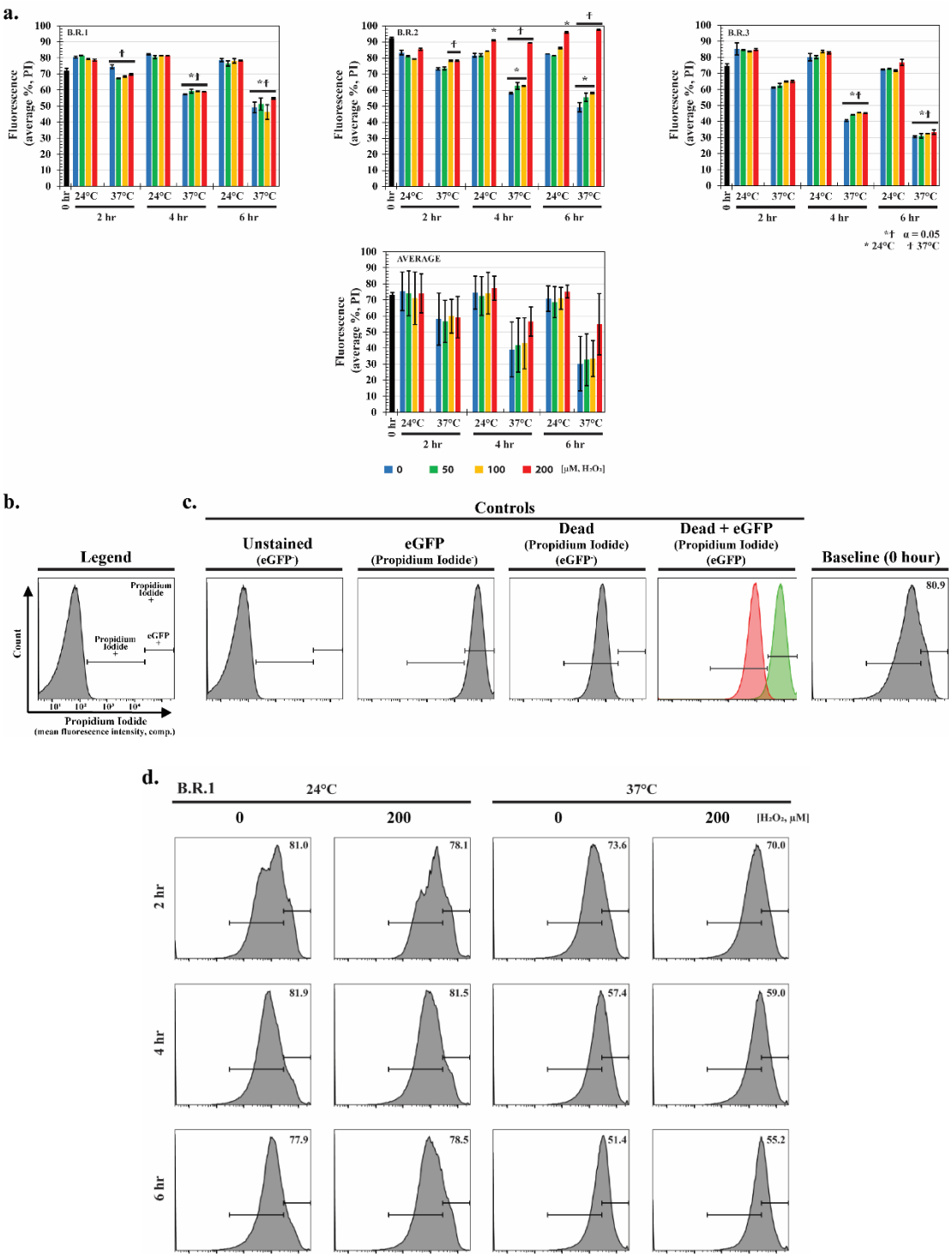
a.
B.R.1
B.R.2
B.R.3
AVERAGE
Fluorescence (average %, PI)
0 hr
24°C
37°C
2 hr
4 hr
6 hr
*† α = 0.05
* 24°C † 37°C
0
50
100
200 [μM, H2O2]
b.
Legend
Propidium Iodide +
eGFP +
Count
Propidium Iodide (mean fluorescence intensity, comp.)
c.
Controls
Unstained (eGFP-)
eGFP (Propidium Iodide-)
Dead (Propidium Iodide) (eGFP-)
Dead + eGFP (Propidium Iodide) (eGFP)
Baseline (0 hour)
80.9
d.
B.R.1
24°C
37°C
0
200
[H2O2, μM]
2 hr
4 hr
6 hr
81.0
78.1
73.6
70.0
81.9
81.5
57.4
59.0
77.9
78.5
51.4
55.2

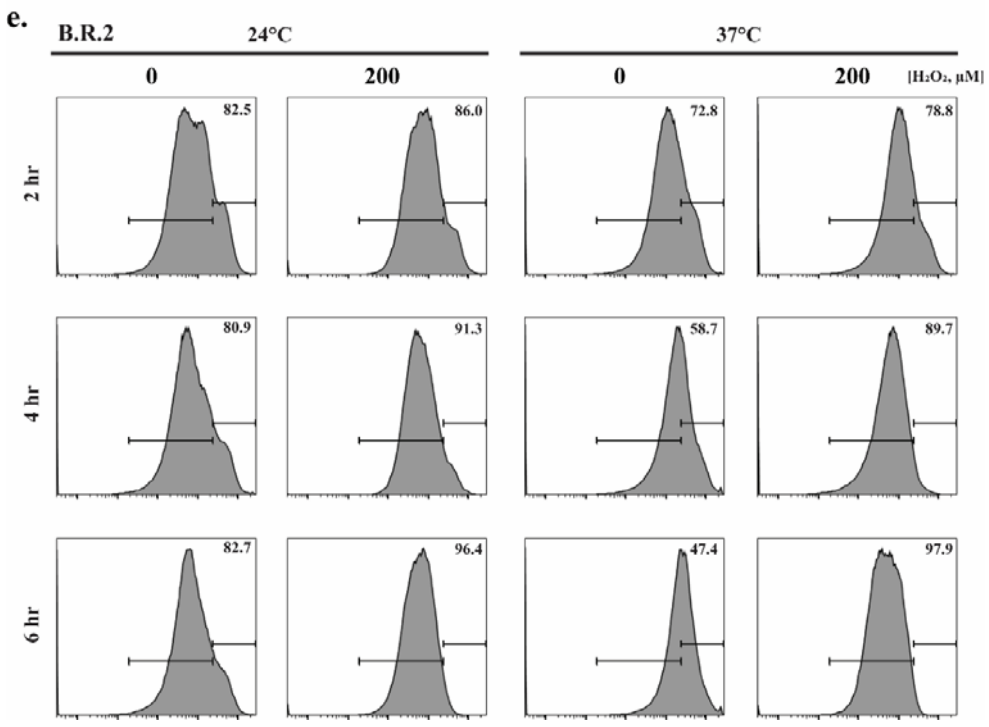

Figure 36 – FACS Analysis of H_2O_2-dosing-E7 lysis with increased metabolic burden. *a. Average percentage of propidium-iodide (dead) stained cells. HCW01-pHW02-E7 + pET200-t5-eGFP were induced with 0-200 µM H_2O_2, and sampled and dosed every 2 hours. Tukey-Kramer ANOVA and multiple comparisons analyses were performed with α = 0.05. * indicates the samples differed significantly from 24°C. † indicates the samples differed significantly from 37°C. b. FACS histogram legend for PI-stained cells with eGFP. The percentage of PI-stained (dead) cells is in the upper right corner. c. Control and Baseline histograms. Control histograms are unstained WT-pHW02, unstained HCW01-pFZY1 + pET200-t5-eGFP, and PI-stained dead HCW01-pHW02-E7 cells. The overlaid histogram shows the spectral bleedover of the green into the red which was negated using compensation. The Baseline histogram is the 0 hr timepoint for HCW01-pHW02-E7 + pET200-t5-eGFP lysis. d. HCW01-pHW02-E7 biological replicate 1 histograms. e. HCW01-pHW02-E7 biological replicate 2 histograms. The biological replicate histograms show only 0 and 200 µM H_2O_2 over time.*

Previously, percent lysis with increased metabolic burden was calculated using PI-staining and FACS. However, this did not indicate whether the cells were dead and/or expressing eGFP. Confocal microscopy was conducted using the same samples as the growth and FACS experiments to qualitatively express the presence or absence of PI and/or eGFP. Single color controls were used to set the laser (**Figure 37-a**); cells that were both red and green (dead and containing eGFP) looked yellow in the image overlay. B.R.1 images (0, 200 µM H_2O_2) reflected the data obtained by FACS, in that over time, there were red and yellow cells (indicating lysis) but also a significant portion of green cells (**Figure 37-b**). Also, a

portion of the cells were extremely long and red, indicating that they were replicating without dividing and eventually dying.

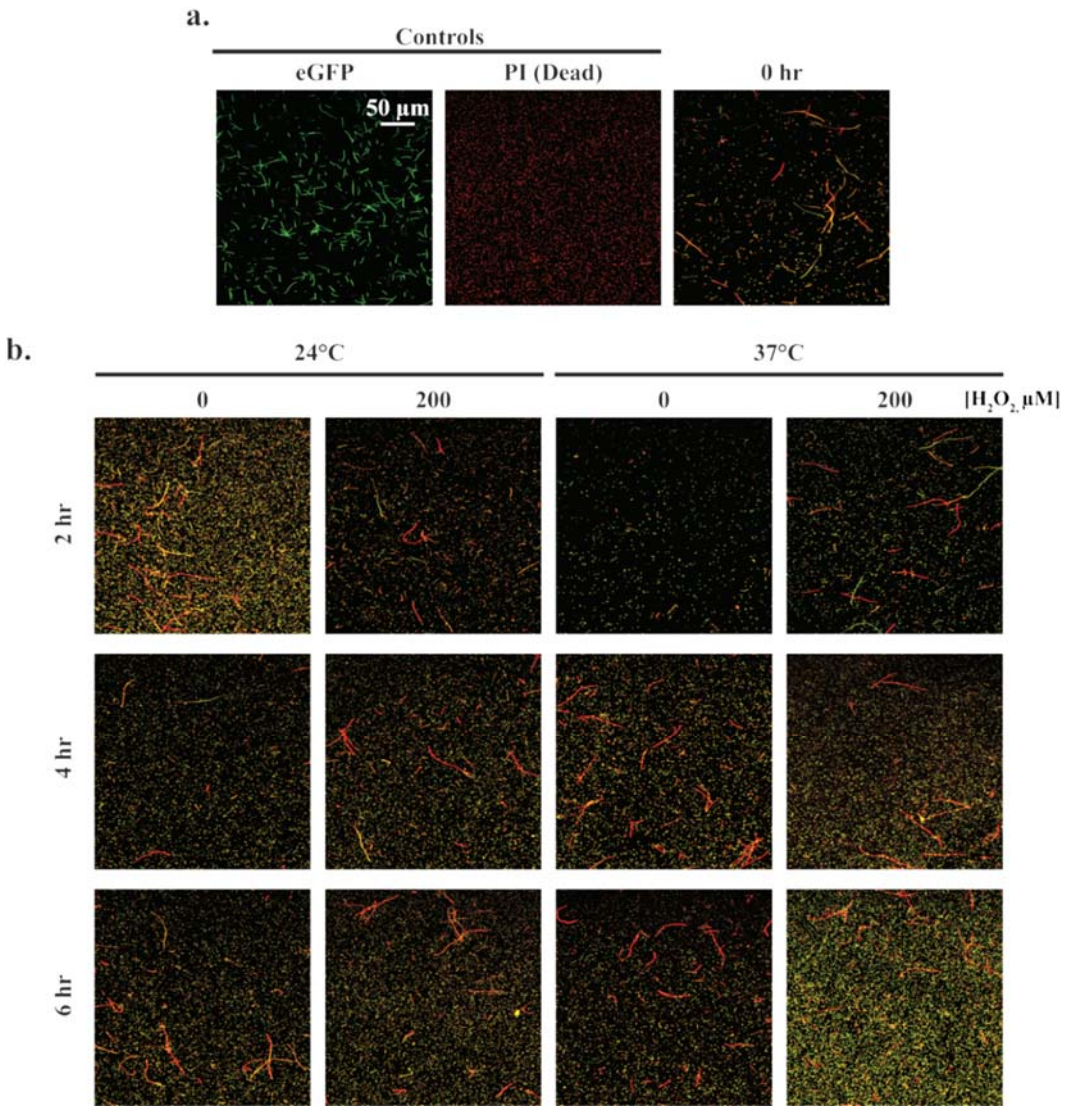

Figure 37 – Confocal microscopy of Biological Replicate 1 lysis. *The biological replicate images show only 0 and 200 µM H_2O_2 over time. Images were taken from the representative FACS samples. a. Control images and 0 hr. images. HCW01-pFZY1 + pET200-t5-eGFP is the green single color control. HCW01-pHW02-E7 dead (PI-stained) is the red single color control. Bacteria both green and red show as yellow in the images. b. Biological Replicate 1 images of 0 and 200 µM H_2O_2 over time.*

On the contrary, when examining B.R.2 images (0, 200 µM H_2O_2) over time, I observed complete lysis and release of eGFP after 6 hours of induction with 200 µM H_2O_2 (**Figure 38-**

a). Additional microscopy imaging conducted before the B.R.2 samples were fixed showed only cell debris with no eGFP fluorescence after 6 hours of induction with 200 µM H_2O_2.

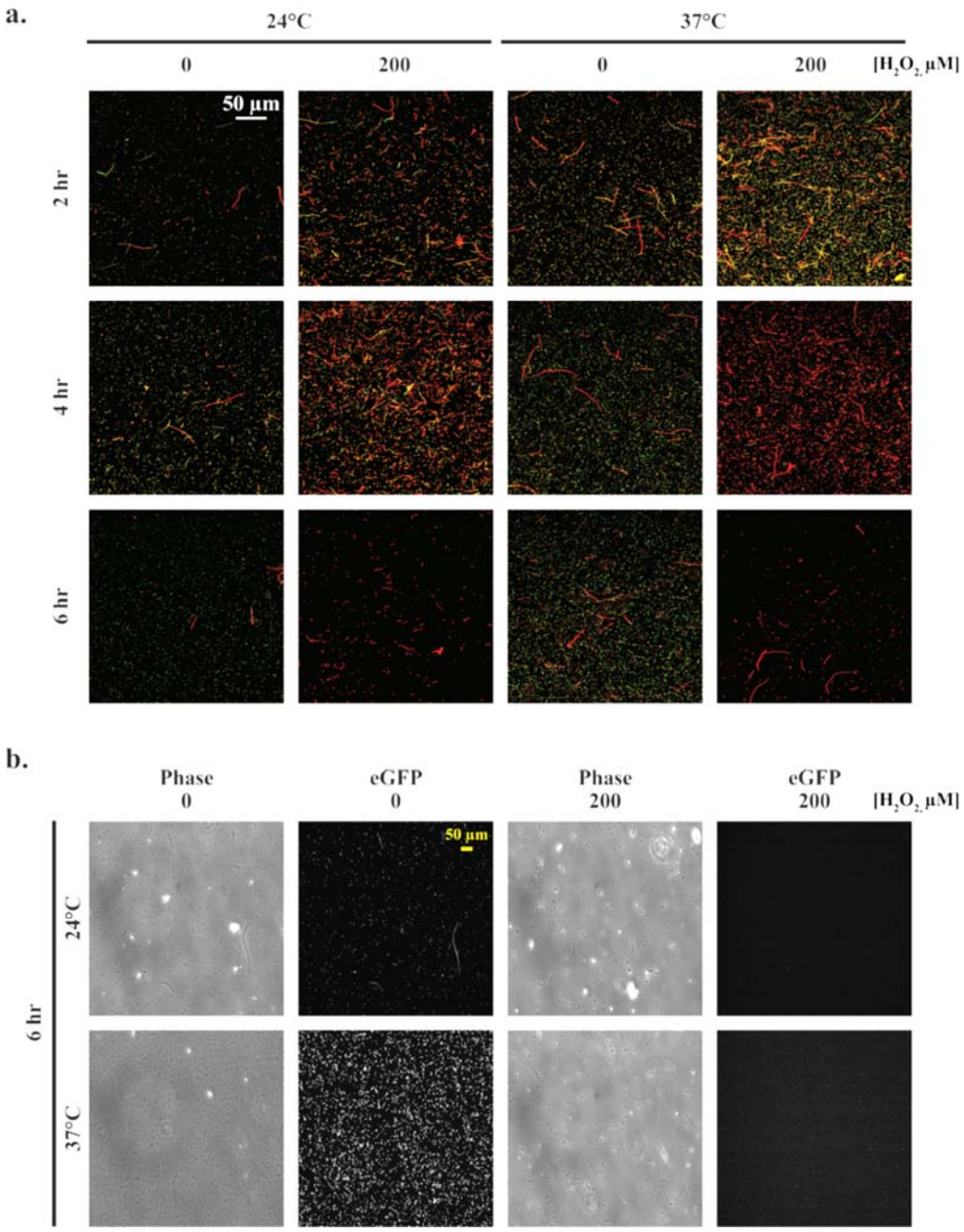

Figure 38 – Confocal microscopy of Biological Replicate 2 lysis. *The biological replicate images show only 0 and 200 µM H_2O_2 over time. Images were taken from the representative FACS samples. a. Biological Replicate 2 images of 0 and 200 µM H_2O_2 over time. b. 6 hr. phase contrast microscopy of Biological Replicate 2 samples. Phase contrast and GFP images were taken at the 6 hr. timepoint for 24°C and 37°C (0 and 200 µM H_2O_2) samples. Images were taken before PI staining and fixing for FACS.*

In order to observe the effects of increased metabolic burden on lysis and intracellular protein release, the supernatants from the growth/FACS experimental samples (0, 2-6 hrs) were concentrated and loaded in an SDS-PAGE gel (**Figure 39**). There were distinct, discrete bands visible in the WT-pFZY1 (non-lysed) sample (**Figure 39-a; Lane 1**), opposite to the 0 hour sample (**Figure 39-b; Lane 2**), compared to HCW01-pHW02-E7. For samples induced at 24°C (**Figure 39-a**), after 2 hours (Lanes 3-6, 0-200 μM), I observed significant, low levels of protein across all sizes; after 4 hours (Lanes 7-10, 0-200 μM) and 6 hours (Lanes 11-14, 0-200 μM), the bands appear to be darker, indicating more protein release. Importantly, when samples were induced at 37°C (**Figure 39-b**), increased levels of protein were visible across all time points (darker and/or thicker bands); markedly more protein was observed after 4 hours (Lanes 8-11, 0-200 μM) and 6 hours (Lanes 11-14, 0-200 μM). These results indicated that despite the increased metabolic burden and variation between biological replicates, the intracellular protein was still released into the supernatant.

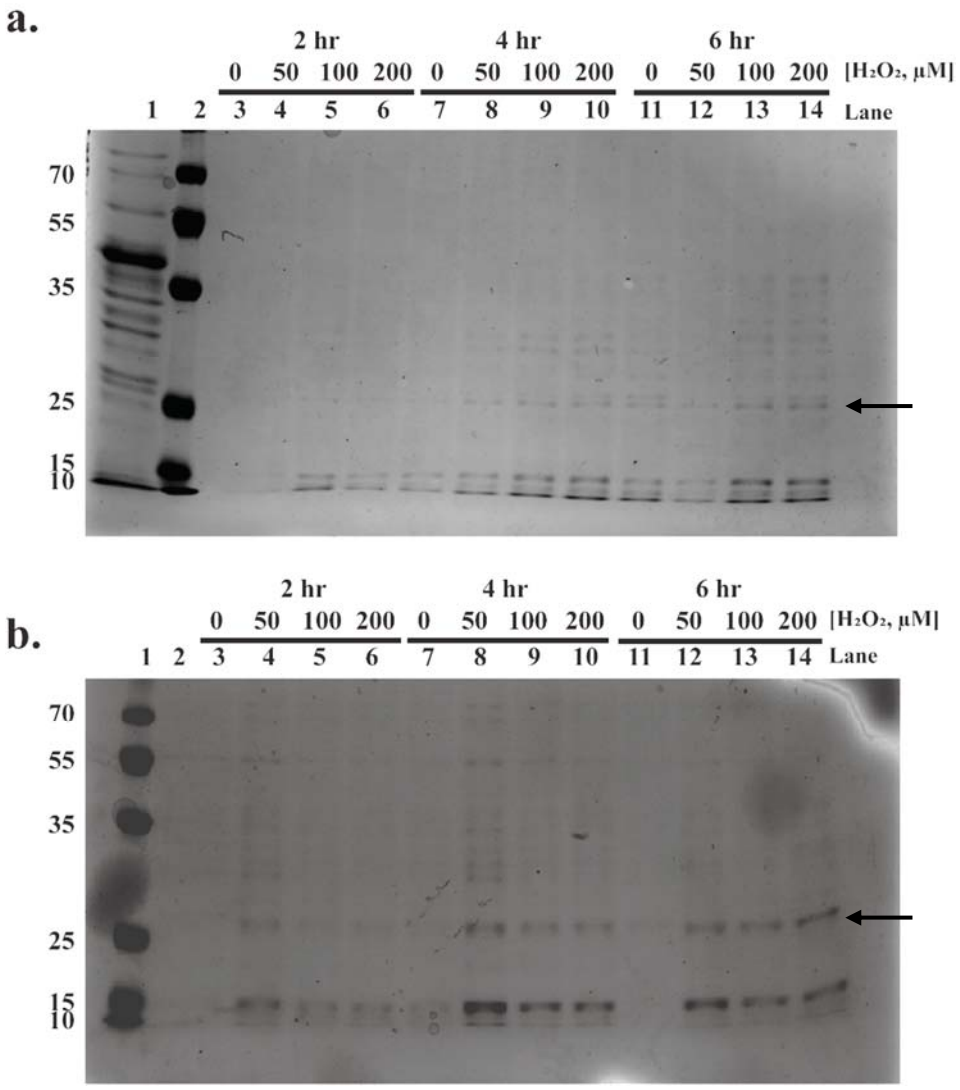

Figure 39 – B.R.2 HCW01-pHW02-E7 + pET200-t5-eGFP cell supernatant SDS PAGE. *a. HCW01-pHW02-E7 + pET200-t5-eGFP samples induced at 24°C. Lane 1 is WT-pFZY1. Lane 2 is the PageRuler Plus Prestained Ladder. Lanes 3-6 are the cell surpernatant after 2 hours of lysis (0-200 µM H_2O_2). Lanes 7-10 are the cell surpernatant after 2 hours of lysis (0-200 µM H_2O_2). Lanes 11-14 are the cell surpernatant after 2 hours of lysis (0-200 µM H_2O_2). b. HCW01-pHW02-E7 + pET200-t5-eGFP samples induced at 37°C. Lane 1 is the PageRuler Plus Prestained Ladder. Lane 2 is the 0 hour timepoint. Lanes 3-6 are the cell surpernatant after 2 hours of lysis (0-200 µM H_2O_2). Lanes 7-10 are the cell surpernatant after 2 hours of lysis (0-200 µM H_2O_2). Lanes 11-14 are the cell surpernatant after 2 hours of lysis (0-200 µM H_2O_2).*

In addition to the FACS analysis, a semi-quantitative analysis was performed to determine the mean grayscale intensity across the bands (indicated by the arrow in the SDS-PAGE images) (**Figure 40**). When comparing the average band intensity of not induced (-, 0 µM H_2O_2) versus induced (+, 50-200 µM H_2O_2, averaged), there was no dose-dependent

response of protein released. However, there was an increase in protein amount with increasing time (darker bands) (**Figure 40-a, b-24°C**). Conversely, at 37°C and with increased metabolic burden, there was an H_2O_2-dose-dependent response to amount of protein release over time (darker bands for induced samples) (**Figure 40-b-37°C**).

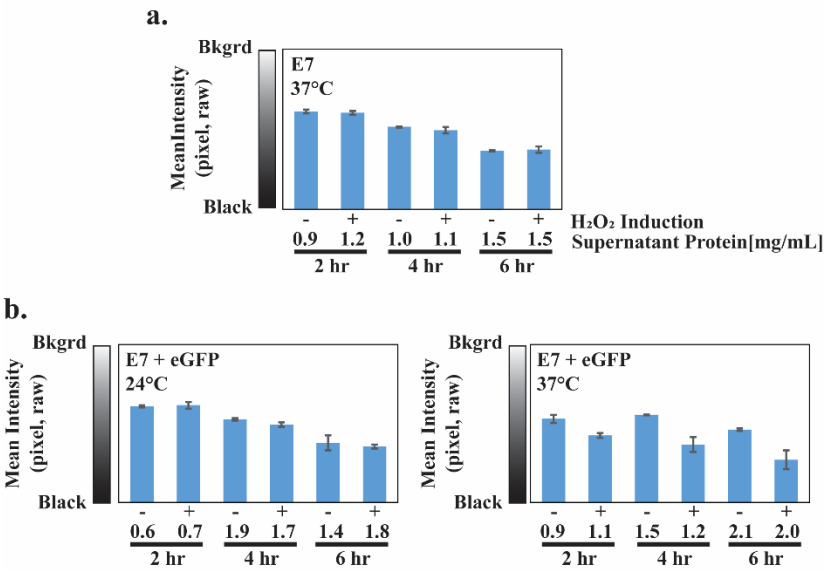

Figure 40 – Cell supernatant SDS PAGE analysis. *a. HCW01-pHW02-E7 samples induced at 24°C. b. HCW01-pHW02-E7 + pET200-t5-eGFP samples induced at 24°C. – samples are not induced. + samples are an average of the H_2O_2 induced range (50-200 µM H_2O_2). Total supernatant protein concentrations are listed below the – and +. Total supernatant protein*

Additionally, in order to observe and characterize whether the decreases and increases in percent of PI-stained cells indicated if B.R.2 cells were still alive or dead, respectively, I plated 20 µL of cells from designated induction concentrations and times (**Figure 41**). Despite induction with 200 µM H_2O_2 for 2 and 6 hours at 24°C, the plates grew bacterial lawns. More importantly, induction with 200 µM H_2O_2 for 6 hours at 37°C showed no bacterial colonies, confirming FACS and confocal results that nearly 100% lysis was achieved by 6 hours.

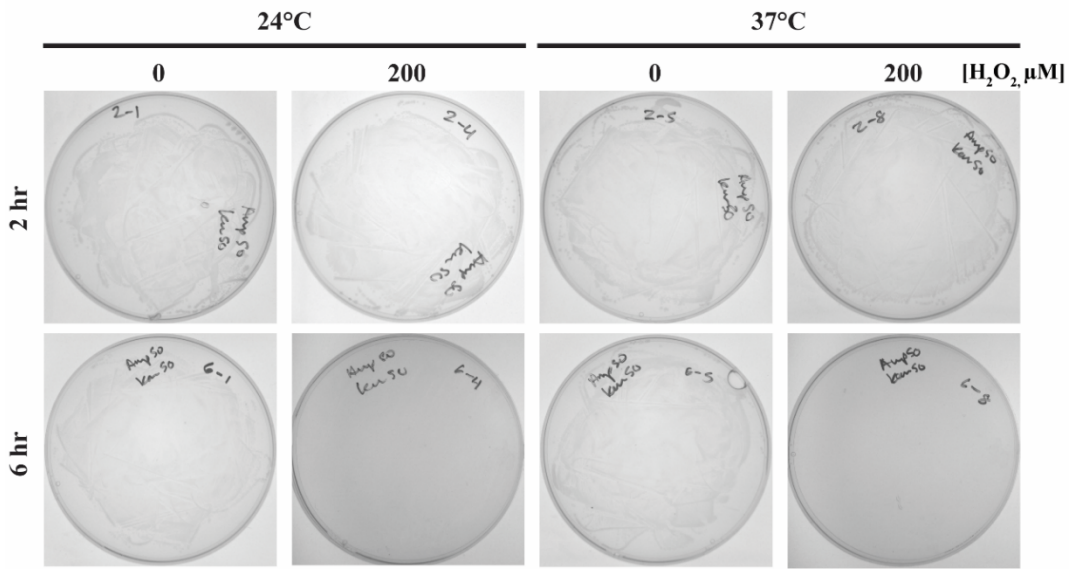

Figure 41 – HCW01-pHW02-E7 + pET200-t5-eGFP Biological Replicate 2 survival. *20 µL of Biological Replicate 2 cells from the designated H_2O_2 induction, temperature, and time were plated on LB agar plates (ampicillin and kanamycin, 50 µg/mL) to compare H_2O_2-induced E7 lysis efficiency with increased metabolic burden. Plates were incubated overnight at 37°C.*

5.3.3 Characterizing mTG biotherapeutic release with the E7 lysis system

In **5.3.2**, I showed that despite the increased metabolic burden, HCW01-pHW02-E7 still lysed and released protein into the supernatant. Based on these results and previous studies in **4.3.2**, I transformed HCW01 with pHW02-E7 and pET32aΔ-SNTGA to test whether mTG as a model biotherapeutic could be released into the supernatant and maintain its solubility and activity. When SNTGA was induced aerobically and with shaking at 24°C, low levels of soluble SNTGA (~1 µg/mL) was purified from the supernatant, regardless of H_2O_2-lysis induction concentration and temperature. Low activity levels of 3.5 U/mg (24°C lysis induction) 6.5 U/mg (37°C lysis induction) were calculated. To try to increase mTG production and solubility and decrease non-induced cell lysis, I induced SNTGA anaerobically, without shaking at 24°C. Although low levels of soluble SNTGA were purified from the supernatant (< 5 µg/mL), higher levels of activity were calculated from the H_2O_2-induced lysis samples. 10.2 and 12.8 U/mg enzyme activity were determined from 24°C and

37°C induced lysis, respectively, which is more comparable to the activity reported by Yu *et al.*[51].

5.4 Conclusion

While HCW01-pHW02-E7 did not result in H_2O_2-dose-dependent lysis for the single plasmid system, initially significant lysis of 60%-70% occurred at both 24°C and 37°C after 2 hours induction time. However, as time increased, percent lysis decreased, indicating that a surviving portion of bacteria were replicating, as seen in the bimodal population FACS histograms, and skewing the percent dead calculation, despite repeated H_2O_2 doses. Despite the decrease in percent dead, protein gels showed that a broad range of intracellular proteins were being released into the supernatant. When pHW02-E7 was induced with constitutive eGFP expression, higher percent lysis occurred after 2 hours of induction. Higher variation was observed and calculated between the two biological replicates. However, B.R.2 expressed a dose-dependent response to 200 μM H_2O_2, achieving nearly 100% lysis after 6 hours. Using FACS, confocal microscopy, and agar plates, I observed and confirmed that when lysis decreased in the biological replicates, a portion of bacteria were surviving and replicating, except for B.R.2 with 200 μM H_2O_2 doses. Despite the decrease in lysis, increased amounts of intracellular proteins were released into the supernatant, compared to the single plasmid system. Using these results, I characterized mTG (SNTGA) expression and release into the supernatant using pHW02-E7. Using aerobic versus anaerobic mTG induction conditions, I was able to purify the mTG and achieve 10.2-12.8 U/mL of activity, comparable to the activity calculated by Yu *et al.*[51]. Through further optimization, pHW02-E7 can potentially serve as an effective targeted motility lysis system for engineered delivery of biotherapeutics.

Chapter 6: Conclusions

6.1 Results Summary

In Chapters 2 and 3, the bacterial motility gene CheZ was engineered under H_2O_2 control via the OxyR/S gene-promoter system (pHW02) to control bacterial running towards H_2O_2, known as pseudotaxis. I used multiple methods, including standard growth curves, qPCR, Western Blot, and H_2O_2 consumption, to characterize and demonstrate the genotypic dose-dependent response. Then, the H_2O_2 dose-dependent and time-dependent responses and pseudotaxis were phenotypically expressed and quantified using transwells, motility plates, microscopy tracking, and a microfluidic device. When induced with either low concentrations of H_2O_2 for 10-15 minutes or high concentrations of H_2O_2 for 5 minutes, HCW01-pHW02 recovered motility speeds similar to native speeds. Additionally, when pET200-t5-eGFP was added to HCW01-pHW02, I characterized and quantified the motility burden placed on the bacteria. This simple synthetic H_2O_2-responsive bacterial running system restored swimming motility while only minimally altering native circuitry.

In Chapter 4, I engineered Protein G, an IgG (antibody) binding domain, with AIDA1 to display Protein G on the bacterial outer surface. I improved Protein G surface display to have high, uniform levels while using low levels of inducer and a short induction time (2 hours) at 24ºC. This allows bacteria to be docked at the target site while minimizing metabolic burden and allowing for temperature-sensitive biotherapeutic expression. Additionally, I engineered the SNTGA system under H_2O_2 control in a low copy plasmid. Although Yu *et al.* optimized SNTGA conditions for high protein and activity yields, I showed that H_2O_2-SNTGA could be expressed within 6 hours and have mTG activity at different activation temperatures.

Finally, I engineered the E7 lysis gene under H_2O_2 control in pHW02 for the release of intracellular protein into the supernatant and cell death. Using multiple methods, including standard growth curves, PI staining with FACS, and SDS PAGE, I characterized and demonstrated that lysis was independent of H_2O_2 induction but sensitive to induction time. Further studies characterized lysis with increased metabolic burden; additional methods, including confocal microscopy and agar plates, confirmed lysis in the samples and a dose-dependent response in B.R.2. Finally, pHW02-E7 + pET32aΔ-SNTGA experiments showed that mTG, a biotherapeutic for wound healing, can be expressed intracellularly, released into the supernatant via E7 lysis, and maintain relatively high amounts of its activity.

Overall, I was able to show that the engineered HCW01-pHW02 bacteria were able to rapidly consume and swim towards the H_2O_2, rather than away, within 10-45 minutes. Importantly, I used physiologically-relevant concentrations of H_2O_2, 0-300 μM, for the *in vitro* and microfluidic experiments. Separately, I optimized Protein G-AIDA1 surface display as a potential biotherapeutic docking system, and expressed mTG relatively quickly (6 hours) that retained its activity as a potential wound healing biotherapeutic. Finally, I engineered bacterial lysis also under H_2O_2 control in the already established pHW02 motility system for release of intracellular proteins and the biotherapeutic. I developed, characterized, and optimized extensive surface display and H_2O_2 *in vitro* testing methods to characterize both qualitatively and quantitatively the different components of the potential wound-healing engineered bacterial system.

6.2 Challenges and Future Directions

6.2.1 Microbial Transglutaminase

Although I engineered Trx-proTGase under H_2O_2 control (**Chapter 4**), the amount of soluble protein and activity were low. Additionally, when pET32aΔ-SNTGA was co-

transformed with pHW02-E7, the amount of soluble mTG was low (**Chapter 5**). In order to overcome the concentration of mTG and activity issues, I would remove the oxyR/S promoter from pST39-OxyR-pOxyS-Trx–proTGase and replace it with the t5 promoter. First, this would increase the amount of soluble Trx-proTGase without overburdening metabolic function and motility because it is in a low-copy plasmid, compared to pET32a; additionally, because E7 can lyse bacteria within 2 hours, this would prevent extreme accumulation of Trx-proTGase. By increasing the amount of soluble protein, the amount of active protein increases, thus reducing the mTG therapeutic crosslinking time.

6.2.2 Protein G Surface Display

I successfully showed that the pG-AIDA1 bacteria highly and uniformly surface display Protein G with bound fluorescent antibody at >90% (**Chapter 4**). However, the stability of the bond *in vivo* was not tested. Potential complications can arise when the engineered bacteria are introduced into a mouse or human model, with varying conditions throughout the GI tract. Rigorous *in vivo* testing needs to be done to determine whether the antibody stays bound to Protein G. If not, Protein G could be engineered to also covalently bind the antibody, thus providing a more robust binding complex.

Also, if the bacterial therapeutic is encapsulated, the engineered bacteria could continue to grow and divide. This potentially produces the engineered bacteria without site-specific antibody preloaded. To overcome this, the site-specific antibody can be introduced into the liquid suspension inside the encapsulated therapeutic for binding.

6.2.3 H_2O_2-controlled E7 Lysis

H_2O_2-controlled E7 lysis exhibited unpredictable results with variable or no dependency on H_2O_2 dose. In order to overcome this, either the oxyR gene needs to be modified through to tighten repression, change the ribosome binding sequence, and/or

increase the copy number of oxyR genes expressed. Through directed evolution of oxyR, in combination with a more optimal ribosome binding site, a library of oxyR mutants can be expressed and characterized based on repression tightness. This would allow for reduced leakiness, increased biotherapeutic expression, and H_2O_2-specific lysis at the wound site, without compromising motility and H_2O_2-guided pseudotaxis. Alternatively, lysis can instead be regulated by a non-native *E. coli* promoter, such as IL-6, IL-8, or IL-10, which are cytokines up-regulated at the wound site during the inflammatory phase[19,95,99]; this promoter would need to be engineered for recombinant expression of a human promoter for *E. coli*.

6.2.3 Future Directions

Once the obstacles described previously are overcome, the entire therapeutic system can be engineered in two plasmids to reduce metabolic burden. Then, E7 lysis can be characterized with motility in the single engineered bacteria. For *in vitro* testing, TumbleScore motility video experiments can be performed again to qualitatively and quantitatively characterize metabolic and motility burdens before lysis. Additionally, the static microfluidic device experiments can be repeated to characterize the pseudotaxis response. Separately, microfluidic-based experiments can be used to determine the maximum distance necessary for the engineered bacteria to sense and swim towards the H_2O_2 (at physiologically relevant levels, ≤ 300 μM). Next, transwells and wound transwell assays can be performed with gut epithelial cells to model the engineered bacteria's response and the rapidity in which the bacteria consume the H_2O_2 over time. Further *in vivo* tests can look at different modes of delivery, i.e. capsules for oral delivery or a cream or patch for dermal delivery. While biotherapeutics are still a relatively new concept, by interacting early and often with the FDA and the Gut Microbiome Project, biotherapeutics serve as a potential alternative to antibiotics and current therapies.

References

1. Lee, T. C., Carrick, M. M., Scott, B. G., Hodges, J. C. & Pham, H. Q. Incidence and clinical characteristics of methicillin-resistant Staphylococcus aureus necrotizing fasciitis in a large urban hospital. *Am. J. Surg.* **194,** 809-12–3 (2007).

2. Seres Therapeutics. at <http://serestherapeutics.com/>

3. Smith, P. A. Pill Extracted From Poop Treats Antibiotic-Resistant Infections - Businessweek. *Bloomberg Business Week* (2014). at <http://www.businessweek.com/articles/2014-10-16/pill-extracted-from-poop-treats-antibiotic-resistant-infections>

4. Mende, K. *et al.* Phenotypic and Genotypic Changes over Time and across Facilities of Serial Colonizing and Infecting Escherichia coli Isolates Recovered from Injured Service Members. *J. Clin. Microbiol.* **52,** 3869–77 (2014).

5. Healy, M. Healing warriors by making a census of combat wounds' microbiota. *LA Times* (2014). at <http://www.latimes.com/science/sciencenow/la-sci-sn-combat-wounds-microbiome-20140618-story.html>

6. Wampler, S. LLNL technology detects bacterial pathogens in soldiers' combat wounds | Lawrence Livermore National Laboratory. (2014). at <https://www.llnl.gov/news/llnl-technology-detects-bacterial-pathogens-soldiers-combat-wounds#.VE_T9PnF-Sr>

7. Locke, J. C. W., Young, J. W., Fontes, M., Hernández Jiménez, M. J. & Elowitz, M. B. Stochastic pulse regulation in bacterial stress response. *Science* **334,** 366–9 (2011).

8. Mehra, S., Charaniya, S., Takano, E. & Hu, W.-S. A bistable gene switch for

antibiotic biosynthesis: the butyrolactone regulon in Streptomyces coelicolor. *PLoS One* **3,** e2724 (2008).

9. Silva-Rocha, R., de Jong, H., Tamames, J. & de Lorenzo, V. The logic layout of the TOL network of Pseudomonas putida pWW0 plasmid stems from a metabolic amplifier motif (MAM) that optimizes biodegradation of m-xylene. *BMC Syst. Biol.* **5,** 191 (2011).

10. Wong, W. W., Tsai, T. Y. & Liao, J. C. Single-cell zeroth-order protein degradation enhances the robustness of synthetic oscillator. *Mol. Syst. Biol.* **3,** 130 (2007).

11. Zhang, Y., Perry, K., Vinci, V. A. & Powell, K. Genome shuffling leads to rapid phenotypic improvement in bacteria. **415,** 5–7 (2002).

12. Stricker, J. *et al.* A fast, robust and tunable synthetic gene oscillator. *Nature* **456,** 516–9 (2008).

13. Regot, S. *et al.* Distributed biological computation with multicellular engineered networks. *Nature* **469,** 207–11 (2011).

14. Saeidi, N. *et al.* Engineering microbes to sense and eradicate Pseudomonas aeruginosa, a human pathogen. *Mol. Syst. Biol.* **7,** 521 (2011).

15. Kanta, J. The role of hydrogen peroxide and other reactive oxygen species in wound healing. *Acta Medica Cordoba.* **54,** 97–101 (2011).

16. Arwert, E. N., Hoste, E. & Watt, F. M. Epithelial stem cells, wound healing and cancer. *Nat. Rev. Cancer* **12,** 170–80 (2012).

17. Roy, S., Khanna, S. & Sen, C. K. Redox regulation of the VEGF signaling path and tissue vascularization: Hydrogen peroxide, the common link between physical

exercise and cutaneous wound healing. *Free Radic. Biol. Med.* **44,** 180–92 (2008).

18. Cho, M., Hunt, T. K., Hussain, M. Z. & Hus-, M. Z. Hydrogen peroxide stimulates macrophage vascular endothelial growth factor release. **280,** 2357–2363 (2001).

19. Iizuka, M. & Konno, S. Wound healing of intestinal epithelial cells. *World J. Gastroenterol.* **17,** 2161–2171 (2011).

20. Sturm, A. & Dignass, A. U. Modulation of gastrointestinal wound repair and inflammation by phospholipids. *Biochim. Biophys. Acta - Mol. Cell Biol. Lipids* **1582,** 282–288 (2002).

21. Niethammer, P., Grabher, C., Look, A. T. & Mitchison, T. J. A tissue-scale gradient of hydrogen peroxide mediates rapid wound detection in zebrafish. *Nature* **459,** 996–9 (2009).

22. Gardner, A. M. *et al.* Apoptotic vs. nonapoptotic cytotoxicity induced by hydrogen peroxide. *Free Radic. Biol. Med.* **22,** 73–83 (1996).

23. Roy, S., Khanna, S., Nallu, K., Hunt, T. K. & Sen, C. K. Dermal wound healing is subject to redox control. *Mol. Ther.* **13,** 211–220 (2006).

24. Bibiloni, R., Mangold, M., Madsen, K. L., Fedorak, R. N. & Tannock, G. W. The bacteriology of biopsies differs between newly diagnosed , untreated , Crohn ' s disease and ulcerative colitis patients. *J. Med. Microbiol.* **55,** 1141–1149 (2006).

25. Strus, M. *et al.* A role of hydrogen peroxide producing commensal bacteria present in colon of adolescents with inflammatory bowel disease in perpetuation of the inflammatory process. *J. Physiol. Pharmacol.* **60,** 49–54 (2009).

26. Zheng, M., Aslund, F. & Storz, G. Activation of the OxyR transcription factor by

reversible disulfide bond formation. *Science* **279,** 1718–1721 (1998).

27. Åslund, F., Zheng, M., Beckwith, J. & Storz, G. Regulation of the OxyR transcription factor by hydrogen peroxide and the cellular thiol-disulfide status. *Proc. Natl. Acad. Sci. U. S. A.* **96,** 6161–6165 (1999).

28. González-Flecha, B. & Demple, B. Role for the oxyS Gene in Regulation of Intracellular Hydrogen Peroxide in Escherichia coli. *J. Bacteriol* **181,** 3833–3836 (1999).

29. Wei, Q. *et al.* Global regulation of gene expression by OxyR in an important human opportunistic pathogen. *Nucleic Acids Res.* **40,** 4320–33 (2012).

30. D'Autréaux, B. & Toledano, M. B. ROS as signalling molecules: mechanisms that generate specificity in ROS homeostasis. *Nat. Rev. Mol. Cell Biol.* **8,** 813–24 (2007).

31. Rubens, J. R., Selvaggio, G. & Lu, T. K. Synthetic mixed-signal computation in living cells. *Nat. Commun.* **7,** 11658 (2016).

32. Toledano, M. B. *et al.* Redox-dependent shift of OxyR-DNA contacts along an extended DNA-binding site: A mechanism for differential promoter selection. *Cell* **78,** 897–909 (1994).

33. Green, J. & Paget, M. S. Bacterial redox sensors. *Nat. Rev. Microbiol.* **2,** 954–66 (2004).

34. Lee, C. *et al.* Redox regulation of OxyR requires specific disulfide bond formation involving a rapid kinetic reaction path. *Nat. Struct. Mol. Biol.* **11,** 1179–85 (2004).

35. Waters, C. M. & Bassler, B. L. Quorum sensing: cell-to-cell communication in bacteria. *Annu. Rev. Cell Dev. Biol.* **21,** 319–346 (2005).

36. Servinsky, M. D. *et al.* Directed assembly of a bacterial quorum. *ISME J.* **10,** 1–12 (2015).

37. Jayaraman, A. & Wood, T. K. Bacterial quorum sensing: signals, circuits, and implications for biofilms and disease. *Annu. Rev. Biomed. Eng.* **10,** 145–167 (2008).

38. DeLisa, M. P., Valdes, J. J. & Bentley, W. E. Quorum signaling via AI-2 communicates the 'Metabolic Burden' associated with heterologous protein production in Escherichia coli. *Biotechnol Bioeng* **75,** 439–450 (2001).

39. He, K. & Bauer, C. E. Chemosensory signaling systems that control bacterial survival. *Trends Microbiol.* **22,** 389–98 (2014).

40. Rao, C. V, Kirby, J. R. & Arkin, A. P. Design and diversity in bacterial chemotaxis: a comparative study in Escherichia coli and Bacillus subtilis. *PLoS Biol.* **2,** E49 (2004).

41. Parkinson, S. E. Coli chemotaxis. at <http://chemotaxis.biology.utah.edu/Parkinson_Lab/projects/ecolichemotaxis/ecolichemotaxis.html>

42. Lorand, L. & Graham, R. M. Transglutaminases: crosslinking enzymes with pleiotropic functions. *Nat. Rev. Mol. Cell Biol.* **4,** 140–56 (2003).

43. Fraij, B. M. 'Activation of tissue tranglutsaminase by removal of carboxyl-terminal peptides'. *J. Cell. Biochem.* **112,** 3469–81 (2011).

44. Shi, Q., Kim, S.-Y., Blass, J. P. & Cooper, A. J. L. Expression in Escherichia coli and purification of hexahistidine-tagged human tissue transglutaminase. *Protein Expr. Purif.* **24,** 366–73 (2002).

45. Oteng-Pabi, S. K. & Keillor, J. W. Continuous enzyme-coupled assay for microbial

transglutaminase activity. *Anal. Biochem.* **441,** 169–73 (2013).

46. Stachel, I., Schwarzenbolz, U., Henle, T. & Meyer, M. Cross-linking of type I collagen with microbial transglutaminase: Identification of cross-linking sites. *Biomacromolecules* **11,** 698–705 (2010).

47. O Halloran, D. M., Collighan, R. J., Griffin, M. & Pandit, A. S. Characterization of a microbial transglutaminase cross-linked type II collagen scaffold. *Tissue Eng.* **12,** 1467–74 (2006).

48. Yung, C. W. *et al.* Transglutaminase crosslinked gelatin as a tissue engineering scaffold. *J. Biomed. Mater. Res. A* **83,** 1039–46 (2007).

49. Yang, G. *et al.* Enzymatically crosslinked gelatin hydrogel promotes the proliferation of adipose tissue-derived stromal cells. *PeerJ* **4,** e2497 (2016).

50. Chen, T. *et al.* Gelatin-based biomimetic tissue adhesive. Potential for retinal reattachment. *J. Biomed. Mater. Res. B. Appl. Biomater.* **77,** 416–22 (2006).

51. Yu, Y. J. *et al.* Overproduction of soluble recombinant transglutaminase from Streptomyces netropsis in Escherichia coli. *Appl. Microbiol. Biotechnol.* **81,** 523–532 (2008).

52. Maurer, J., Jose, J., Meyer, T. F., Maurer, J. & Jose, J. Autodisplay : one-component system for efficient surface display and release of soluble recombinant proteins from Escherichia coli . Autodisplay : One-Component System for Efficient Surface Display and Release of Soluble Recombinant Proteins from Escheric. *J. Bacteriol.* **179,** 794–804 (1997).

53. Gustavsson, M., Bäcklund, E. & Larsson, G. Optimisation of surface expression using

the AIDA autotransporter. *Microb. Cell Fact.* **10,** 72 (2011).

54. Pohlner, J., Halter, R., Beyreuther, K. & Meyer, T. F. Gene structure and extracellular secretion of Neisseria gonorrhoeae IgA protease. *Nature* **325,** 458–462 (1987).

55. Wang, N., Guo, X. & Ng, I. S. Simultaneous release of recombinant cellulases introduced by coexpressing colicin E7 lysis in Escherichia coli. *Biotechnol. Bioprocess Eng.* **21,** 491–501 (2016).

56. James, R., Kleanthous, C. & Moore, G. R. The biology of E colicins: Paradigms and paradoxes. *Microbiology* **142,** 1569–1580 (1996).

57. Cascales, E. *et al.* Colicin Biology. *Microbiol. Mol. Biol. Rev.* **71,** 158–229 (2007).

58. Lin, L. J. R., Liao, C. C., Chen, Y. R. & Chak, K. F. Induction of membrane permeability in Escherichia coli mediated by lysis protein of the ColE7 operon: Research letter. *FEMS Microbiol. Lett.* **298,** 85–92 (2009).

59. González-Flecha, B. & Demple, B. Role for the oxyS Gene in Regulation of Intracellular Hydrogen Peroxide in E. coli. *J. Bacteriol* **181,** 3833–3836 (1999).

60. Zhang, A. *et al.* The OxyS regulatory RNA represses rpoS translation and binds the Hfq (HF-I) protein. *EMBO J.* **17,** 6061–6068 (1998).

61. Alon, U. *et al.* Response regulator output in bacterial chemotaxis. *EMBO J.* **17,** 4238–4248 (1998).

62. Chen, H. *et al.* A novel OxyR sensor and regulator of hydrogen peroxide stress with one cysteine residue in Deinococcus radiodurans. *PLoS One* **3,** e1602 (2008).

63. Zheng, M. *et al.* Computation-Directed Identification of OxyR DNA Binding Sites in

Escherichia coli. *J. Bacteriol.* **183,** 4571–4579 (2001).

64. Tschirhart, T. *et al.* Electronic control of gene expression and cell behaviour in Escherichia coli through redox signalling. *Nat. Commun.* **8,** (2017).

65. Canton, B., Labno, A. & Endy, D. Refinement and standardization of synthetic biological parts and devices. *Nat. Biotechnol.* **26,** 787–793 (2008).

66. Damton, N. C., Turner, L., Rojevsky, S. & Berg, H. C. Dynamics of bacterial swarming. *Biophys. J.* **98,** 2082–2090 (2010).

67. Turner, L., Zhang, R., Darnton, N. C. & Berg, H. C. Visualization of flagella during bacterial swarming. *J. Bacteriol.* **192,** 3259–3267 (2010).

68. Zhang, R., Turner, L. & Berg, H. C. The upper surface of an Escherichia coli swarm is stationary. *Proc. Natl. Acad. Sci. U. S. A.* **107,** 288–290 (2010).

69. Zargar, A. *et al.* Constructing 'quantized quorums' to guide emergent phenotypes through quorum quenching capsules. *Biotechnol. Bioeng.* 1–23 (2016). doi:10.1002/bit.26080

70. Terrell, J. L. *et al.* Nano-guided cell networks as conveyors of molecular communication. *Nat. Commun.* **6,** 8500 (2015).

71. Imlay, J. A. & Linn, S. Bimodal pattern of killing of DNA-repair-defective or anoxically grown Escherichia coli by hydrogen peroxide. *J. Bacteriol.* **166,** 519–527 (1986).

72. Sen, C. K. & Roy, S. Redox signals in wound healing. *Biochim. Biophys. Acta* **1780,** 1348–61 (2008).

73. Pottash, A. E., Mckay, R., Virgile, C. R., Ueda, H. & Bentley, W. E. TumbleScore : Run and tumble analysis for low. *Biotechniques* **62,** 1–6 (2017).

74. Division, C. and M. S. D. R. *AD819081 Hydrogen Peroxide Manual*. (1967).

75. Wu, H.-C. *et al.* Autonomous bacterial localization and gene expression based on nearby cell receptor density. *Mol. Syst. Biol.* **9,** 1–8 (2013).

76. Shang, W. *et al.* A simple and reusable bilayer membrane-based microfluidic device for the studies of gradient-mediated bacterial behaviors. *Biomicrofluidics* **11,** (2017).

77. Hwang, I. Y. *et al.* Reprogramming microbes to be pathogen-seeking killers. *ACS Synth. Biol.* **3,** 228–37 (2014).

78. McKay, R. *et al.* Controlling Localization of E. coli Populations Using a Two-Part Synthetic Motility Circuit: An Accelerator and Brake. *Biotechnol. Bioeng.* (2017).

79. Benov, L. & Fridovich, I. Escherichia coli exhibits negative chemotaxis in gradients of hydrogen peroxide, hypochlorite, and N-chlorotaurine: products of the respiratory burst of phagocytic cells. *Proc. Natl. Acad. Sci. U. S. A.* **93,** 4999–5002 (1996).

80. Girgis, H. S., Liu, Y., Ryu, W. S. & Tavazoie, S. A comprehensive genetic characterization of bacterial motility. *PLoS Genet.* **3,** 1644–60 (2007).

81. Diao, J. *et al.* A three-channel microfluidic device for generating static linear gradients and its application to the quantitative analysis of bacterial chemotaxis. *Lab Chip* **6,** 381–8 (2006).

82. Junge, W. Commentary ATP synthase and other motor proteins. *Prot. Natl. Acad. Sci.* **96,** 4735–4737 (1999).

83. Minamino, T., Morimoto, Y. V, Kinoshita, M., Aldridge, P. D. & Namba, K. The bacterial flagellar protein export apparatus processively transports flagellar proteins even with extremely infrequent ATP hydrolysis. *Sci. Rep.* **4,** 1–8 (2014).

84. Loo, A. E. K. *et al.* Effects of Hydrogen Peroxide on Wound Healing in Mice in Relation to Oxidative Damage. *PLoS One* **7,** (2012).

85. Liu, Y. *et al.* Biofabrication to build the biology–device interface. *Biofabrication* **2,** 22002 (2010).

86. Patel, R. & Dupont, H. L. New approaches for bacteriotherapy: Prebiotics, new-generation probiotics, and synbiotics. *Clin. Infect. Dis.* **60,** S108–S121 (2015).

87. Akerstrom, B., Brodin, T., Reis, K. & Bjorck, L. Protein G : a powerful tool for binding and detection of monoclonal and polyclonal antibodies. *J. Immunol.* **135,** 2589–2592 (1985).

88. Watanabe, H. *et al.* Optimizing pH response of affinity between protein G and IgG Fc. How electrostatic modulations affect protein-protein interactions. *J. Biol. Chem.* **284,** 12373–12383 (2009).

89. Akerstrom, B. & Bjorck, L. A physicochemical study of protein G, a molecule with unique immunoglobulin G-binding properties. *J. Biol. Chem.* **261,** 10240–10247 (1986).

90. Hajela, K. Significance of Fc receptors. *Biochem. Educ.* **19,** 50–57 (1991).

91. Mach, T. Clinical usefulness of probiotics in inflammatory bowel diseases. *J. Physiol. Pharmacol.* **57 Suppl 9,** 23–33 (2006).

92. Wang, L., Li, J., March, J. C., Valdes, J. J. & Bentley, W. E. luxS-Dependent Gene

Regulation in Escherichia coli K-12 Revealed by Genomic Expression Profiling. *Society* **187,** 8350–8360 (2005).

93. Biolabs, N. E. Gibson Assembly Master Mix. *Manual* 1–16 (2012). doi:10.1073/pnas.88.17.7585

94. Folk, J. E. & Cole, P. W. Mechanism of Action of Guinea Pig Liver Transglutaminase. *J. Bol. Chem.* **241,** 5518–5525 (1966).

95. Leoni, G., Neumann, P.-A., Sumagin, R., Denning, T. L. & Nusrat, A. Wound repair: role of immune–epithelial interactions. *Mucosal Immunol.* **8,** 959–968 (2015).

96. Lerner, A. & Matthias, T. Food Industrial Microbial Transglutaminase in Celiac Disease: Treat or Trick. *Int. J. Celiac Dis.* **3,** 1–6 (2015).

97. Chak, K. F., Kuo, W., Lu, F. & James, R. Cloning and Characterization of the ColE7 plasmid. *J. Gen. Microbiol.* **137,** 91–100 (1991).

98. Schindelin, J. *et al.* Fiji: an open-source platform for biological-image analysis. *Nat Meth* **9,** 676–682 (2012).

99. Liu, L. N. *et al.* Protective effects of Rheum tanguticum polysaccharide against hydrogen peroxide-induced intestinal epithelial cell injury. *World J. Gastroenterol.* **11,** 1503–1507 (2005).